

LU TP 19-21  
June 2019

# FLAVOUR-ORDERING IN THE NONLINEAR SIGMA MODEL WITH MORE DERIVATIVES AND LEGS

**Mattias Sjö**

Department of Astronomy and Theoretical Physics,  
Lund University

Master's thesis supervised by  
Johan Bijnens and Karol Kampf



**LUND**  
UNIVERSITY

## Abstract

We present a generalisation of the flavour-ordering method applied to the chiral nonlinear sigma model with any number of flavours. We use an extended Lagrangian with terms containing any number of derivatives, organised in a power-counting hierarchy. The method allows diagrammatic computations at tree-level with any number of legs at any order in the power-counting. Using an automated implementation of the method, we calculate amplitudes ranging from 12 legs at leading order,  $\mathcal{O}(p^2)$ , to 6 legs at next-to-next-to-next-to-leading order,  $\mathcal{O}(p^8)$ .

## Contents

|  |           |
|--|-----------|
| Populärvetenskaplig beskrivning . . . . .                                    | iii       |
| Popular science description . . . . .  | iv        |
| <b>1 Introduction</b>  | <b>1</b>  |
| 1.1 The structure of this thesis . . . . .                                   | 2         |
| <b>2 The NLSM and its Lagrangian</b>   | <b>2</b>  |
| 2.1 Some Lie algebra . . . . .   | 2         |
| 2.2 A toy example: the linear sigma model and its low-energy limit . . . . . | 3         |
| 2.3 The general NLSM . . . . .   | 5         |
| 2.4 The chiral NLSM Lagrangian . . . . .                                     | 6         |
| 2.4.1 The lowest-order Lagrangian terms . . . . .                            | 8         |
| 2.4.2 The Cayley-Hamilton theorem . . . . .                                  | 9         |
| 2.4.3 Higher-order Lagrangian terms . . . . .                                | 9         |
| <b>3 Flavour-ordering</b>  | <b>12</b> |
| 3.1 Some notation . . . . .  | 12        |
| 3.2 NLSM vertices . . . . .  | 13        |
| 3.3 Stripped vertex factors . . . . .  | 14        |
| 3.4 Constructing diagrams . . . . .  | 15        |
| 3.5 Flavour-ordered diagrams . . . . .                                       | 16        |
| 3.6 The singlet problem and its solution . . . . .                           | 19        |
| 3.7 Uniqueness of stripped amplitudes . . . . .                              | 21        |
| <b>4 NLSM amplitudes</b>   | <b>22</b> |
| 4.1 Dependence on the parametrisation . . . . .                              | 23        |
| 4.2 Generalised Mandelstam invariants . . . . .                              | 24        |
| 4.3 Reduced stripped amplitudes . . . . .                                    | 26        |
| 4.4 Adler zeroes and soft limits . . . . .                                   | 27        |
| 4.5 Reconstruction from soft limits . . . . .                                | 29        |

|          |  |           |
|----------|--|-----------|
| <b>5</b> | <b>Practical calculation methods</b>                                   | <b>31</b> |
| 5.1      | Diagrams as polygon partitions . . . . .                               | 32        |
| 5.2      | Generating partitioned polygons . . . . .                              | 33        |
| 5.3      | A symmetry-respecting representation of partitions . . . . .           | 33        |
| 5.4      | Determining diagram symmetries . . . . .                               | 36        |
| <b>6</b> | <b>Examples of amplitudes</b>  | <b>37</b> |
| 6.1      | 4-point amplitudes . . . . .   | 37        |
| 6.1.1    | The $\mathcal{O}(p^2)$ amplitude . . . . .                             | 37        |
| 6.1.2    | The $\mathcal{O}(p^4)$ amplitude . . . . .                             | 38        |
| 6.1.3    | The $\mathcal{O}(p^6)$ amplitude . . . . .                             | 38        |
| 6.1.4    | The $\mathcal{O}(p^8)$ amplitude . . . . .                             | 39        |
| 6.2      | The $\mathcal{O}(p^2)$ 6- and 8-point amplitudes . . . . .             | 39        |
| 6.3      | The $\mathcal{O}(p^4)$ 6-point amplitude . . . . .                     | 40        |
| 6.4      | Further amplitudes . . . . .   | 41        |
| <b>7</b> | <b>First steps towards generalisation</b>                              | <b>43</b> |
| 7.1      | A brief look at $\chi$ PT . . . . .                                    | 43        |
| 7.2      | Flavour-ordering and mass . . . . .                                    | 44        |
| 7.2.1    | Scalar meson masses . . . . .  | 44        |
| 7.2.2    | Massive propagators, equal-mass case . . . . .                         | 46        |
| 7.2.3    | Massive propagators, general case . . . . .                            | 46        |
| 7.3      | Flavour-ordering and loops . . . . .                                   | 48        |
| <b>8</b> | <b>Summary, conclusions and outlook</b>                                | <b>49</b> |
| <b>A</b> | <b>The Lie algebra of <math>SU(N_f)</math> and <math>U(N_f)</math></b> | <b>51</b> |
| A.1      | General definitions . . . . .  | 51        |
| A.2      | Conventional values . . . . .  | 52        |
| A.3      | Contractions in traces . . . . .                                       | 52        |
| A.4      | The adjoint representation . . . . .                                   | 53        |
| <b>B</b> | <b>The orthogonality of flavour structures</b>                         | <b>54</b> |
| <b>C</b> | <b>The double soft limit</b>   | <b>55</b> |
| <b>D</b> | <b>Closed Mandelstam bases</b>   | <b>56</b> |
| D.1      | The basis for $R = \{2, 4\}$ . . . . .                                 | 56        |
| D.2      | The basis for $R = \{3, 3\}$ . . . . .                                 | 57        |
| D.3      | The basis for $R = \{2, 2, 2\}$ . . . . .                              | 58        |
| <b>E</b> | <b>Implementation details</b>  | <b>59</b> |
| E.1      | The FORM library . . . . .   | 59        |
| E.2      | The diagram generator <code>fodge</code> . . . . .                     | 60        |

## Populärvetenskaplig beskrivning

Världen som vi känner den hålls samman av fyra grundläggande krafter. Gravitationskraften drar oss mot jorden och håller samman planeter, stjärnor och galaxer. Den elektromagnetiska kraften styr i princip allt annat vi upplever i vår vardag. Den starka kärnkraften håller samman protoner och neutroner i atomkärnor och binder de kvarkar som i sin tur bygger upp dessa partiklar, och den svaga kärnkraften styr radioaktivt sönderfall.

Alla dessa krafter är var för sig väl förstådda av vetenskapen, fast bland kärnkrafterna och elektromagnetismen, som förenas av den så kallade Standardmodellen, är den starka kärnkraften något av ett sorgebarn. Vid extremt höga energier, som när partikelfysiker splittrar materiens allra minsta beståndsdelar i enorma accelerators, släpper den starka kärnkraften sitt grepp, och de kvarkar och gluoner som den binder kan studeras. Men så fort de enorma energierna avtar, blir den starka kärnkraften starkare och binder sina partiklar så hårt att fria kvarkar och gluoner aldrig kan observeras direkt. Tänk på det — med ett skutt övervinner du för en sekund hela jordens gravitation, och med en ballong mot håret sliter du lätt loss miljardtals elektroner mot elektromagnetismens protester, men ingenting vetenskapen har att uppbringa kan skilja kvarkar åt när den starka kärnkraften binder dem.

Den starka kärnkraftens styrka gör det svårt att studera partiklar som hålls samman av den. Innehållet i en atom är en förhållandevis enkel struktur där elektroner och en kärna binds av den elektromagnetiska kraften, men innehållet i en proton är en oöverskådlig soppa av kvarkar och gluoner, där även partikelfysikens mest avancerade verktyg måste anstränga sig för att dra ens de enklaste slutsatser.

Denna sopps ogenomtränglighet kan dock användas till vår fördel. Den starka kärnkraften knyter sina partiklar så hårt att de, om en inte gräver runt för mycket, kan uppfattas som fundamentala punktpartiklar snarare än de invecklade klumpar de egentligen är. Med denna uppfattning går det att ta fram modeller som beskriver dessa punktpartiklar på samma sätt som Standardmodellen beskriver de verkliga elementarpartiklarna. Den enklaste av dessa modeller är den icke-linjära sigmamodellen (engelska: *nonlinear sigma model*), som är vårt arbetes fokus. All komplexitet i partiklarnas inre kokas ner till en uppsättning tal, som kan mätas och sedan stoppas in i modellen för att förutsäga partiklarnas beteende.

Den icke-linjära sigmamodellen är välstuderad, men oftast handskas forskarna bara med de enklaste och viktigaste bitarna av den. Den kompletta modellen innehåller en oändlig lista med allt mer komplicerade, men också allt mer oviktiga, bitar. Vi utvecklar diverse beräkningsmetoder så att vi kan inkludera några fler av dessa bitar, vilket gör modellens förutsägelser mer exakta.

Det vi gör är viktigt av flera skäl, för partiklar sammansatta genom den starka kärnkraften spelar en avgörande roll i vetenskapen och universum. Skurar av dessa partiklar bär fingeravtrycket från de nya processer, som sker i en partikelaccelerators hjärta, fram till våra detektorer. Nästan all materia vi känner till är uppbyggd av protoner och neutroner, och andra partiklar (så kallade mesoner) fungerar som den starka kärnkraftens budbärare i atomkärnors inre. Allt detta gör förståelsen av den starka kärnkraftens bundna partiklar en avgörande pusselbit i mänsklighetens jakt på kunskap.

## Popular science description

The world as we know it is held together by four fundamental forces. The force of gravity pulls us to the Earth and holds planets, stars and galaxies together. The electromagnetic force governs essentially all other things we experience in our daily lives. The strong nuclear force holds protons and neutrons together in atomic nuclei and binds the quarks that in turn make up these particles, and the weak nuclear force governs radioactive decay.

All these forces are separately well understood by science, but among the nuclear forces and electromagnetism, which are united by the so-called Standard Model, the strong nuclear force is a bit troublesome. At extremely high energies, like when particle physicists shatter the minutest constituents of matter in enormous accelerators, the strong nuclear force loosens its grip, and the quarks and gluons it binds can be studied. But as soon as the enormous energies fade, the strong nuclear force grows even stronger and binds its particles so hard that free quarks and gluons can never be observed directly. Just think of that — with a jump, you defeat the gravity of the entire Earth for a second, and with a balloon to your hair, you easily rip off billions of electrons against the protests of electromagnetism, but nothing science has to offer can ever separate quarks against the pull of the strong nuclear force.

The strength of the strong nuclear force makes it difficult to study particles built through it. The contents of an atom is a comparatively simple structure where electrons and a nucleus are bound by the electromagnetic force, but the contents of a proton is an intractable soup of quarks and gluons, where even the most advanced tools of particle physics must struggle to come to even the simplest of conclusions.

The opacity of this soup can be used to our advantage, though. The strong nuclear force ties its particles so hard that they, as long as one does not dig around too much, can be seen as fundamental point particles rather than the intricate lumps they actually are. With this view, one can produce models that describe these point particles the same way that the Standard Model describes the true elementary particles. The simplest such theory is the nonlinear sigma model, which is the focus of our work. All the complexity in the interior of the particles is boiled down to a set of numbers, which can be measured and plugged into the model to predict the behaviour of the particles.

The nonlinear sigma model is well studied, but scientists usually only handle the simplest and most important pieces of it. The complete model contains an infinite sequence of more and more complicated, but also less and less important, pieces. We develop some calculation methods that allow us to include some more of these pieces, which makes the predictions of the model more precise.

What we do is important for several reasons, as particles built with the strong force play a crucial role in science and the Universe. Showers of these particles carry to our detectors the fingerprint of the new processes that take place in the heart of a particle accelerator. Almost all matter we know of is made from protons and neutrons, and other particles (so-called mesons) serve as the messengers of the strong nuclear force in the interiors of atomic nuclei. All of this makes the understanding of the bound particles of the strong nuclear force a decisive piece in the puzzle of humanity's search for knowledge.

# 1 Introduction

Quantum chromodynamics (QCD) is currently understood to be the complete theory describing the strong interactions of quarks and gluons within the framework of the Standard Model (SM) of particle physics. However, the path from the elegance of its Lagrangian to the phenomena it generates is not at all clear. Due to the running of the QCD coupling, the perturbative treatment that allows predictions from other parts of the SM breaks down in the low-energy limit. Instead, quark confinement arises, and the interiors of composite strongly interacting particles (mesons, baryons, and more exotic hadrons) become intractable soups of quarks and gluons. Even deducing the mass of the such a familiar particle as the proton from its constituents remains difficult.

There are several approaches to tackling low-energy QCD. One is lattice QCD, where the continuity of spacetime is sacrificed for the ability to perform direct simulations. Another is to use effective field theories (EFTs), that in general model the degrees of freedom that emerge from an underlying theory in some limit. In the context of QCD, the quark and gluon degrees of freedom disappear in the low-energy limit and give way to mesons and baryons. With no direct reference to their interior, these particles can be modeled perturbatively under a well-chosen EFT. In this work, we follow the EFT approach.

In 1960, Gell-Mann and Lévy [1] proposed a number of models for mesons and nucleons. Two of these, the linear and nonlinear sigma models, were extended to highly general quantum field theories that now serve in many different fields (see [2] for an example in quantum spin systems). The nonlinear sigma model (NLSM) was also found to be a decent theory of meson interactions, and was extended by Weinberg [3] and by Gasser and Leutwyler [4, 5] into chiral perturbation theory ( $\chi$ PT), an EFT of low-energy QCD that is widely used today.

The main focus of this thesis is not  $\chi$ PT but rather its backbone, the NLSM, which models light mesons as massless pseudoscalar bosons. Its Lagrangian contains an infinite number of interaction terms organised in a power-counting hierarchy<sup>1</sup>, so the calculation of scattering amplitudes beyond the simplest cases is a daunting task. So far, tree-level scattering has been calculated for up to 10 particles at the leading order in the power counting [6], and 4-point scattering [7] and pion decays [8] in  $\chi$ PT have been calculated to high orders. No NLSM results beyond this were known when we started, but near the completion of our work, the 6-point tree-level amplitude at next-to-leading order in the power counting was published [9].

We aim to expand both the number of particles and the power-counting order for which tree-level NLSM amplitudes are known. Both [6] and [9] reached their results using various recursion relations, in which amplitudes are constructed recursively from simpler amplitudes. We will take the somewhat more direct approach of flavour-ordering, which simplifies diagrammatic computations by reducing the vast number of terms to a subset that carries all essential information. This method was introduced in [6] and will be generalised

---

<sup>1</sup>“The NLSM” often refers to the leading-order term in the power counting, while we use the term to refer to the generalised form including higher-order terms. See section 2 for more details.

by us. It is analogous to the colour-ordering methods in perturbative QCD, which were introduced by Berends and Giele [10]; see [11] and particularly [12] for an approach that is very similar to ours.

## 1.1 The structure of this thesis

In section 2, we give an introduction to the NLSM and some related models. We aim for a gradual buildup in line with contemporary introductions such as [13]. We then state the four lowest power-counting orders of its Lagrangian, the highest of which was only recently determined [14], and present it in a new, compact notation.

In section 3, we describe the powerful method of flavour-ordering and generalise it to handle the higher-order Lagrangians. Rather than directly stating the result, the section is laid out as a gradual development roughly modeled on how we progressed in this work. It is our hope that this helps with understanding the reasoning behind the method, since flavour-ordering forms the core result of this thesis.

In section 4, we present some additional technology mainly related to the kinematic structure of NLSM amplitudes, with an eye to more general EFTs. Much of this is merely introduced for completeness, but some is generalised to apply to higher-order amplitudes.

In section 5, we introduce the algorithms used for automating the calculation of amplitudes using flavour-ordering, and in section 6, we give a tour of some of the more manageable amplitudes produced this way.

Lastly, we introduce some possible ways to extend flavour-ordering to NLSM loop diagrams and  $\chi$ PT in section 7, and summarise the work in section 8.

## 2 The NLSM and its Lagrangian

### 2.1 Some Lie algebra

In this and the following sections, we will make heavy use of the Lie algebra of  $SU(N_f)$  or  $U(N_f)$ . The main definitions are given here; a more thorough summary and the derivation of the relevant identities are given in appendix A.

The Lie algebra is given in terms of its generators  $t^a$ . For  $SU(N_f)$ , they are a set of  $N_f^2 - 1$  hermitian and traceless  $N_f \times N_f$  matrices, with  $a$  starting at 1. For  $U(N_f)$ , the generators also include the non-traceless generator  $t^0 \propto \mathbb{1}$ , where  $\mathbb{1}$  is the unit matrix. The index  $a$  is referred to in this context as a *flavour index*, since it is closely tied to the flavours of the particles involved in the model.

The generators form a basis for the space of (traceless) hermitian matrices, and obey the trace orthogonality relation

$$\langle t^a t^b \rangle = \tau \delta^{ab}, \quad (2.1)$$

where  $\langle \dots \rangle$  denotes a trace, and  $\tau$  is a normalisation that is left unspecified to conform to

the conventions of various authors. They also obey the (anti)commutator relations

$$[t^a, t^b] = i\kappa f^{abc}t^c, \quad \{t^a, t^b\} = \frac{2\tau}{N_f}\delta^{ab} + \kappa d^{abc}t^c, \quad (2.2)$$

where  $\kappa$  is another normalisation, and  $f^{abc}$  and  $d^{abc}$  are some real numbers called the structure constants of the algebra.  $f^{abc}$  is totally antisymmetric in its indices, and  $d^{abc}$  is totally symmetric. Here and in all other places, the Einstein summation convention is used, with no distinction between upper and lower flavour indices.

## 2.2 A toy example: the linear sigma model and its low-energy limit

Rather than directly presenting the NLSM, it is useful to first gain some intuition about its origin by considering its simpler cousin, the linear sigma model (LSM), as was done historically [1]. This section closely follows the approach taken by [13].

Let us construct a toy Lagrangian containing a vector of four real (pseudo)scalar fields,  $\Phi = (\sigma, \pi^a)$ , where  $a$  runs from 1 to 3. The  $\phi^4$ -style Lagrangian is

$$\mathcal{L} = \frac{1}{2}\partial_\mu\Phi^T\partial^\mu\Phi - \frac{\lambda}{4}(\Phi^T\Phi - v^2)^2, \quad (2.3)$$

and is invariant under  $SO(4)$  rotations of  $\Phi$ . With  $v^2 < 0$ , the theory would contain four degenerate fields of squared mass  $-\lambda v^2$ , but if  $v^2 > 0$ , the potential assumes a ‘‘Mexican hat’’ shape, with minima at all field configurations with  $\Phi^T\Phi = v^2$ . We adopt the vacuum where  $\langle 0|\sigma|0\rangle = v$  and  $\langle 0|\pi^a|0\rangle = 0$ , and make the field redefinition  $\sigma \rightarrow \hat{\sigma} + v$ , so that all four fields  $(\hat{\sigma}, \pi^a)$  again have zero vacuum expectation value. After this redefinition, the Lagrangian has the form

$$\mathcal{L} = \frac{1}{2}[\partial_\mu\hat{\sigma}\partial^\mu\hat{\sigma} + \partial_\mu\pi^a\partial^\mu\pi^a - 2\lambda v^2\hat{\sigma}^2] - \lambda v\hat{\sigma}(\hat{\sigma}^2 + \pi^a\pi^a) - \frac{\lambda}{4}(\hat{\sigma}^2 + \pi^a\pi^a)^2, \quad (2.4)$$

which endows the redefined  $\hat{\sigma}$  with a squared mass  $2\lambda v^2$ , but leaves  $\pi^a$  massless. The vacuum choice has broken the  $SO(4)$  symmetry and leaves only  $SO(3)$  symmetry among  $\pi^a$ ;  $\hat{\sigma}$  is left as a singlet. In light of the Nambu-Goldstone theorem, we interpret  $\pi^a$  as the Nambu-Goldstone fields corresponding to the  $\dim[SO(4)] - \dim[SO(3)] = 3$  broken generators of the symmetry. Here,  $a$  serves as our first practical example of a flavour index that distinguishes the elements of a multiplet of otherwise identical fields.

This Lagrangian can be recast in a more illuminating form, bringing us closer to the NLSM. We rearrange the four fields into a  $2 \times 2$  matrix like

$$\Sigma = \sigma\mathbf{1} + \frac{2i}{\tau}t^a\pi^a, \quad (2.5)$$

where  $t^a$  are the generators of  $SU(2)$ , e.g. the Pauli matrices; as stated in appendix A,  $\{\mathbf{1}, t^a\}$  is a basis for all  $2 \times 2$  matrices. In terms of this field, (2.3) becomes

$$\mathcal{L} = \frac{1}{4}\langle\partial_\mu\Sigma^\dagger\partial^\mu\Sigma\rangle - \frac{\lambda}{16}(\langle\Sigma^\dagger\Sigma\rangle - v^2)^2. \quad (2.6)$$



Due to the appearance of the trace,  $\mathcal{L}$  is explicitly invariant under a global symmetry  $SU(2)_R \times SU(2)_L$ , which can be defined to act as

$$\Sigma \xrightarrow{g} g_R \Sigma g_L^\dagger, \quad g = (g_R, g_L) \in SU(2)_R \times SU(2)_L. \quad (2.7)$$

However, the vacuum expectation value  $\langle 0|\Sigma|0\rangle = v\mathbb{1}$  is only conserved by the subgroup where  $g_R = g_L$ . Therefore, the spontaneous symmetry breaking appears again, this time in the form  $SU(2)_R \times SU(2)_L \rightarrow SU(2)_V$ .<sup>2</sup>

The reformulation in terms of  $\Sigma$  mixed the massive and massless fields. We can separate them again by rewriting  $\Sigma$  in the polar form

$$\Sigma = [v + S] \exp\left(\frac{it^a \phi^a}{v}\right) = [v + S]U(\phi), \quad (2.8)$$

where  $(S, \phi^a)$  is a new set of scalar fields defined in terms of  $(\hat{\sigma}, \pi^a)$ . For consistency,  $S$  must be invariant under  $SU(2)_R \times SU(2)_L$ , while the composite field  $U(\phi)$  inherits the transformation properties of  $\Sigma$ . This, in turn, means that the fields  $\phi^a$  transform nonlinearly. With this field redefinition, the Lagrangian becomes

$$\mathcal{L} = \frac{v^2}{4} \left(1 + \frac{S}{v}\right)^2 \langle \partial_\mu U^\dagger \partial^\mu U \rangle + \frac{1}{2} (\partial_\mu S \partial^\mu S - M^2 S^2) - \frac{M^2}{2v} S^3 - \frac{M^2}{8v^2} S^4, \quad (2.9)$$

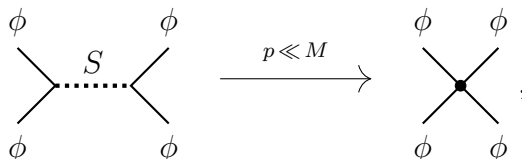
where  $M^2 = 2\lambda v^2$ . This confirms that the  $\phi$  fields are the massless Nambu-Goldstone bosons of the symmetry breaking, and the polar form (2.8) supports the interpretation that  $\phi^a$  represent rotations within the minimum of the potential, while  $S$  represents massive excitations out of the minimum.

When  $M$  is much larger than the momentum scale  $p$  of a process,  $S$  can be integrated out from the Lagrangian, in line with the central idea of EFTs. Doing so leaves an effective Lagrangian for the Nambu-Goldstone bosons with the very simple form

$$\mathcal{L}_{\text{eff}} = \frac{v^2}{4} \langle \partial_\mu U^\dagger \partial^\mu U \rangle. \quad (2.10)$$

We have now transitioned from the LSM to our first example of the NLSM: the massive field has been fully untangled from the massless ones, at the cost of replacing our original fields  $\pi^a$  with the nonlinear  $U(\phi)$ .

The interactions between  $\phi$  (contained in  $U$ ) and  $S$  in (2.9) give rise to corrections to this effective Lagrangian. The leading correction is conceptually given by the  $S$ -mediated scattering



$$\begin{array}{ccc} \begin{array}{c} \phi & & \phi \\ \diagdown & & / \\ & \text{---} S \text{---} & \\ / & & \diagdown \\ \phi & & \phi \end{array} & \xrightarrow{p \ll M} & \begin{array}{c} \phi & & \phi \\ \diagdown & & / \\ & \bullet & \\ / & & \diagdown \\ \phi & & \phi \end{array}, \end{array} \quad (2.11)$$

<sup>2</sup>The existence of two equivalent symmetry breakings is no surprise, since the Lie algebra of  $SO(4)$  is homeomorphic to that of  $SU(2) \times SU(2)$ , and the Lie algebra of  $SO(3)$  is homeomorphic to that of  $SU(2)$ .

where the two  $\phi\phi S$  vertex factors and the propagator, which reduces to  $\sim 1/M^2$  at the small momentum scale  $p$ , are condensed into a single vertex in the EFT. Doing this for all possible diagrams gives rise to a series of corrections of the form

$$\mathcal{L}_{\text{eff}} = \frac{v^2}{4} \langle \partial_\mu U^\dagger \partial^\mu U \rangle + \frac{v^2}{8M^2} \langle \partial_\mu U^\dagger \partial^\mu U \rangle^2 + \mathcal{O} \left( \frac{p^4}{M^4} \right), \quad (2.12)$$

where the leading correction is suppressed by a factor of  $p^2/M^2 \ll 1$  compared to the first term. Such a series of derivative-coupled interaction terms is typical of an EFT.

### 2.3 The general NLSM

In the previous section, the effective Lagrangian (2.10) and its extension (2.12) were derived from a Lagrangian containing the additional massive field  $\sigma$ , recast as  $S$ , and then sending the mass of that field to infinity. A similar but more general model can be derived in a theory-agnostic fashion, using only the symmetry breaking and not the explicit form of the underlying fields. We still follow [13] closely.

Consider some general global symmetry breaking  $G \rightarrow H$ , of which the scenario  $SU(2)_R \times SU(2)_L \rightarrow SU(2)_V$  above was a special case. Here,  $G$  can be any simple compact Lie group with  $H$  as a subgroup. By the Nambu-Goldstone theorem, this generates  $N_{\text{NGB}} = \dim(G) - \dim(H)$  Nambu-Goldstone bosons  $\phi_a$ , which we arrange as  $\phi = (\phi_1, \dots, \phi_{N_{\text{NGB}}})$ . They will not be invariant under  $G$ , but instead transform in some non-trivial way as

$$\phi \xrightarrow{g} \mathcal{G}_g(\phi), \quad (2.13)$$

where  $g \in G$ . To respect the group structure of  $G$ , the mapping  $\mathcal{G}$  must satisfy  $\mathcal{G}_{g_1}(\mathcal{G}_{g_2}(\phi)) = \mathcal{G}_{g_1 g_2}(\phi)$  and  $\mathcal{G}_e(\phi) = \phi$ , where  $e$  is the identity element of  $G$ . Furthermore, each field configuration  $\phi$  should be possible to obtain from the vacuum  $\phi_0$  with some  $g \in G$  like

$$\phi = \mathcal{G}_g(\phi_0) = \mathcal{G}_{gh}(\phi_0), \quad h \in H. \quad (2.14)$$

The second equality holds for any  $h \in H$  since  $H$  is defined to preserve the vacuum. Thus, the above defines a mapping from the coset  $gH = \{gh \mid h \in H\}$  to the field configuration  $\phi$ .<sup>3</sup> This mapping is invertible, since if two cosets  $g_1H, g_2H$  map to the same  $\phi$ , then

$$\mathcal{G}_{g_1}(\phi_0) = \mathcal{G}_{g_2}(\phi_0) \quad \Rightarrow \quad \mathcal{G}_{g_1^{-1}g_2}(\phi_0) = \mathcal{G}_e(\phi_0) \quad \Rightarrow \quad g_1^{-1}g_2 \in H \quad \Rightarrow \quad g_2 \in g_1H. \quad (2.15)$$

Thus,  $g_2 = g_1 h'$  for some  $h' \in H$ . But since  $h'h \in H$  for any  $h \in H$ , this proves that  $g_1H = g_2H$ . Therefore, each field configuration  $\phi$  corresponds to a unique coset, and may be replaced by a representative  $\xi(\phi)$  taken from that coset. The representatives transform by group element composition, but if  $\xi(\phi)$  is a representative of  $g_1H$ , then  $g_2\xi(\phi)$  is not necessarily *the* representative that was chosen from  $g_2g_1H$  to represent  $\mathcal{G}_{g_2}(\phi)$ . Therefore,

---

<sup>3</sup>Recall that  $gH = \{gh \mid h \in H\}$  is the *definition* of a (left) coset, and that the space of all such cosets  $gH$  for  $g \in G$  is denoted  $G/H$ .

we must apply a compensating transformation  $h(\xi(\phi), g_2) \in H$  to recover our chosen representative. This endows  $\xi$  with the transformation property

$$\xi(\phi) \xrightarrow{g} g\xi(\phi)h(\xi(\phi), g)^\dagger = \xi(\mathcal{G}_g(\phi)). \quad (2.16)$$

This coset representation forms a convenient basis for further developments.

Let us now restrict ourselves to a highly useful special case, namely when  $G$  is the chiral symmetry group  $SU(N_f)_R \times SU(N_f)_L$ . Among other things, this group (with  $N_f$  being the number of quark flavours) is a global symmetry of the massless QCD Lagrangian,

$$\mathcal{L}_{\text{QCD}} = i\bar{q}_L\gamma^\mu D_\mu q_L + i\bar{q}_R\gamma^\mu D_\mu q_R - \frac{1}{4}G_{\mu\nu}^a G_a^{\mu\nu}, \quad (2.17)$$

where the left- and right-handed quark  $N_f$ -plets transform as

$$q_L \xrightarrow{g} g_L q_L, \quad q_R \xrightarrow{g} g_R q_R, \quad g = (g_L, g_R) \in G \quad (2.18)$$

and the gluon fields contained in  $D_\mu$  and  $G_{\mu\nu}^a$  are invariant under  $G$ . This symmetry is not conserved in the hadronic spectrum generated in low-energy QCD, but is instead broken to  $H = SU(N_f)_V$ . This symmetry breaking generates  $\dim(G) - \dim(H) = N_f^2 - 1$  Nambu-Goldstone bosons, which may be identified with the pion triplet (for  $N_f = 2$ ) or the light meson octet (for  $N_f = 3$ ). This identification is supported by the introduction of masses in section 7.2.

In reality, these mesons are light but not massless, and many are electrically charged, so the identification with massless Nambu-Goldstone bosons that only interact strongly can only serve as a first approximation. In section 7.1, we will briefly cover the extensions that reintroduce masses, electroweak couplings, and other interactions beyond those that can be derived from (2.17), turning the NLSM into chiral perturbation theory ( $\chi$ PT). Still, the NLSM serves as the backbone of its more complete counterpart. Therefore, we shall continue to develop it as the main focus of this thesis without dwelling on its limitations.

## 2.4 The chiral NLSM Lagrangian

As we saw in the preceding section, the Nambu-Goldstone fields of the chiral NLSM<sup>4</sup> can be expressed in terms of coset representatives, which we split to represent the chiral structure:  $\xi(\phi) = (\xi_L(\phi), \xi_R(\phi)) \in [SU(N_f)_L \times SU(N_f)_R]/SU(N_f)_V$ . In line with (2.16), they gain the transformation properties

$$\xi_L(\phi) \xrightarrow{g} g_L \xi_L(\phi) h^\dagger(\xi(\phi), g), \quad \xi_R(\phi) \xrightarrow{g} g_R \xi_R(\phi) h^\dagger(\xi(\phi), g). \quad (2.19)$$

The compensating transformation  $h(\xi(\phi), g)$  is the same in both cases, since  $H$  is invariant under a parity transformation that interchanges  $L$  and  $R$ .

---

<sup>4</sup>That is, the NLSM for the chiral symmetry group  $G = SU(N_f)_L \times SU(N_f)_R$ . From now on, we will mostly focus on the chiral NLSM, and therefore drop the qualifier and simply call it “the NLSM”.

Without loss of generality, we may choose  $\xi_R(\phi) = \xi_L^\dagger(\phi) = u(\phi)$ . A highly convenient parametrisation of  $u$  in terms of  $\phi$  is

$$u(\phi) = \exp\left(\frac{i\Phi(\phi)}{F\sqrt{2}}\right), \quad \Phi(\phi) = \frac{t^a \phi^a}{\sqrt{\tau}} \quad (2.20)$$

with the flavour index with  $a$  running from 1 to  $N_f^2 - 1$ . Here,  $t^a$  are the generators of  $SU(N_f)$ ,  $F$  is an overall scale, and the factor of  $\sqrt{2}$  is conventional. The above expression for  $u(\phi)$  is only one of many possible ways to parametrise the field; for a discussion on alternative parametrisations, see section 4.1.

We now desire to determine the most general Lagrangian consistent with the chiral symmetry. However,  $u$  still transforms with the nontrivial  $h(u(\phi), g)$ . An object with simpler transformation properties is

$$U = u^2 = \exp\left(\frac{i\sqrt{2}\Phi}{F}\right), \quad U \xrightarrow{g} g_R U g_L^\dagger, \quad (2.21)$$

(we drop the explicit dependence on  $\phi$  from now on) which generalises the  $U$  we defined in (2.8). This field serves as a good building block for the Lagrangian, since  $\langle \mathcal{O}_1 U^\dagger \mathcal{O}_2 U \dots \rangle$  will be invariant under chiral transformations as long as  $\mathcal{O}_i$  are operators such that  $\mathcal{O}_i U^{(\dagger)}$  transform the same way as  $U^{(\dagger)}$ . For the NLSM, the simplest examples are 1 and  $\partial_\mu$ .

The construction of the Lagrangian is not entirely unconstrained. Lorentz invariance dictates that the number of derivatives must be even, and parity requires the number of  $U$ 's to be even as well. Thanks to the unitarity of  $U$ , we only need to consider Lagrangian terms with purely derivative couplings, since we can use the identity

$$0 = \partial_\mu(U^\dagger U) = \partial_\mu U^\dagger U + U^\dagger \partial_\mu U \quad (2.22)$$

to move all derivative-less  $U$ 's together so that  $U^\dagger U = 1$  can be used to eliminate them. With higher derivatives present, derivatives of (2.22) supply the necessary identities.

Instead of building the Lagrangian from  $U, U^\dagger$  and their derivatives, we will employ an alternative basis introduced in [15] and used in e.g. [14]. It is less straightforward in its definition, but is more readable and, most importantly, generalises more readily to full  $\chi$ PT; see section 7.1. The basis replaces  $U^{(\dagger)}$  with the building block

$$u_\mu = i(u^\dagger \partial_\mu u - u \partial_\mu u^\dagger), \quad u_\mu \xrightarrow{g} h(u, g) u_\mu h(u, g)^\dagger, \quad (2.23)$$

which includes the obligatory first derivative. Higher derivatives are applied through the covariant derivative

$$\nabla_\mu X = \partial_\mu X + [\Gamma_\mu, X], \quad \Gamma_\mu = \frac{1}{2}(u^\dagger \partial_\mu u + u \partial_\mu u^\dagger), \quad (2.24)$$

which again is defined to make generalisation to  $\chi$ PT easier. It has the properties that  $\nabla_\mu X$  transforms the same way as  $X$ , and that

$$\nabla_\mu u_\nu - \nabla_\nu u_\mu = 0 \quad (2.25)$$

just as for plain second derivatives.

When no higher derivatives are present, it is easy to convert between the building blocks. Firstly, unitarity and (2.22) gives

$$\partial_\mu U^\dagger \partial_\nu U = -(U^\dagger \partial_\mu U)(U^\dagger \partial_\nu U), \quad (2.26)$$

and furthermore, using (2.22) and (2.23),

$$U^\dagger \partial_\mu U = u^\dagger u^\dagger \partial_\mu u u - \partial_\mu u^\dagger u = -i u^\dagger u_\mu u. \quad (2.27)$$

This makes  $U^\dagger \partial_\mu U$  wholly interchangeable with  $-i u_\mu$  as long as a trace is present to eliminate the excess  $u$ 's and  $u^\dagger$ 's. When higher derivatives are included, the translation is not as directly obvious, and we will keep to the  $u_\mu$  basis alone.

### 2.4.1 The lowest-order Lagrangian terms

With the above definitions, the simplest valid term in the NLSM Lagrangian is

$$\mathcal{L}_2 = \frac{F^2}{4} \langle \partial_\mu U^\dagger \partial^\mu U \rangle = \frac{F^2}{4} \langle u_\mu u^\mu \rangle, \quad (2.28)$$

where the constant in front is chosen such that the first term in the expansion in terms of  $\phi^a$  becomes the canonical kinetic term  $\frac{1}{2} \partial_\mu \phi^a \partial^\mu \phi^a$ . We recognise this from (2.10); this is the universal lowest-order NLSM term.

Beyond this first term, there is an infinite sequence of increasingly complex terms permitted by the symmetries.<sup>5</sup> These can be organised into a hierarchy based on power counting, using the momentum scale  $p$  of whatever process is studied with the model. Since each derivative in the Lagrangian brings down one factor of  $p$  into an amplitude, both  $u_\mu$ ,  $\partial_\mu$  and  $\nabla_\mu$  are  $\mathcal{O}(p)$ , whereas  $U^{(\dagger)}$  alone contributes nothing to the power counting. Thus, we may split the Lagrangian as

$$\mathcal{L} = \sum_{n=1}^{\infty} \mathcal{L}_{2n}, \quad (2.29)$$

where  $\mathcal{L}_{2n}$  is  $\mathcal{O}(p^{2n})$  and contains  $2n$  derivatives carrying  $n$  pairs of Lorentz indices. Assuming a low momentum scale, we may then ignore all terms above a certain  $n$ .

The four-derivative  $\mathcal{O}(p^4)$  Lagrangian is, for general  $N_f$  [4, 5, 16],

$$\mathcal{L}_4 = L_0 \langle u_\mu u_\nu u^\mu u^\nu \rangle + L_1 \langle u_\mu u^\mu \rangle \langle u_\nu u^\nu \rangle + L_2 \langle u_\mu u_\nu \rangle \langle u^\mu u^\nu \rangle + L_3 \langle u_\mu u^\mu u_\nu u^\nu \rangle. \quad (2.30)$$

We use the more readable  $u_\mu$  basis from here on. The  $L_i$  are independent coupling constants, so-called low-energy constants (LECs). By comparing with (2.12), we see that the LSM gives  $L_1 = v^2/8M^2$  and  $L_0 = L_2 = L_3 = 0$ . It is in principle possible to derive the LECs from any underlying theory (e.g. QCD), but in practice, they are unknown parameters that must be measured by experiments or lattice simulations.

---

<sup>5</sup>Many authors refer to  $\mathcal{L}_2$  as the full Lagrangian of the NLSM. We instead use “the NLSM” to refer to the more general version, which includes all permitted terms.

### 2.4.2 The Cayley-Hamilton theorem

$\mathcal{L}_4$  presents the first case in which effects of finite  $N_f$  changes the number of independent Lagrangian terms. These effects manifest themselves through the Cayley-Hamilton theorem, which states that for any  $N_f \times N_f$  matrix  $M$ , the characteristic polynomial

$$p(\lambda) = \det(\lambda \mathbb{1} - M), \quad (2.31)$$

which is zero whenever  $\lambda$  is an eigenvalue of  $M$ , also satisfies  $p(M) = 0$  when viewed as a matrix polynomial. For a traceless  $N_f = 2$  matrix, the characteristic polynomial is  $p(M) = M^2 - \frac{1}{2}\langle M^2 \rangle$ , and if expanded as  $M = A + B$  (with  $A$  and  $B$  traceless), we get

$$0 = A^2 + \{A, B\} + B^2 - \frac{1}{2}\langle A^2 + \{A, B\} + B^2 \rangle \Rightarrow \{A, B\} = \langle AB \rangle, \quad (2.32)$$

where we use the fact that  $A$  and  $B$  satisfy their own characteristic polynomials. With a traceless  $3 \times 3$  matrix  $M = A + B + C$ , a similar process yields

$$\sum_{\text{permutations of } \{ABC\}} \langle ABCD \rangle = \sum_{\text{cyclic permutations of } \{ABC\}} \langle AB \rangle \langle CD \rangle \quad (2.33)$$

after multiplying by a fourth matrix  $D$  and taking the trace.

In the context of this Lagrangian, we may choose  $A = C = u_\mu$  and  $B = D = u_\nu$ ; these are traceless as a consequence of the identity  $\partial_\mu \det(A) = \det(A) \langle A^{-1} \partial_\mu A \rangle$ , which holds for any invertible matrix  $A$ , and which reduces to  $\langle A^\dagger \partial_\mu A \rangle = 0$  when  $A \in SU(N_f)$ . In the  $N_f = 3$  case, this use of the Cayley-Hamilton theorem gives one linear relation between the terms of  $\mathcal{L}_4$ , so one term (historically,  $L_0$ ) may be eliminated. In the  $N_f = 2$  case, we may eliminate two terms. Many terms can be eliminated from higher-order Lagrangians using these identities.<sup>6</sup>

### 2.4.3 Higher-order Lagrangian terms

The explicitly known Lagrangian of  $\chi$ PT (and therefore, the NLSM) also includes  $\mathcal{L}_6$  [16] and  $\mathcal{L}_8$  [14], but the number of terms grows extremely rapidly, so a simple listing such as (2.30), or even a tabulation of the terms, becomes rather difficult to overview. Instead, we can look at the more basic ingredients of a Lagrangian term: a pattern of pairwise contracted Lorentz indices, and a pattern of how they are placed inside traces.

To represent such patterns in a neat fashion, we will use a graphical notation known as *chord diagrams*.<sup>7</sup> A chord diagram is defined as  $2n$  points on a circle, with  $n$  chords

<sup>6</sup>A less-studied effect is how the finite dimension  $D$  of spacetime limits the number of independent terms. For instance, with  $D = 1$ ,  $u_\mu u^\mu u_\nu u^\nu = u_\mu u_\nu u^\mu u^\nu = u_0 u_0 u_0 u_0$ , so the  $\mathcal{O}(p^4)$  Lagrangian has 2 independent terms, not 4. It is easy to check that  $D = 2$  imposes similar restrictions at  $\mathcal{O}(p^6)$ . In general, terms are removed by the Schouten identity  $(\epsilon^{\mu\nu\rho\cdots} u_\mu u_\nu u_\rho \cdots)^2 = 0$ , which holds whenever the Levi-Civita tensor  $\epsilon^{\mu\nu\rho\cdots}$  carries more than  $D$  indices. Therefore, it gives additional linear relations in the  $\mathcal{O}(p^{2D+2})$  Lagrangian, so the physically relevant  $D = 4$  does not affect any of the Lagrangians used in this work.

<sup>7</sup>Chord diagrams are familiar in mathematics, but do not appear to have been used in the present context before. See [17] for a counting formula and generation algorithms for chord diagrams.

connecting the points pairwise so that each point is connected to exactly one chord. For our purposes, we will generalise these diagrams in several ways.

Lorentz index patterns naturally map to chord diagrams: the  $2n$  indices correspond to the points in cyclic order, and the  $n$  contractions correspond to the chords. This captures the freedom to relabel dummy indices (all chords look the same) and the cyclicity of the trace (the circle is round). Compared to directly handling the indices, such a diagram provides a very clear view of the distinct patterns; consider, for instance,

$$\langle u^\mu u^\nu u^\rho u_\mu u^\sigma u_\nu u_\rho u_\sigma \rangle = \text{Diagram} \left( \text{more explicitly, } \begin{array}{c} \rho \quad \nu \quad \mu \\ \mu \quad \sigma \\ \sigma \quad \nu \quad \rho \end{array} \right) \quad (2.34)$$

which is a complicated Lorentz index pattern but a simple chord diagram.

Trace patterns can be represented in a visually compatible fashion by using chords that have been generalised to connect more than two points. Each point is still connected to exactly one generalised chord, and cyclicity applies within each generalised chord rather than to the circle as a whole. To capture the fact that traces commute, we can require the generalised chords to be noncrossing and sorted by size around the circle. Any Lagrangian term with no higher derivatives can then be created by overlaying an index pattern with a trace pattern. Thus, the terms of  $\mathcal{L}_2$  in (2.28) and  $\mathcal{L}_4$  in (2.30) can be represented as

$$\frac{F^2}{4} \text{Diagram}, \quad L_0 \text{Diagram}, \quad L_1 \text{Diagram}, \quad L_2 \text{Diagram} = L_2 \text{Diagram}, \quad L_3 \text{Diagram}, \quad (2.35)$$

where the grey blobs represent the generalised chords of the trace patterns. The cyclicity of the traces can be used in different ways; for instance,  $L_2$  can be made to look more analogous to  $L_1$  (left) or  $L_0$  (right) depending on which is considered clearer. At higher orders, such display choices get quite involved.

At  $\mathcal{O}(p^6)$  and above, additional covariant derivatives can not be avoided, but representing them is easy: allow each point to connect to more than one chord. With a 1-chord point representing  $u_\mu$ , a 2-chord point represents  $\nabla_\mu u_\nu$ , and so on. Due to (2.25), it does not matter which chord is which.<sup>8</sup> For instance, the first term in the  $\mathcal{O}(p^6)$  Lagrangian (see table 1) is

$$L_{6,1} \langle u_\mu \nabla_\nu u_\rho \rangle \langle u^\mu \nabla^\rho u^\nu \rangle = L_{6,1} \text{Diagram} = L_{6,1} \text{Diagram}, \quad (2.36)$$

where we use the notation  $L_{m,n}$  to denote the  $n$ th LEC in the  $\mathcal{O}(p^m)$  Lagrangian.

Using this notation, the 19-term  $\mathcal{O}(p^6)$  Lagrangian and the 135-term  $\mathcal{O}(p^8)$  Lagrangian are presented in tables 1 and 2, respectively. The  $\mathcal{O}(p^8)$  Lagrangian is taken directly as the NLSM subset of the full  $\chi$ PT Lagrangian presented in [14], and uses the same numbering of the terms. The  $\mathcal{O}(p^6)$  Lagrangian is similarly taken from unpublished work done in conjunction with [14]. The older published version [16] yields redundant terms when naïvely constrained to the NLSM, and uses a less convenient notation.

<sup>8</sup>With more than one covariant derivative, the commutator  $[\nabla_\mu, \nabla_\nu]u_\rho$  is nonzero, but can be absorbed into other Lagrangian terms. Therefore, the indices remain interchangeable for our purposes.

| $\mathcal{O}(p^6)$ | 0 | 1 | 2 | 3 | 4 | 5 | 6 | 7 | 8 | 9 |
|--------------------|---|---|---|---|---|---|---|---|---|---|
| 0                  |   |   |   |   |   |   |   |   |   |   |
| 10                 |   |   |   |   |   |   |   |   |   |   |

Table 1: The terms of the  $\mathcal{O}(p^6)$  NLSM Lagrangian  $\mathcal{L}_6$ , represented as generalised chord diagrams. Each diagram is associated with a LEC  $L_{6,r+c}$ , where  $r$  and  $c$  are its row and column labels, respectively. An asterisk (\*) next to a diagram indicates that it is asymmetric, and that the full Lagrangian term is the sum of the diagram and its mirror image, which is not included. A number (2 or 3) next to a diagram indicates the lowest  $N_f$  at which it is kept in the Lagrangian. At  $N_f = 3$  or  $N_f = 2$ , all terms with higher number, or no number at all, are eliminated through the Cayley-Hamilton relations; see section 2.4.2. The choice of which terms to keep follows that made in [14].

| $\mathcal{O}(p^8)$ | 0 | 1 | 2 | 3 | 4 | 5 | 6 | 7 | 8 | 9 |
|--------------------|---|---|---|---|---|---|---|---|---|---|
| 0                  |   |   |   |   |   |   |   |   |   |   |
| 10                 |   |   |   |   |   |   |   |   |   |   |
| 20                 |   |   |   |   |   |   |   |   |   |   |
| 30                 |   |   |   |   |   |   |   |   |   |   |
| 40                 |   |   |   |   |   |   |   |   |   |   |
| 50                 |   |   |   |   |   |   |   |   |   |   |
| 60                 |   |   |   |   |   |   |   |   |   |   |
| 70                 |   |   |   |   |   |   |   |   |   |   |
| 80                 |   |   |   |   |   |   |   |   |   |   |
| 90                 |   |   |   |   |   |   |   |   |   |   |
| 100                |   |   |   |   |   |   |   |   |   |   |
| 110                |   |   |   |   |   |   |   |   |   |   |
| 120                |   |   |   |   |   |   |   |   |   |   |
| 130                |   |   |   |   |   |   |   |   |   |   |

Table 2: The terms of the  $\mathcal{O}(p^8)$  NLSM Lagrangian  $\mathcal{L}_8$ , represented as generalised chord diagrams. Each diagram is associated with a LEC  $L_{8,r+c}$ , where  $r$  and  $c$  are its row and column labels, respectively. See table 1 for further details on the presentations.



Several new features show up at these orders. Most importantly, some terms are not PT invariant, so they must be added to their PT conjugate to form a valid term. PT invariance maps directly to mirror symmetry of the chord diagrams. In the tables, an attempt has been made to display symmetric diagrams in such a way that they also look symmetric, although with more complicated trace structures, this is not always possible.

### 3 Flavour-ordering

With the structure of the NLSM established, we are ready to use it for perturbative calculations of scattering amplitudes. However, the infinite number of interaction terms requires the use of some scheme for restricting it to a manageable subset. Even then, the resulting vertex factors are very intricate, both in their dependence on the particle momenta, and in their group-algebraic structure. This leaves only the simplest Feynman diagrams tractable by hand, and even computer algebra becomes highly time-consuming when tackling more complicated cases directly.

In this section, we will direct much effort towards the development of simpler ways to perform these calculations. As we will see, the group-algebraic structure of the flavour indices carried by the particles can be used to condense an amplitude into a much more easily manageable expression, for which simpler calculation rules exist. We will mostly follow the derivation of  $\mathcal{O}(p^2)$  flavour-ordering as presented in [6], but insert the notation to support our own generalisations to higher-order vertices.

#### 3.1 Some notation

In this section, we will write many expressions such as  $\langle t^{a_1} t^{a_3} \rangle \langle t^{a_2} t^{a_4} \rangle$ . Since these describe how the flavour indices of particles are combined via group algebra, we will call them *flavour structures*. In order to make them both more readable and easier to formalise, we will introduce some shorthand notation. Firstly, we will often omit the  $t$ 's and write the indices directly inside the traces:  $\langle a_1 a_3 \rangle \langle a_2 a_4 \rangle$  means the same as  $\langle t^{a_1} t^{a_3} \rangle \langle t^{a_2} t^{a_4} \rangle$ . We will use the symbol  $\mathcal{F}_\sigma(r_1, r_2, \dots, r_k)$  for a general flavour structure split into  $k$  traces with  $r_1, r_2, \dots$  flavour indices each. Here,  $\sigma \in \mathcal{S}_n$  is a permutation of  $\{1, 2, \dots, n\}$  that describes the order in which the indices appear. For example,  $\langle a_1 a_3 \rangle \langle a_2 a_4 \rangle = \mathcal{F}_{1324}(2, 2)$ , and  $\langle a_1 a_2 \dots a_n \rangle = \mathcal{F}_{\text{id}}(n)$ , where  $\text{id}(i) = i$  is the identity permutation. In general,

$$\mathcal{F}_\sigma(r_1, r_2, \dots, r_k) = \langle a_{\sigma(1)} \dots a_{\sigma(r_1)} \rangle \langle a_{\sigma(r_1+1)} \dots a_{\sigma(r_1+r_2)} \rangle \dots \langle a_{\sigma(r_1+\dots+r_{k-1}+1)} \dots a_{\sigma(r_1+\dots+r_k)} \rangle. \quad (3.1)$$

For easier handling, we may encapsulate the arguments  $r_i$  of  $\mathcal{F}_\sigma$  as a *flavour splitting*  $R = \{r_1, r_2, \dots, r_{|R|}\}$ , and write  $\mathcal{F}_\sigma(R)$  rather than  $\mathcal{F}_\sigma(r_1, \dots)$ . For a structure with  $n$  indices, we impose the restrictions

$$\sum_{i=1}^{|R|} r_i = n, \quad r_1 \leq r_2 \leq \dots \leq r_{|R|}. \quad (3.2)$$

The second can be imposed without loss of generality, since the traces commute.

Lastly, we see that the cyclicity of a trace makes  $\mathcal{F}_\sigma(n)$  invariant when  $\sigma$  is changed by a cyclic permutation. Therefore, we can restrict  $\sigma$  to be in  $\mathcal{S}_n/\mathbb{Z}_n$  rather than the full group of permutations. Similarly, we define  $\mathbb{Z}_R$  to be the group of permutations that leave  $\mathcal{F}_\sigma(R)$  invariant. This includes cyclic permutations within each individual trace, but when several traces are the same size, it also includes reordering of the traces, i.e. swapping blocks of indices. For instance,

$$\begin{aligned}\mathbb{Z}_{\{2,2\}} &= \{12\ 34, 21\ 34, 12\ 43, 21\ 43, 34\ 12, 43\ 12, 34\ 21, 43\ 21\}, \\ \mathbb{Z}_{\{2,4\}} &= \{12\ 3456, 21\ 3456, 12\ 4563, 21\ 4563, 12\ 5634, 21\ 5634, 12\ 6345, 21\ 6345\},\end{aligned}\tag{3.3}$$

where we have inserted spaces between blocks of indices corresponding to different traces.<sup>9</sup>

In this notation, we can also generalise the notion of two permutations being equivalent modulo a cyclic permutation: we write  $\sigma \equiv \rho \pmod{\mathbb{Z}_R}$  if  $\mathcal{F}_\sigma(R) = \mathcal{F}_\rho(R)$ . For instance,  $1234 \equiv 2341 \pmod{\mathbb{Z}_{\{4\}}}$  and  $1234 \equiv 2134 \pmod{\mathbb{Z}_{\{2,2\}}}$ , but not vice versa.

## 3.2 NLSM vertices

Let us now look at how the NLSM Lagrangian produces vertices and amplitudes. When expanded in terms of  $\phi$ , e.g.

$$\mathcal{L}_2 = \frac{1}{2} \langle t^a t^b \rangle \partial_\mu \phi^a \partial^\mu \phi^b + \frac{1}{F^2} \langle t^a t^b t^c t^d \rangle \left( \frac{1}{6} \phi^a \partial_\mu \phi^b \phi^c \partial^\mu \phi^d - \frac{1}{12} \phi^a \phi^b \partial_\mu \phi^c \partial^\mu \phi^d \right) + \dots,\tag{3.4}$$

each term in the Lagrangian produces an infinite series of interaction terms, each with some combinatorial coefficient. If the term contains several traces, like for  $L_1$  and  $L_2$  from  $\mathcal{L}_4$  in (2.30), the flavour indices will be distributed between the traces in several ways for each term.

By parity, only terms with an even number of particles are allowed, as can be easily verified by examining the expansion of  $\partial_\mu U^\dagger \partial_\nu U$ , in which the odd powers of  $\phi$  vanish.<sup>10</sup>

---

<sup>9</sup>As can be seen by considering compositions of its elements,  $\mathbb{Z}_{\{2,2\}}$  is isomorphic to the dihedral group  $D_4$ . Other  $\mathbb{Z}_R$  are not isomorphic to named groups, but  $\mathbb{Z}_{\{2,4\}} \simeq \mathbb{Z}_2 \times \mathbb{Z}_4$ , and in general,  $\mathbb{Z}_R \simeq \mathbb{Z}_{r_1} \times \mathbb{Z}_{r_2} \times \dots$  whenever all  $r_i$  are different. When some  $r_i$  are equal (say,  $m$  in a row), the group will be non-abelian and isomorphic to a semidirect product, e.g.  $\mathbb{Z}_{\{2,2,2\}} \simeq (\mathbb{Z}_2 \times \mathbb{Z}_2 \times \mathbb{Z}_2) \rtimes \mathcal{S}_3$ . In general,  $\mathbb{Z}_R \simeq (\mathbb{Z}_{r_1} \times \mathbb{Z}_{r_2} \times \dots) \rtimes (\mathcal{S}_{m_1} \times \mathcal{S}_{m_2} \times \dots)$ , where each  $m_j$  is the length of a stretch of equal  $r_i$ . The proof follows from the following definition of the semidirect product: if a group  $G$  has a subgroup  $H$  and a normal subgroup  $N$ , then  $G = N \rtimes H$  if  $G = \{nh \mid n \in N, h \in H\}$  and  $N \cap H = \{e\}$ , with  $e$  being the identity element. The groups  $N \simeq (\mathbb{Z}_{r_1} \times \dots)$  of cyclings within traces and  $H \simeq (\mathcal{S}_{m_1} \times \dots)$  of swaps of equal-size traces are clearly subgroups of  $G = \mathbb{Z}_R$ , and  $N$  is normal since  $gng^{-1} \in N$  for any  $n \in N$ ,  $g \in G$  — any trace swaps in  $g$  are cancelled by  $g^{-1}$ , leaving only cyclings. Any permutation in  $\mathbb{Z}_R$  is the composition of a cycling and a trace swap, and the only element shared by  $N$  and  $H$  is id, which completes the proof.

<sup>10</sup>It is possible to make additions to NLSM (or, more generally,  $\chi$ PT) that include an odd number of  $U$ 's contracted with an odd-parity Levi-Civita symbol. This is the so-called Wess-Zumino-Witten term [18, 19]. For an introduction in the context of  $\chi$ PT, see [13, section 7], and for the EFT point of view, see [20].

For the same reason, split-trace terms such as  $L_1$  only ever allocate an even number of indices to each trace, so it results in flavour splittings like  $\{2, 2\}$  and  $\{2, 4\}$ , but never  $\{3, 3\}$ . This is broken at higher orders, since  $\mathcal{L}_6$  and above contains terms with an odd number of  $u_\mu$ 's in each trace. Therefore,  $\mathcal{O}(p^6)$  interaction terms (for instance, the ones connected to  $L_{6,1}$ ) may be split  $\{3, 3\}$ .

The interaction terms quickly grow complicated and opaque, and listing even the simpler vertex factors of the NLSM is a rather futile exercise. Instead, we organise the inventory of vertices by only looking at their power-counting orders and flavour splittings. Thus, the  $1/F^2$  term in (3.4) makes up the  $\mathcal{O}(p^2)$   $\{4\}$ -vertex, and the  $\mathcal{O}(p^4)$   $\{2, 2\}$ -vertex contains contributions from both  $L_1$  and  $L_2$ . By bundling different interaction terms based on these properties, we greatly simplify the palette with which we later draw Feynman diagrams.

### 3.3 Stripped vertex factors

Equipped with these notions and notations, we can express the  $n$ -particle vertex factor of order  $\mathcal{O}(p^N)$  and flavour splitting  $R$  as

$$\mathcal{V}_{N,R}^{a_1 a_2 \dots a_n}(p_1, p_2, \dots, p_n) = \sum_{\sigma \in \mathcal{S}_n / \mathbb{Z}_R} \mathcal{F}_\sigma(R) \mathcal{V}_{N,R,\sigma}(p_1, p_2, \dots, p_n), \quad (3.5)$$

where the  $a$ 's and  $p$ 's are the flavour indices and momenta of the particles interacting through the vertex, and  $\mathcal{V}_{N,R,\sigma}$  contains whatever kinematic factors come attached to that specific flavour structure. Here and in all other places, we treat all momenta as ingoing. Since  $\mathcal{F}_\sigma(R)$  is invariant under  $\mathbb{Z}_R$ , the kinematic factors must also have this symmetry, i.e.

$$\mathcal{V}_{N,R,\sigma}(p_1, p_2, \dots, p_n) = \mathcal{V}_{N,R,\sigma}(p_{\rho(1)}, p_{\rho(2)}, \dots, p_{\rho(n)}) \quad (3.6)$$

for any  $\rho \in \mathbb{Z}_R$ . Also, Bose symmetry implies that the act of rearranging the legs of the vertex by any permutation  $\rho \in \mathcal{S}_n$  must have the effect

$$\mathcal{V}_{N,R,\sigma \circ \rho}(p_1, p_2, \dots, p_n) = \mathcal{V}_{N,R,\sigma}(p_{\rho(1)}, p_{\rho(2)}, \dots, p_{\rho(n)}), \quad (3.7)$$

where  $\circ$  denotes composition of permutations. A special case of this is

$$\mathcal{V}_{N,R,\sigma}(p_1, p_2, \dots, p_n) = \mathcal{V}_{N,R}(p_{\sigma(1)}, p_{\sigma(2)}, \dots, p_{\sigma(n)}), \quad (3.8)$$

where  $\mathcal{V}_{N,R} = \mathcal{V}_{N,R,\text{id}}$  is called a *stripped* vertex factor, since it contains the same information as the full vertex, but in a smaller format with the flavour structure stripped away.<sup>11</sup> It can be “dressed” into a full vertex factor by the simple act of multiplying by  $\mathcal{F}_{\text{id}}(R)$  and then summing over all  $\sigma \in \mathcal{S}_n / \mathbb{Z}_R$ .

A stripped vertex factor has the property of being *flavour-ordered*, since it is the kinematic factor attached to  $\mathcal{F}_{\text{id}}(R)$ , where all flavour indices are sorted in ascending order.

---

<sup>11</sup>The word “stripped” is typical in the context of EFTs. For the analogous concept in perturbative QCD (where “flavour” is replaced by “colour”), the word “primitive” is used instead; see e.g. [11, 12]. In older literature, the word “dual” is common.

Thanks to this, its explicit form can be derived by expanding the relevant Lagrangian terms and discarding all terms where any flavour index appears out of order. This saves a significant amount of work for the more complicated vertices.

Stripped vertices serve as the first ingredient in the method we are developing. In the following sections, we will treat diagrams and amplitudes along the same lines.

### 3.4 Constructing diagrams

Like the vertices, we may organise the diagrams by their power-counting order and flavour structure. The order can be determined by using Weinberg’s power-counting formula,

$$D = 2 + 2L + \sum_d (d - 2)N_d, \quad (3.9)$$

which states that a diagram containing  $L$  loops and  $N_d$   $\mathcal{O}(p^d)$  vertices is  $\mathcal{O}(p^D)$  overall. Due to the form  $(d - 2)$ , any number of  $\mathcal{O}(p^2)$  vertices, and therefore any number of legs, may be added to a diagram without changing the overall power. To construct higher-order diagrams, a vertex may be “upgraded” by 2 orders of momenta, or a loop may be added, both of which increase  $D$  by 2. Therefore, tree-level  $\mathcal{O}(p^4)$  diagrams may contain a single  $\mathcal{O}(p^4)$  vertex, while  $\mathcal{O}(p^6)$  tree-level diagrams may contain one  $\mathcal{O}(p^6)$  vertex or two  $\mathcal{O}(p^4)$  vertices, and so on.

As for the vertex factors, the flavour structure provides a useful handle to the kinematic and combinatorial intricacies of a diagram. The NLSM Feynman rule for a propagator with momentum  $q$  has the simple form

$$\begin{array}{c} q \\ \hline a \qquad b \end{array} = \frac{i\delta^{ab}}{q^2 + i\epsilon}, \quad (3.10)$$

so when two  $\phi$ ’s are Wick contracted together to form a propagator, their corresponding flavour indices are also contracted by the Kronecker delta. Therefore, we need a contraction identity for traces of generators, which for  $SU(N_f)$  is

$$\frac{1}{\tau} \langle X t^a \rangle \langle t^a Y \rangle = \langle XY \rangle - \frac{1}{N_f} \langle X \rangle \langle Y \rangle \quad (3.11)$$

for arbitrary  $X$  and  $Y$  (see appendix A for a derivation). This is perhaps the most important identity in this work, so for future reference, we will name its terms. For reasons that will become apparent in section 3.6, we will call the first term on the right-hand side the *multiplet term*, and the second one the *singlet term*. Importantly, (3.11) is only valid for  $SU(N_f)$ ; for  $U(N_f)$ , the corresponding identity only contains the multiplet term. For other groups, the analogous identity may be greatly different or not exist at all.

The identity (3.11) describes the effect on the flavour structures when two vertices or sub-diagrams are joined at tree level by a propagator. The multiplet term concatenates the structures inside the traces, but the singlet term keeps the traces split. Therefore,

we would guess that the amplitude represented by a  $SU(N_f)$  NLSM Feynman diagram contains traces split in very many ways, both due to vertices with split traces, and because of the singlet term.

There also exists an alternative version of (3.11) that covers contractions inside a trace:

$$\frac{1}{\tau} \langle X t^a Y t^a \rangle = \langle X \rangle \langle Y \rangle - \frac{1}{N_f} \langle XY \rangle. \quad (3.12)$$

Like (3.11), the  $U(N_f)$  analogue only uses the first term. In the context of diagrams, it only comes into play when loops are included, but it is useful in other ways; see e.g. appendix B.

### 3.5 Flavour-ordered diagrams

Even the simplest scattering amplitudes in the NLSM are quite lengthy, and even with the aid of computer algebra, they quickly grow unmanageable at higher orders and more legs. The complications mainly come from the fact that for each diagram topology, there are many different permutations of internal and external particles that contribute to the amplitude. Therefore, our main goal should be to reduce the number of permutations that are counted.

In a manner similar to (3.5), we may write the  $\mathcal{O}(p^N)$   $n$ -particle amplitude as

$$\mathcal{M}_{N,n}^{a_1 a_2 \dots a_n}(p_1, p_2, \dots, p_n) = \sum_{R \in \mathcal{R}(N,n)} \sum_{\sigma \in \mathcal{S}_n / \mathbb{Z}_R} \mathcal{F}_\sigma(R) \mathcal{M}_{N,R,\sigma}(p_1, p_2, \dots, p_n), \quad (3.13)$$

where  $\mathcal{M}_{N,R,\sigma}$  carries all kinematic factors, and  $\mathcal{R}(N,n)$  contains all flavour splittings that contribute to the amplitude.

Now, the same arguments that allowed us to define the stripped vertex factor in section 3.3 allows us to define the *stripped amplitude*  $\mathcal{M}_{N,R}$  with the property

$$\mathcal{M}_{N,R,\sigma}(p_1, p_2, \dots, p_n) = \mathcal{M}_{N,R}(p_{\sigma(1)}, p_{\sigma(2)}, \dots, p_{\sigma(n)}). \quad (3.14)$$

It is sufficient to compute the stripped amplitude, since plugging it into

$$\mathcal{M}_{N,n}^{a_1 a_2 \dots a_n}(p_1, p_2, \dots, p_n) = \sum_{R \in \mathcal{R}(N,n)} \sum_{\sigma \in \mathcal{S}_n / \mathbb{Z}_R} \mathcal{F}_\sigma(R) \mathcal{M}_{N,R}(p_{\sigma(1)}, p_{\sigma(2)}, \dots, p_{\sigma(n)}) \quad (3.15)$$

to get the full amplitude is a straightforward operation.

The stripped amplitude offers quite a lot of simplification for any group, but with  $SU(N_f)$  or  $U(N_f)$ , it makes an enormous difference. Since the stripped amplitude is the kinematic factor associated with  $\mathcal{F}_{\text{id}}(R)$ , it is flavour-ordered. The amplitude is built from vertex factors via the contraction identity (3.11), which preserves the flavour-ordering of  $X$  and  $Y$ . Therefore, the stripped amplitude only gets contributions from flavour-ordered vertex factors, and exactly all diagrams constructed from flavour-ordered vertex factors

contribute to the stripped amplitude. Such flavour-ordered diagrams are quite intuitive to construct; for 4, 6 and 8 particles at  $\mathcal{O}(p^2)$  with single-trace flavour structures, they are

$$(3.16)$$

respectively. In each diagram, each leg should be seen as equipped with a label  $i$ , indicating flavour index  $a_i$  and ingoing momentum  $p_i$ . Flavour-ordering corresponds to having the labels in cyclic order around the diagram. Since a labeling is not unique, each diagram should be summed over all cyclically ordered labelings that give *distinct* kinematic factors. For instance, the second 6-point diagram above should be seen as the sum of

$$(3.17)$$

Labeling clockwise or counterclockwise is a matter of convention. These three labelings obviously give distinct kinematic factors, since they result in propagator momenta  $(p_1 + p_2 + p_3)^2$ ,  $(p_2 + p_3 + p_4)^2$ , and  $(p_3 + p_4 + p_5)^2$ , respectively. Due to the symmetry of the diagram, the remaining three cyclic permutations are not distinct from these three (remember that with all momenta ingoing,  $\sum_i p_i = 0$  due to conservation of momentum), so they should not be counted. All other labelings fail to be flavour-ordered, and can be ignored.

Stripped vertex factors are completely symmetric under cyclings by virtue of (3.6), so single-vertex diagrams always have only one distinct labeling. Therefore, the 4-point diagram and the first 6-point diagram in (3.16) should not be summed over other labelings. The 8-point diagrams have 1, 8, 4, and 8 distinct labelings, respectively, as can be seen from their symmetry. Note that the last two 8-point diagrams are topologically the same if viewed as ordinary Feynman diagrams, but must be treated as different for the purposes of flavour-ordering, and have different symmetry properties. This is a general tradeoff: each diagram becomes simpler to evaluate, but the number of topologies becomes larger.

Above  $\mathcal{O}(p^2)$ , we begin to encounter flavour-split vertices, but they can be integrated into the flavour-ordering routine. We still label the legs according to the identity permutation, but instead of summing over cyclic permutations, we sum over  $\mathbb{Z}_R$ , and once again only consider distinct labelings.

At higher orders, we also need to distinguish vertices of different order, which is done by attaching a number to all vertices above  $\mathcal{O}(p^2)$ . In order to distinguish vertices with split flavour structures, we leave a gap in the vertex, so that each contiguous piece of a diagram resides in a single trace. For instance, the 4-point  $\mathcal{O}(p^4)$  diagrams are

$$(3.18)$$

for  $R = \{4\}$  and  $R = \{2, 2\}$ , respectively. Neither diagram has more than one distinct labeling, since they contain only a single vertex each. The four lines in the right diagram

are still kinematically connected, but are separated flavour-wise. Since there is a direct correspondence between traces in a flavour structure and flavour-separated pieces of a diagram, we will simply refer to the pieces as *traces*.

Some adjustment to the intuition is needed when handling split diagrams. Since  $\langle X \rangle \langle Y \rangle = \langle Y \rangle \langle X \rangle$ , the traces may “float” around the diagram. For instance,

(3.19)

are the same. By our conventions, the distinct labelings of the above diagram are

(3.20)

Labels 1 and 2 are applied to the smaller trace (as per (3.2)), and no cycling is needed due to the symmetry of the vertex. Labels 3456 must be summed over all four cyclings, since each cycling gives a different propagator. No other labeling is considered flavour-ordered; in particular,

(3.21)

which would be valid on a single-trace diagram, should not be counted, since it has flavour structure  $\mathcal{F}_{\text{id}}(4, 2)$  in disagreement with (3.2). Including it would be double-counting, since it is obtained from (3.20) via a permutation in  $\mathcal{S}_6/\mathbb{Z}_{\{2,4\}}$  when executing (3.15).

Interesting structures sometimes show up. For instance, the two  $\mathcal{O}(p^4)$  diagrams

(3.22)

emerge from different orientations of the same three vertices, but have completely different properties. In the first diagram, the smaller trace should not be cycled at all, and the larger trace only halfway, since it is symmetric (compare to the  $\mathcal{O}(p^2)$  6-point diagram). In the second diagram, all  $4 \cdot 4$  combined cyclings of the two traces are distinct, but due to the symmetry of the diagram, swapping them, e.g.

(3.23)

does not produce a distinct kinematic structure and should not be counted.

In the  $\mathcal{O}(p^6)$  diagrams

(3.24)

the other component of  $\mathbb{Z}_R$ , swapping of equal-size traces, does play a role. In the first diagram, we may place either 12 or 34 in the trace straddling the propagator, and we must sum over both placements. In addition to that, we must sum over cyclings of the trace that straddles the propagator, but not the other two, again due to the symmetry of the vertices. In the second diagram, the two smaller traces are equivalent under the  $\mathbb{Z}_{\{2,2,2\}}$  symmetry of the vertex, and we should not sum over both ways of placing the labels 12 and 34.

### 3.6 The singlet problem and its solution

The construction of flavour-ordered diagrams hinges heavily on the use of (3.11), or specifically the multiplet term,  $\langle XY \rangle$ . The singlet term,  $\langle X \rangle \langle Y \rangle / N_f$ , is problematic, since it is invariant under different permutations. Consider the diagrams

$$(3.25)$$

The first two have the same flavour structure (i.e.  $\langle 123456 \rangle$ ) under the multiplet term, but not under the singlet ( $\langle 123 \rangle \langle 456 \rangle$  and  $\langle 234 \rangle \langle 561 \rangle$ , respectively). On the other hand, the first and the last diagrams have the same flavour structure (i.e.  $\langle 123 \rangle \langle 456 \rangle$ ) under the singlet, but not the multiplet (the last diagram has  $\langle 312645 \rangle$ ). In fact, the last diagram should not really be regarded as flavour-ordered, since the flavour indices appear out of order. This different treatment of the two terms is a serious threat to the methods we are trying to develop.

There is, however, an elegant solution. As stated previously, the singlet term in (3.11), which has the potential of breaking flavour-ordering, is not present in  $U(N_f)$ . Therefore, in the  $U(N_f)$  NLSM we may always do flavour-ordering at any order in the Lagrangian. We can extend this to  $SU(N_f)$  by taking advantage of its similarity to  $U(N_f)$ .

Remember (see appendix A) that the  $U(N_f)$  algebra differs from the  $SU(N_f)$  algebra by a non-traceless generator  $t^0$  that commutes with all other generators. Due to the latter property, its associated field  $\phi^0$  forms a  $U(1)$  singlet separate from the  $SU(N_f)$  multiplet  $\phi^a$ . With this in mind, a more elucidating form of (3.11) is

$$\sum_{a=1}^{N_f^2-1} \langle X t^a \rangle \langle t^a Y \rangle = \sum_{a=0}^{N_f^2-1} \langle X t^a \rangle \langle t^a Y \rangle - \langle X t^0 \rangle \langle t^0 Y \rangle, \quad (3.26)$$

where we temporarily suppress Einstein summation. This expression suggests that a  $SU(N_f)$  propagator (left) represents a  $U(N_f)$  propagator (right) minus the singlet propagator, and explains our naming of the terms. The  $N_f^{-1}$  is absorbed into  $t^0$ .

Now, if we extend our Lagrangian-building field like

$$\hat{\Phi}(\phi^0, \phi) = \frac{t^0 \phi^0}{\sqrt{\tau}} + \Phi(\phi), \quad \hat{U}(\phi^0, \phi) = \exp\left(\frac{i\hat{\Phi}\sqrt{2}}{F}\right) = \exp\left(\frac{i\phi^0 t^0}{F} \sqrt{\frac{2}{\tau}}\right) U(\phi), \quad (3.27)$$



where  $U(\phi) \in SU(N_f)$  and  $\hat{U}(\phi^0, \phi) \in U(N_f)$ , we see that

$$\hat{U}^\dagger \partial_\mu \hat{U} = \left( \frac{i\sqrt{2}}{F\sqrt{N_f}} \right) \partial_\mu \phi^0 + U^\dagger \partial_\mu U \quad (3.28)$$

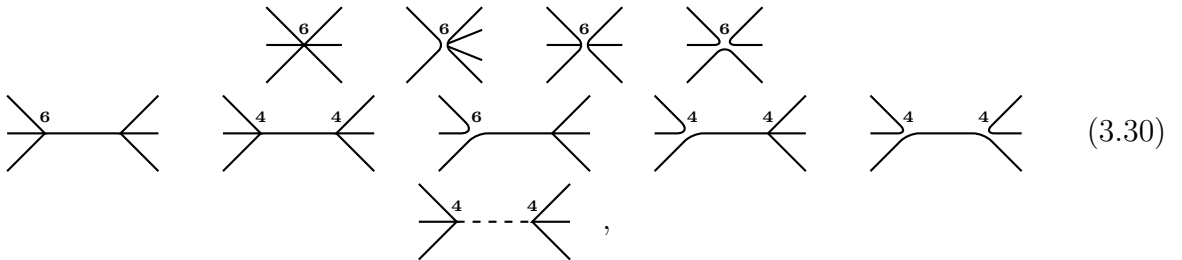
(remembering that  $U^\dagger \partial_\mu U$  is equivalent to  $u_\mu$ ), and therefore

$$\hat{\mathcal{L}}_2 = \frac{1}{2} \partial_\mu \phi^0 \partial^\mu \phi^0 + \frac{F^2}{4} \langle u_\mu u^\mu \rangle. \quad (3.29)$$

At this order, the singlet decouples from the other fields and forms a free theory. Therefore, no  $\mathcal{O}(p^2)$  vertex involves the singlet, so there is no distinction between  $U(N_f)$  and  $SU(N_f)$  amplitudes at this order, and we may ignore the singlet term in (3.11).

This observation was sufficient in [6], but we must handle the singlet problem beyond  $\mathcal{O}(p^2)$ . At higher orders, this decoupling does not happen, and indeed  $\mathcal{L}_4$  and all higher-order Lagrangians introduce vertices that mix the singlet with the other particles. However, a singlet propagator can only exist if both vertices at its ends couples to it. Since this requires at least two vertices of at least  $\mathcal{O}(p^4)$ , the diagram as a whole must be at least  $\mathcal{O}(p^6)$  to include such complications.<sup>12,13</sup> Therefore, we can flavour-order at  $\mathcal{O}(p^4)$  with no other complications than the introduction of split vertices.

At  $\mathcal{O}(p^6)$  and above, we can at last not avoid the singlet term in (3.11) in  $SU(N_f)$ , but the interpretation of (3.26) still holds. In order to build a  $SU(N_f)$  amplitude, we first work in  $U(N_f)$  to build flavour-ordered diagrams using only the multiplet term. Then, we construct all diagrams with singlet propagators in a similar fashion, maintaining flavour-ordering independently. For instance, the full suite of  $\mathcal{O}(p^6)$  6-point diagrams is



including one singlet propagator, indicated by a dashed line. It implicitly includes a factor of  $-N_f^{-1}$ , and its flavour structure is split  $\{3, 3\}$  over the propagator, in accordance with the behaviour of the singlet term. All cyclings of the two traces should be counted as distinct, since the vertices are invariant under  $\mathbb{Z}_4$ , not  $\mathbb{Z}_3$ .

<sup>12</sup>If the singlet forms a loop, only one  $\mathcal{O}(p^4)$  vertex is necessary, but the loop itself increases the power counting, so  $\mathcal{O}(p^6)$  is needed in this case as well.

<sup>13</sup>An interesting parallel can be seen in [11], where  $U(1)$  gluons similar to our singlets must be introduced in perturbative QCD. While our singlets only emerge with at least two higher-order vertices, their  $U(1)$  gluons cancel unless the diagram contains at least two quark lines. In general, there are several intriguing analogies between the inclusion of quark lines in gluon scattering (where there are no higher-order vertices) and the inclusion of higher-order vertices in the NLSM (where there are no quark lines).

Once all diagrams are listed, we add the singlet diagrams to the rest, and arrive at the stripped  $SU(N_f)$  amplitude. By keeping the singlet diagrams independent from the others, we avoid any issues with mismatched flavour-ordering. We can be sure that the full amplitude will be the same as if we had constructed it directly without flavour-ordering thanks to the uniqueness of stripped amplitudes, which we will prove below.

### 3.7 Uniqueness of stripped amplitudes

Above, we have blindly trusted the definition of the stripped amplitude as everything that comes attached to the flavour-ordered structure  $\mathcal{F}_{\text{id}}(R)$ . It is this that allows us to treat the singlet diagrams as diagrams in its own right, and not as order-breaking corrections. If the stripped amplitude could not be uniquely constructed from this definition, our methods would break down. However, we can show that the stripped amplitude is indeed unique, using a generalisation of a method presented by [21] and adapted to flavour-ordering by [6]. Therefore, we can be sure that our methods are correct.

The uniqueness hinges on an orthogonality relation that reads

$$\mathcal{F}_\sigma(Q) \cdot [\mathcal{F}_\rho(R)]^* = \tau^n N_f^{n-2} (N_f^2 - 1) \begin{cases} 1 + \mathcal{O}(N_f^{-2}) & \text{if } Q = R \text{ and } \sigma \equiv \rho \pmod{\mathbb{Z}_R}, \\ \mathcal{O}(N_f^{-\gamma}) & \text{otherwise } (\gamma \geq 1; \text{ see below}) \end{cases} \quad (3.31)$$

using the notation defined in section 3.1. The dot in the left-hand side indicates contraction over all flavour indices. If  $Q \neq R$ ,  $\gamma \geq 1$ , and if  $\sigma \not\equiv \rho \pmod{\mathbb{Z}_R}$ ,  $\gamma \geq 2$ ; therefore, the single-trace version (i.e. that given in [6]) has  $\mathcal{O}(N_f^{-2})$  as its second case. The more different the flavour structures are, the greater  $\gamma$  is.

The relation (3.31) is proven in appendix B and states that any given flavour structure  $\mathcal{F}_\sigma(Q)$  is orthogonal at leading order in  $N_f$  to all other flavour structures whose permutations are not equivalent to  $\sigma$ , or whose flavour splittings are not equal to  $Q$ . The more different the flavour structures are, the greater  $\gamma$  is. In the context of stripped amplitude uniqueness, it can be applied as follows. In analogy with (3.5) and (3.15), we write some arbitrary quantity  $\mathcal{X}$  in the form

$$\mathcal{X}^{a_1 \dots a_n} = \sum_{R \in \mathcal{R}} \sum_{\sigma \in \mathcal{S}_n / \mathbb{Z}_R} \mathcal{F}_\sigma(R) \mathcal{X}_{\sigma, R}, \quad (3.32)$$

where  $\mathcal{R}$  is some appropriate selection of flavour splits. Then, we use the orthogonality relation (3.31) to perform the projection

$$\mathcal{X}^{a_1 \dots a_n} [\mathcal{F}_{\text{id}}(R)]^* = \tau^n N_f^{n-2} (N_f^2 - 1) \left[ \mathcal{X}_{\text{id}, R} + \mathcal{O}\left(\frac{1}{N_f}\right) \right]. \quad (3.33)$$

This means that we can always project out the stripped  $\mathcal{X}$ , and that any overlap with other terms must come suppressed by at least  $N_f^{-1}$ . In a stripped amplitude of  $\mathcal{O}(p^4)$  or lower, the stripped amplitude can not contain any powers of  $N_f^{-1}$  due to the decoupling of the

singlet, so there can be no overlap for arbitrary  $N_f$ . This proves that stripped amplitudes are unique at  $\mathcal{O}(p^4)$  or below.

At higher orders, things are not as simple, since there are possibly many factors of  $N_f^{-1}$ . This would allow mixing between different stripped  $\mathcal{X}$ 's, threatening to break uniqueness. However, it can be resolved by expressing  $\mathcal{X}^{a_1 \cdots a_n}$  as a polynomial in  $N_f^{-1}$ ,

$$\mathcal{X}^{a_1 \cdots a_n} = \mathcal{X}_0^{a_1 \cdots a_n} + \frac{1}{N_f} \mathcal{X}_1^{a_1 \cdots a_n} + \frac{1}{N_f^2} \mathcal{X}_2^{a_1 \cdots a_n} + \dots \quad (3.34)$$

such that each  $\mathcal{X}_i^{a_1 \cdots a_n}$ , and therefore also its stripped counterpart, is independent of  $N_f^{-1}$ . We then apply the projection to each  $\mathcal{X}_i^{a_1 \cdots a_n}$  independently, and ignore the  $\mathcal{O}(N_f^{-1})$  completely. Thus, stripped amplitudes, vertex factors, and other analogous quantities are unique to all orders.<sup>14,15</sup>

This result has significant consequences. Most importantly, it guarantees the correctness of our method of flavour ordering with split traces and singlets: it provides *a* way to produce something with the properties of a stripped amplitude, so its result must in fact be *the* unique stripped amplitude. Also, uniqueness allows many properties of the full amplitude to carry over to the stripped amplitude, as is discussed below.

A second consequence is worthy of note. The full amplitude of some  $\mathcal{O}(p^N)$   $n$ -particle process is constructed from  $|\mathcal{R}(N, n)|$  different stripped amplitudes. When summed over permutations according to (3.15), the total number of flavour structures grows to

$$\mathcal{N}_{N,n} \sim \sum_{R \in \mathcal{R}(N,n)} \frac{|\mathcal{S}_n|}{|\mathbb{Z}_R|}, \quad (3.35)$$

which is a very rapidly growing number — even at  $\mathcal{O}(p^2)$ ,  $\mathcal{N}(2, n) \sim (n-1)!$ . Since the flavour structures are not truly orthogonal, the expression for the cross section of the process, proportional to  $\mathcal{M}_{N,n}^{a_1 \cdots a_n} [\mathcal{M}_{N,n}^{a_1 \cdots a_n}]^\dagger$ , grows in length as  $(\mathcal{N}_{N,n})^2$ . However, the expression for the cross section contracts the flavour structures as in (3.31), which suppresses products of non-equivalent flavour structures by a factor of  $N_f^{-1}$  for each difference (or  $N_f^{-2}$  in the single-trace case). Therefore, in the limit  $N_f \rightarrow \infty$ , flavour structures *are* orthogonal, and the cross section only grows as  $\mathcal{N}_{N,n}$ . Even with finite  $N_f$ , most cross-terms will be heavily suppressed, and can most likely be ignored.

## 4 NLSM amplitudes

Equipped with the tools of flavour-ordering, we can take on the computation of amplitudes in the NLSM. However, there exists more useful amplitude-related structure that is worthy of discussion. This section covers some of these topics.

<sup>14</sup>This uniqueness is of course only up to a permutation in  $\mathbb{Z}_R$ , but since we sum over those in the definition of the stripped quantity, they are unique for our purposes.

<sup>15</sup>The orthogonality may be broken if there are additional relations among the flavour structures, such as those given by the Cayley-Hamilton theorem at some fixed  $N_f$ . In practice, we must assume that such relations have been exhausted to simplify the Lagrangian, so that no further applications are possible.

## 4.1 Dependence on the parametrisation

When defining the NLSM, we used the exponential definition (2.20) of  $u(\phi)$ . However, this is not the only possible choice, since the equivalence theorem [26] guarantees that all amplitudes are invariant under a reparametrisation of the form

$$\phi^a \rightarrow \phi^a + F^a(\phi), \quad F^a = \mathcal{O}(\phi^2). \quad (4.1)$$

Equivalently, we can redefine  $u(\phi)$  in any desired way as long as the changes only occur at quadratic order and above. Since stripped amplitudes are unique, they must also be invariant under such reparametrisations. However, stripped vertex factors are not required to be invariant, since the full vertex factors are parametrisation-dependent.

A more general form of parametrisation is

$$u(\phi) = \sum_{k=0}^{\infty} a_k \left( \frac{i\Phi(\phi)}{F\sqrt{2}} \right)^k, \quad (4.2)$$

where  $a_0 = a_1 = 1$  to conform with (2.20) below quadratic order. In our context, three parametrisations are relevant:

- The *exponential parametrisation*, which corresponds to (2.20) and  $a_k = 1/k!$ . This is the “default” parametrisation and is useful for general proofs, such as that of singlet decoupling in section 3.6. On the other hand, the explicit stripped vertex factors and diagrams become more complicated than in the other parametrisations considered in this section.

As was proven in [27], the exponential parametrisation is the only one among the class (4.2) that is valid for the  $SU(N_f)$  NLSM at  $N_f > 2$ . We have no such restraints at  $N_f = 2$ , or at  $\mathcal{O}(p^4)$  or below, where amplitudes are identical with those of  $U(N_f)$ . There also exist valid parametrisations not in the form (4.2) (see e.g. [28]).

- The *Cayley parametrisation* [6], which uses a Cayley transform to map an antihermitian matrix (proportional to  $i\Phi$ ) to a special unitary matrix,  $u(\phi)$ . A convenient form is

$$u(\phi) = \frac{1 + \frac{x(\phi)}{2}}{1 - \frac{x(\phi)}{2}} \Leftrightarrow a_k = \frac{1}{2^{k-1}} \quad (4.3)$$

for  $k \geq 2$ , where  $x(\phi) = i\Phi(\phi)/F\sqrt{2}$ . Due to the simplicity of the  $a_k$ 's, the stripped vertex factors assume a very simple form. Many can be easily derived by hand, and there is a noticeable speedup even with computer algebra. However, the simplification disappears at the diagram level, where this parametrisation is on equal footing with the exponential.

- The *minimal parametrisation* [29], which corresponds to

$$u(\phi) = x(\phi) + \sqrt{1 + [x(\phi)]^2}, \quad \Leftrightarrow \quad a_{2k} = \frac{(-1)^{k+1}}{2^{2k-1}} C_{k-1}, \quad a_{2k+1} = 0 \quad (4.4)$$

for  $k > 1$ , where  $C_k$  are the Catalan numbers and  $x(\phi)$  is the same as for the Cayley parametrisation. This parametrisation has the peculiar property that at  $\mathcal{O}(p^2)$ , the vertex factors do not depend on whether their legs are on-shell or not. Therefore, there is no difference between an  $n$ -point vertex and an  $n$ -particle single-vertex diagram. This greatly simplifies the expressions at the diagram level, and there are fewer cancellations when diagrams are summed to form stripped amplitudes. In [6], it is used as the key to computing amplitudes through semi-on-shell recursion relations. However, its benefits appear to vanish at  $\mathcal{O}(p^4)$  or above, and it is entirely unusable in the cases where the exponential parametrisation is the only valid one.

## 4.2 Generalised Mandelstam invariants

At tree level, a general stripped amplitude will be a linear combination of rational functions of products of momenta. However, using momenta directly leads to cluttered expressions, and also obfuscates many consequences of on-shellness and conservation of momentum — for instance,  $(p_1 + p_2 + p_3)^2 = (p_4 + p_5 + p_6)^2$  is not at all obvious when the squares are expanded and intermixed with other terms.

The solution is to use a generalisation of Mandelstam invariants, which for 4-particle processes with all momenta ingoing are defined as

$$s = (p_1 + p_2)^2 = (p_3 + p_4)^2, \quad t = (p_1 + p_3)^2 = (p_2 + p_4)^2, \quad u = (p_2 + p_3)^2 = (p_4 + p_1)^2. \quad (4.5)$$

Since NLSM particles are massless,  $p_i^2 = 0$ , and we may simply write  $s = 2p_1 \cdot p_2$ , and so on. Due to this masslessness, the invariants also obey  $s + t + u = 0$ , so one is redundant and can be eliminated in terms of the others.

At higher orders, we similarly define generalised Mandelstam invariants

$$s_{ijk\dots} = (p_i + p_j + p_k + \dots)^2, \quad (4.6)$$

which are kinematic invariants just like the 4-particle ones. We seek a selection of Mandelstam invariants such that any product of momenta can be expressed as a linear combination of them — that is, a complete basis for the space of kinematic invariants. There are  $n(n+1)/2$  distinct products  $p_i \cdot p_j$  for an  $n$ -particle amplitude, but on-shellness removes the  $n$  products  $p_i \cdot p_i$ . Conservation of momentum allows one momentum to be eliminated in terms of the others, removing another  $n$  products. Thus, there are  $n(n-3)/2$  independent products of momenta. This number is consequently the dimension of a complete basis of Mandelstam invariants.

This counting of the number of invariants does not take the dimension  $D$  of spacetime into account. Since each new momentum adds only  $D - 1$  degrees of freedom (the  $-1$  being due to  $(p_i)^2 = 0$ ), the number of independent kinematic invariants can only grow as  $n(D - 1) \sim n$ , not  $n(n - 3)/2 \sim n^2$ , when  $n \gg D$ . The first such limitation enters at  $n = D + 2$ , when the Gram determinant becomes zero, adding an extra relation among

the Mandelstam invariants.<sup>16</sup> However, such finite-dimensional effects are algebraically very messy, so for practical purposes it is better to ignore them and construct Mandelstam invariants as if  $D \gg n$ .

For  $n$  momenta (restricting ourselves to even  $n$ ), we may derive a practical Mandelstam basis from the observation that

$$\begin{aligned}
2p_i \cdot p_{i+1} &= s_{i(i+1)}, \\
2p_i \cdot p_{i+2} &= s_{i(i+1)(i+2)} - s_{i(i+1)} - s_{(i+1)(i+2)}, \\
2p_i \cdot p_{i+3} &= s_{i(i+1)(i+2)(i+3)} - s_{i(i+1)(i+2)} - s_{(i+1)(i+2)(i+3)} + s_{(i+1)(i+2)}, \\
&\vdots \\
2p_i \cdot p_j &= s_{i\dots j} - s_{i\dots(j-1)} - s_{(i+1)\dots j} + s_{(i+1)\dots(j-1)}.
\end{aligned} \tag{4.7}$$

The principle is to take an invariant containing the desired product, subtract the unwanted cross-terms, and then add back the cross-terms that were subtracted twice. All terms on the right-hand side are generalised Mandelstam invariants with consecutive indices, and since this formula clearly allows description of all possible products of momenta, such invariants form a complete basis. With indices cycling around, i.e.  $p_{i-n} = p_i = p_{i+n} = \dots$ , we see that the distance between  $i$  and  $j$  never exceeds  $n/2$ , so we only need invariants with up to  $n/2$  indices. Furthermore, since conservation of momentum implies that

$$s_{i\dots(i+k-1)} = s_{(i+k)\dots(i-1)}, \tag{4.8}$$

we only need half the complete set of invariants with exactly  $n/2$  indices. With this approach, the  $n = 4$  basis is  $\mathcal{B}_{\{4\}} = \{s_{12}, s_{23}\} = \{s, u\}$ , and the  $n = 6$  basis is

$$\mathcal{B}_{\{6\}} = \{s_{12}, s_{23}, s_{34}, s_{45}, s_{56}, s_{61}, \quad s_{123}, s_{234}, s_{345}\}, \tag{4.9}$$

which is complete since, for instance,  $s_{456} = s_{123}$  by (4.8). In the general case, the basis is

$$\mathcal{B}_{\{n\}} = \{s_{12}, s_{23}, \dots, s_{n(n-1)}, s_{n1}, \quad s_{123}, s_{234}, \dots, s_{n12}, \quad \dots, \quad s_{12\dots(n/2)}, \dots, s_{(n/2-1)\dots(n-1)}\}. \tag{4.10}$$

This contains  $n/2 - 1$  sets of  $n$  invariants each, plus one set of  $n/2$  invariants, for a total of  $n(n-3)/2$ . Therefore, it is complete, but not overcomplete, for all even  $n$ .

Using any choice of Mandelstam basis has benefits over just using products of momenta, since on-shellness and conservation of momentum is automatically taken care of. However, the basis choice in (4.10) has the further benefit that  $P^2 \in \mathcal{B}_{\{n\}}$ , where  $P = p_i + p_{i+1} + \dots + p_{i+j}$  is the momentum of any propagator that appears in a flavour-ordered diagram with flavour split  $R = \{n\}$ . This means that denominators containing a sum will never appear in the corresponding stripped amplitudes, which greatly simplifies their algebraic handling. This property does not hold for most  $R \neq \{n\}$ .

---

<sup>16</sup>Remember that the Gram determinant is the determinant of the  $n \times n$  matrix whose element  $ij$  is  $p_i \cdot p_j$ . When  $n > D$ , any set of  $n$  momenta must be linearly dependent, causing the determinant to be zero. At  $n = D + 1$ , this linear dependence is just conservation of momentum, but at  $n \geq D + 2$ , it is an independent effect.

### 4.3 Reduced stripped amplitudes

While we are on the subject of Mandelstam invariants, let us discuss a bit on how the choice of basis affects the form of stripped amplitudes. As a consequence of invariance under  $\mathbb{Z}_R$ , any stripped amplitude can be written in the form

$$\mathcal{M}_{N,R}(p_1, \dots, p_n) = \sum_{\sigma \in \mathbb{Z}_R} \mathbf{m}_{N,R}(p_{\sigma(1)}, \dots, p_{\sigma(n)}) = \mathbf{m}_{N,R}(p_1, \dots, p_n) + [\mathbb{Z}_R], \quad (4.11)$$

where the second equality uses a shorthand for sums over  $\mathbb{Z}_R$ , generalising the familiar idiom “+cycl.”<sup>17</sup> Here,  $\mathbf{m}$  is some smaller expression, which we will dub the *reduced* stripped amplitude. In the simpler cases (see e.g. section 6.2), it is obvious what  $\mathbf{m}$  should be: (6.11) contains  $\mathcal{M}$ , and (6.12) contains  $\mathbf{m}$ . For more complicated amplitudes, writing  $\mathbf{m}$  rather than  $\mathcal{M}$  helps greatly with getting an overview of the amplitude.

Unlike the stripped amplitude,  $\mathbf{m}$  is not unique, and finding it can be difficult in the general case. It helps to decompose  $\mathcal{M}$  into terms of the form

$$\mathcal{M} = \sum_i \mathcal{T}_i, \quad \mathcal{T}_i = \frac{\beta_{i0} \Pi_{i0}}{\Pi_{i1} + \beta_{i2} \Pi_{i2} + \beta_{i3} \Pi_{i3} + \dots} \quad \text{or} \quad \mathcal{T}_i = \beta_{i0} \Pi_{i0}, \quad (4.12)$$

where  $\beta_{ij}$  are numbers and each  $\Pi_{ij}$  is a product of one or more Mandelstam invariants. This decomposition is unique if we require that there is no factor shared by all  $\Pi_{ij}$  in a term (the same condition on the  $\beta_{ij}$  is why we have eliminated  $\beta_{i1}$  in the denominator), and that  $\mathcal{T}_i \propto \mathcal{T}_j$  does not hold for any  $i, j$ . If we define a total ordering on the space of  $\Pi_{ij}$ , we can normalise the terms by requiring that  $\Pi_{i1} \leq \Pi_{i2} \leq \Pi_{i3} \leq \dots$ .<sup>18</sup>

Now, assume that we use some *closed* basis of Mandelstam invariants  $\hat{\mathcal{B}}_R$  with the property that, if we permute the momenta in any  $\Pi_{ij}$  with any  $\sigma \in \mathbb{Z}_R$ , the resulting expression is some other  $\Pi_{i'j'}$ . Then,  $\mathbb{Z}_R$  will map each  $\mathcal{T}_i$  in  $\mathcal{M}_{N,R}$  to some  $\mathcal{T}_{i'}$  also in  $\mathcal{M}_{N,R}$ . This divides the terms of  $\mathcal{M}_{N,R}$  into separate orbits under  $\mathbb{Z}_R$ , where the terms in each orbit map only to each other. Picking a single representative of each orbit then yields  $\mathbf{m}_{N,R}$ . One way to do this is to define a total ordering on the space of  $\mathcal{T}_i$ 's and pick the smallest term in each orbit.<sup>19</sup> This process yields essentially the same choice as if  $\mathbf{m}$  is found by hand, but can be automated and applied to much larger stripped amplitudes.

This process hinges entirely on the existence of the closed basis  $\hat{\mathcal{B}}_R$ . With  $R = \{n\}$ , the choice (4.10) is sufficient, since each of its elements map to a *single* other element under  $\mathbb{Z}_n$ . However, this does not hold if  $R \neq \{n\}$ , since e.g.  $s_{23} \rightarrow s_{13} = s_{123} - s_{12} - s_{23}$  under  $213456 \in \mathbb{Z}_{\{2,4\}}$ . This would map some  $\Pi_{ij}$  to a sum of several different  $\Pi$ 's, breaking the division into orbits.

<sup>17</sup>Remember that  $\mathbb{Z}_R$  is the group of permutations that leaves  $\mathcal{F}_\sigma(R)$  invariant; see section 3.

<sup>18</sup>This relation is of course not the same as the numerical less-than relation when the Mandelstam invariants are given fixed values, but should rather be something akin to lexicographic ordering, e.g.  $s_{12} < s_{23} < \dots < s_{345} < s_{12}^2 < s_{12}s_{23} < \dots$  for  $\mathcal{B}_{\{6\}}$ . In practice, we employ the internal ordering used by FORM; see section 5 for an introduction to our use of FORM.

<sup>19</sup>As with the  $\Pi_{ij}$ 's, we use FORM's internal ordering in practice.

It is not easy to find a basis that is closed under some given  $R$ . A start is to find a basis that contains all squared propagator momenta  $P^2$  admitted by the diagrams with that flavour structure, since the set of  $P^2$ 's is by construction closed under  $\mathbb{Z}_R$ . This also has the benefit that  $\beta_{ij} = 0$  for all  $j \geq 2$ . For  $R = \{2, 4\}$  and  $R = \{2, 2, 2\}$ , one easily finds

$$\begin{aligned}\mathcal{B}_{\{2,4\}} &= \{s_{123}, s_{124}, s_{125}, s_{126}, \quad s_{14}, s_{15}, s_{16}, s_{45}, s_{56}\}, \\ \mathcal{B}_{\{2,2,2\}} &= \{s_{123}, s_{124}, s_{125}, s_{126}, s_{156}, s_{134}, \quad s_{23}, s_{45}, s_{61}\},\end{aligned}\tag{4.13}$$

of which the first 4 and 6 elements, respectively, are the  $P^2$ 's, and the remaining ones are added to complete the basis. For  $R = \{3, 3\}$ , the only  $P^2$  is  $s_{123}$ , so  $\mathcal{B}_{\{3,3\}} = \mathcal{B}_{\{6\}}$  suffices. However, these are likely to be the only solutions — for  $R = \{2, 6\}$ , the set of  $P^2$ 's fails to be linearly independent, and for  $R = \{2, 2, 2, 2\}$ , there are 24 different  $P^2$ 's, which is more than the 20 dimensions of a Mandelstam basis for 8 particles.

Starting with  $\mathcal{B}_R$ , we have found closed bases  $\hat{\mathcal{B}}_R = \{t_1, \dots, t_9\}$  for  $R = \{2, 4\}$ ,  $\{3, 3\}$  and  $\{2, 2, 2\}$ , i.e. all 6-particle flavour structures. For the values of  $t_i$  and details on their derivation, see appendix D. We have not found any closed bases beyond these, but it is not ruled out that closed bases exist for  $\mathbb{Z}_{\{2,6\}}$  and beyond, since it is possible to use linear combinations of  $P^2$ 's even if the  $P^2$ 's themselves can not be used for basis elements.

## 4.4 Adler zeroes and soft limits

There exists a very general statement about the behaviour of a NLSM amplitude when one of the external momenta approaches the soft limit. For any effective field theory emerging from the spontaneous breaking of a global symmetry [22], it holds that

$$\lim_{\varepsilon \rightarrow 0} \mathcal{M}^{a_1 \dots a_n}(p_1, \dots, \varepsilon p_i, \dots, p_n) = 0,\tag{4.14}$$

for any  $i$ . Essentially, the amplitude vanishes whenever an external particle approaches the soft limit. This is known as the Adler zero, and can be proven non-perturbatively in a very general fashion, see e.g. [23]. More specifically, for a general EFT one can define

$$\mathcal{M}^{a_1 \dots a_n}(p_1, \dots, \varepsilon p_i, \dots, p_n) \sim \varepsilon^\sigma\tag{4.15}$$

as  $\varepsilon$  approaches zero. The value of  $\sigma > 0$  is known as the *soft degree*, and serves as a characteristic from which EFTs can be classified and even constructed [20, 24]. The NLSM has  $\sigma = 1$ , so its Adler zeroes are first-order zeroes.<sup>20</sup>

Due to the orthogonality of flavour structures and the uniqueness of stripped amplitudes, Adler zeroes may only exist in the full amplitude if they also exist, with the same soft degree, in the stripped amplitudes. Therefore, (4.14) and any statement relying on it can equally well be applied to the stripped amplitudes.

---

<sup>20</sup>This is not entirely true, as  $\mathcal{O}(p^N)$  4-point amplitudes (see section 6.1) have  $\sigma = N/2$ . However, the amplitude up to  $\mathcal{O}(p^N)$ , including all lower-order contributions, still has  $\sigma = 1$ . At 6-point and above,  $\sigma = 1$  holds order by order.



The presence of Adler zeroes has profound implications, since all amplitudes can in fact be derived from a few “seed” amplitudes using the knowledge about the soft degree (see section 4.5). However, it also has a more directly practical application. Since far from every term in the amplitude is proportional to  $p_i$ , the Adler zero must manifest itself through an intricate scheme of cancellations. Therefore, any error in the amplitude is extremely likely to break these cancellations, causing a finite right-hand side in (4.14). This fact is highly useful for validating the correctness of a complicated stripped amplitude.

Beside the Adler zeroes, there also exists identities for the case when two momenta are sent to zero at the same rate. In some cases, cancellations of the type  $\lim_{\varepsilon \rightarrow 0}(\varepsilon/\varepsilon) \neq 0$  may cause this *double soft limit* to be nonzero. For instance, the double-soft limit of the  $\mathcal{O}(p^2)$  6-point amplitude presented in (6.12) is

$$\lim_{\varepsilon \rightarrow 0} \mathcal{M}_{2,\{6\}}(\varepsilon p_1, \varepsilon p_2, p_3, \dots, p_6) = \frac{i}{4F^4} \left\{ s_{45} + s_{56} - \frac{s_{23}(s_{45} + s_{56})}{s_{123} - s_{12}} - \frac{s_{61}(s_{34} + s_{45})}{s_{612} - s_{12}} \right\}. \quad (4.16)$$

If  $\varepsilon$  is instead applied to  $p_1$  and  $p_3$ , or to  $p_1$  and  $p_4$ , the limit is zero. The right-hand side above contains several copies of  $s_{45} + s_{56}$  and  $s_{34} + s_{45}$ , which are equivalent forms of the kinematic factor in  $\mathcal{M}_{2,\{4\}}(p_3, \dots, p_6)$ , as is presented below in (6.1). In fact, it turns out that the double soft limit of any  $(n+2)$ -particle amplitude can be expressed in terms of  $n$ -particle amplitudes with the soft particles removed; for the NLSM, the specific form is

$$\lim_{\varepsilon \rightarrow 0} \mathcal{M}^{aba_1 \dots a_n}(\varepsilon p, \varepsilon q, p_1, \dots, p_n) = -\frac{\kappa^2}{4F^2} \sum_{i=1}^n f^{abc} f^{a_i dc} \frac{p_i \cdot (p - q)}{p_i \cdot (p + q)} \mathcal{M}^{a_1 \dots a_{(i-1)} da_{(i+1)} \dots a_n}(p_1, \dots, p_n). \quad (4.17)$$

This was conjectured in [25] and proven in [6]. Like the Adler zero, it can be projected to a relation for stripped amplitudes, although the projection is not entirely trivial. The result for single-trace flavour structures is given in [6]. We derive the counterpart for general flavour structures in appendix C, with the result being as follows. At any order  $N$  in the power counting and for any flavour split  $R \in \mathcal{R}(N, n+2)$ , the double soft limit

$$\lim_{\varepsilon \rightarrow 0} \mathcal{M}_{N,R}(p_1, \dots, p_{i-1}, \varepsilon p_i, \dots, \varepsilon p_j, p_{j+1}, \dots, p_{n+2}) \quad (4.18)$$

is zero unless one of the following conditions hold:

1. Indices  $i-1$ ,  $i$ ,  $j$  and  $j+1$  are consecutive and lie within the same trace.
2. There exists some permutation  $\rho \in \mathbb{Z}_R$  such that the above condition is satisfied by applying  $\rho$  to the indices and possibly swapping  $i$  and  $j$ .

If either condition holds, we can without loss of generality assume that the first condition

does, since  $\mathcal{M}_{N,R}$  is invariant under  $\mathbb{Z}_R$ . Under this assumption, the double soft limit is

$$\begin{aligned} & \lim_{\varepsilon \rightarrow 0} \mathcal{M}_{N,R}(p_1, \dots, \varepsilon p_i, \varepsilon p_j, \dots, p_{(n+2)}) \\ &= \frac{1}{4F^2} \left( \frac{p_{(j+1)} \cdot (p_i - p_j)}{p_{(j+1)} \cdot (p_i + p_j)} - \frac{p_{(i-1)} \cdot (p_i - p_j)}{p_{(i-1)} \cdot (p_i + p_j)} \right) \mathcal{M}_{N,R'}(p_1, \dots, p_{(i-1)}, p_{(j+1)}, \dots, p_{(n+2)}), \end{aligned} \quad (4.19)$$

where  $R' \in \mathcal{R}(N, n)$  is  $R$  with the location of the soft particles removed. The result, which generalises that given in [6], is quite remarkable: for properly chosen  $i, j$ , the double soft limit amounts to removing the soft particles from the amplitude and multiplying by a simple kinetic factor. The factor is similar to those that arise in IR divergences, which is understandable — both arise from propagators going on-shell in the soft (IR) limit.

## 4.5 Reconstruction from soft limits

The existence of Adler zeroes (see section 4.4) is not merely a convenient consequence of the NLSM symmetries. For a broad class of scalar EFTs, including the NLSM, the soft limit can be used as an *a priori* assumption from which the rest of the theory is derived [24].

The explicit construction of theories in this manner follows a program of recursion relations that allow more complex amplitudes to be built recursively from simpler ones. The original use of this was BCFW recursion [30, 31] in the context of gauge theories. An  $n$ -point amplitude, viewed as a function of the external momenta, is extended into the complex plane via the shift

$$p_j \rightarrow \hat{p}_j(z) = p_j + zq, \quad p_k \rightarrow \hat{p}_k(z) = p_k - zq \quad (4.20)$$

for some  $j, k$ , with  $q^2 = q \cdot p_j = q \cdot p_k = 0$  to respect on-shellness and conservation of momentum. All other momenta are left as-is:  $\hat{p}_i(z) = p_i$ ,  $i \neq j, k$ . At tree level, the amplitude is a rational function of the momenta, so the shifted amplitude  $\hat{\mathcal{M}}_n(z)$  is a meromorphic function of  $z$ . The physical amplitude is recovered as  $\hat{\mathcal{M}}_n(0)$ , and can be extracted as a residue of  $\hat{\mathcal{M}}_n(z)/z$  through an application of Cauchy's theorem:

$$\hat{\mathcal{M}}_n(0) = \frac{1}{2\pi i} \oint \frac{dz}{z} \hat{\mathcal{M}}_n(z) = - \sum_I \text{Res}_{z=z_I} \left( \frac{\hat{\mathcal{M}}_n(z)}{z} \right), \quad (4.21)$$

where the contour of integration is an infinitesimal circle around the origin, and  $z_I$  are the locations of the poles of  $\hat{\mathcal{M}}_n(z)$ . Since the denominators contained in  $\hat{\mathcal{M}}_n(z)$  consist of squared propagator momenta, all the poles of  $\hat{\mathcal{M}}_n(z)$  occur when some propagator goes on-shell. That is,

$$\hat{P}_I^2(z_I) = 0, \quad \hat{P}_I(z) = \sum_{i \in I} \hat{p}_i(z), \quad (4.22)$$

where  $I$  is the collection of particle indices on one side of a propagator, and  $z_I$  is defined by the above condition. All  $z_I$  are simple poles, so the residues are

$$- \text{Res}_{z=z_I} \left( \frac{\hat{\mathcal{M}}_n(z)}{z} \right) = \hat{\mathcal{M}}_{L_I}(z_I) \frac{1}{P_I^2(0)} \hat{\mathcal{M}}_{R_I}(z_I), \quad (4.23)$$

where  $\hat{\mathcal{M}}_{L_I}$  and  $\hat{\mathcal{M}}_{R_I}$  are the amplitudes corresponding to the sub-diagrams on the left- and right-hand side, respectively, of the propagator carrying  $\hat{P}_I$ . Since the propagator is on-shell, they are physical amplitudes with all external particles on-shell. They have at most  $n - 2$  external particles each, so (4.23) and (4.21) together give a recursion relation for an amplitude in terms of smaller amplitudes. This can be continued until some trivial single-vertex amplitude is reached.

The method described above does unfortunately not work for EFTs, since (4.21) relies on the assumption that  $\mathcal{M}_n(z) \rightarrow 0$  sufficiently fast as  $z \rightarrow \infty$ . This holds for e.g. gluon scattering, but EFT amplitudes scale as a positive power of the momentum, so BCFW recursion fails. In a sense, that is understandable: gluon amplitudes can be recursively built from three- and four-gluon vertices, but in an EFT,  $\mathcal{M}_n$  may contain an  $n$ -point vertex that is not described in terms of anything that is present in smaller amplitudes.

Despite the failure of BCFW recursion, it is possible to construct EFT amplitudes recursively by taking advantage of the information contained in the soft limit, as was first done in [32]. First, we define a different shift that preserves the soft limit,

$$p_i \rightarrow \hat{p}_i(z) = p_i(1 - za_i), \quad 1 \leq i \leq n, \quad (4.24)$$

where  $a_i$  are chosen to respect conservation of momentum, i.e.

$$\sum_{i=1}^n a_i p_i = 0. \quad (4.25)$$

For  $n \leq D$ , where  $D$  is the spacetime dimension, the momenta are linearly independent in general, and the only solution is  $a_i = 0$ . For  $n = D + 1$ , conservation of momentum constrains all  $a_i$  to be equal. Both these cases are useless for recursion, so we require  $n > D + 1$ . For a general set of  $p_i$ 's, the vector  $(a_1 a_2 \dots a_n)^T$  can be any vector in the null space of the matrix whose  $i$ th column is  $p_i$ .

The scaling chosen above has the property that

$$\hat{\mathcal{M}}_n(z) \sim (1 - za_i)^\sigma \quad \text{as } z \rightarrow 1/a_i, \quad (4.26)$$

with the soft degree  $\sigma$  defined in (4.15). We define the product of all such factors as

$$F_n(z) = \prod_{i=1}^n (1 - a_i z)^\sigma, \quad (4.27)$$

such that  $F_n(0) = 1$  and  $F_n(z) \sim z^{n\sigma}$  as  $z \rightarrow \infty$ . We can then apply (4.21) to  $\hat{\mathcal{M}}_n(z)/zF_n(z)$ , which has strongly suppressed large- $z$  behaviour. Also,  $F_n(z)$  is engineered specifically to have exactly the same zeroes as  $\hat{\mathcal{M}}_n(z)$ , so its presence in the denominator does not give any new poles. Therefore, all poles follow from propagators going on-shell at  $z = z_{I\pm}$ , where  $z_{I\pm}$  are the two roots of

$$P_I^2 - 2P_I \cdot Q_I z + Q_I^2 z^2 = 0, \quad P_I = \sum_{i \in I} p_i, \quad Q_I = \sum_{i \in I} a_i p_i. \quad (4.28)$$

With the necessary adjustments, [32] turns this into the recursion relation

$$\hat{\mathcal{M}}_n(0) = \sum_I \sum_{\pm} \left[ 1 - \frac{z_{I\pm}}{z_{I\mp}} \right]^{-1} \frac{\hat{\mathcal{M}}_{L_I}(z_{I\pm}) \hat{\mathcal{M}}_{R_I}(z_{I\pm})}{P_I^2 F_n(z_{I\pm})}. \quad (4.29)$$

This remarkable result implies that any amplitude where  $F_n(z)$  is sufficient to suppress the high- $z$  behaviour can be recursively constructed. The  $n$ -point vertices are not needed as input, but are fixed by the form of the lower-point vertices along with the soft limit.

The explicit calculation of amplitudes this way is unfortunately a nontrivial algebraic task, and is not as amenable to automation as our flavour-ordering methods. In [32], the  $\mathcal{O}(p^2)$  6-point NLSM amplitude is derived along with analogous results for some other EFTs. We have laboriously recreated the  $\mathcal{O}(p^4)$  6-point amplitude (presented in (6.16) and (6.17)) as well. Some additional related tools have been developed by [9], which allowed more convenient computation of the same results with these methods. Using a different kind of recursion that is constrained to  $\mathcal{O}(p^2)$ , [6] reached 10-point. There seem to be no results beyond this.

For the NLSM, the  $\mathcal{O}(p^6)$  6-point amplitude is not possible to construct recursively, since  $F_6(z) \sim z^6$  does not suppress enough. This construction must in fact be impossible, since several features (singlets and 15 of the terms in  $\mathcal{L}_6$ ) that have independent soft limits do not show up at 4-point. In general, the  $\mathcal{O}(p^N)$   $n$ -point amplitude is only constructible if  $N < \sigma n$ , and all lower-point amplitudes must be computed some other way.

## 5 Practical calculation methods

In the preceding sections, we have demonstrated and generalised methods for calculation of tree-level stripped amplitudes in the NLSM using flavour-ordered diagrams. While the methods offer significant simplifications compared to a brute-force diagrammatic approach, the computation of all but the simplest amplitudes requires algebra with expressions too large for human handling. Even handling with most computer algebra systems is hampered with long computation times and memory limitations.

In this work, the computations were successively handled by using FORM, whose ability to perform simple algebra on enormous expressions is well suited for this kind of problem.<sup>21</sup> In conjunction with this thesis, a library of FORM procedures was written that calculates stripped amplitudes using flavour-ordering, with support for vertices up to  $\mathcal{O}(p^8)$  by using the Lagrangian of [14]. The procedures take specifications of vertex factors and diagram structures as input, and allow checking of Adler zeroes among other things. More details are given in appendix E.

On its own, the FORM library requires manual input of all diagrams and vertices. As the order and number of legs increases, flavour-ordered diagrams rapidly grow numerous and complicated, so it is desirable to automate this tedious and error-prone process. However, it is difficult to find a computer-based representation that does not obscure the structure

---

<sup>21</sup>For information about FORM, see [www.nikhef.nl/~form](http://www.nikhef.nl/~form).

of a flavour-ordered diagram. For instance, a natural representation of a tree diagram is a tree, but even in

$$\begin{array}{c} \diagup \quad \diagdown \\ | \quad | \\ \diagdown \quad \diagup \end{array} \sim \begin{array}{c} \diagup \\ | \\ \diagdown \\ | \\ \diagup \end{array}, \quad (5.1)$$

the choice of one vertex as the root hides the symmetry of the diagram. These problems become worse for larger diagrams.

## 5.1 Diagrams as polygon partitions

A more fruitful approach, which is somewhat akin to the chord diagrams used in section 2.4.3, is to draw an  $n$ -leg diagram as a regular  $n$ -gon, with each edge of the polygon representing an external leg. The polygon can then be partitioned by straight, non-crossing lines, where each  $k$ -gon piece corresponds to a  $k$ -particle vertex, and pieces sharing an edge correspond to vertices connected by a propagator.<sup>22</sup> For instance,

$$\begin{array}{c} \diagup \quad \diagdown \\ | \quad | \\ \diagdown \quad \diagup \end{array} \sim \begin{array}{c} \diagup \quad \diagdown \\ | \quad | \\ \diagdown \quad \diagup \end{array}, \quad \begin{array}{c} \diagup \quad \diagdown \\ | \quad | \\ \diagdown \quad \diagup \end{array} \sim \begin{array}{c} \diagup \quad \diagdown \\ | \quad | \\ \diagdown \quad \diagup \end{array} \quad (5.2)$$

Any two partitions that represent the same diagram are equivalent under rotation, and any symmetry of the diagram is manifested as rotational symmetry of the partition. Most importantly, these properties readily translate into a computer-based representation, as we will see below. Before going into details, let us first cover the necessary generalisations for higher-order diagrams.

Since each piece of a partition corresponds to a vertex in a diagram, vertices of different orders can be represented as pieces of different colours. Here, we use white for  $\mathcal{O}(p^2)$  vertices and darker shades of grey for higher orders. For instance, the single-trace  $\mathcal{O}(p^6)$  6-point diagrams are

$$\begin{array}{c} \diagup \quad \diagdown \\ | \quad | \\ \diagdown \quad \diagup \end{array} \quad \begin{array}{c} \diagup \quad \diagdown \\ | \quad | \\ \diagdown \quad \diagup \end{array} \quad \begin{array}{c} \diagup \quad \diagdown \\ | \quad | \\ \diagdown \quad \diagup \end{array} \sim \begin{array}{c} \diagup \quad \diagdown \\ | \quad | \\ \diagdown \quad \diagup \end{array} \quad \begin{array}{c} \diagup \quad \diagdown \\ | \quad | \\ \diagdown \quad \diagup \end{array} \quad \begin{array}{c} \diagup \quad \diagdown \\ | \quad | \\ \diagdown \quad \diagup \end{array} \quad (5.3)$$

Flavour-split vertices can be introduced as a second partition within the pieces, with the new lines representing where the traces are separated. However, this interferes with the geometric view of symmetries and equivalent representations. A multi-trace partition should be imagined as “pulled apart” across the flavour splits, as in

$$\begin{array}{c} \diagup \quad \diagdown \\ | \quad | \\ \diagdown \quad \diagup \end{array} \sim \begin{array}{c} \diagup \quad \diagdown \\ | \quad | \\ \diagdown \quad \diagup \end{array} \rightarrow \begin{array}{c} \diagup \quad \diagdown \\ | \quad | \\ \diagdown \quad \diagup \end{array} \quad \begin{array}{c} \diagup \quad \diagdown \\ | \quad | \\ \diagdown \quad \diagup \end{array} \quad \begin{array}{c} \diagup \quad \diagdown \\ | \quad | \\ \diagdown \quad \diagup \end{array} \quad (5.4)$$

where the dotted lines represent flavour splits. In the view on the right, each trace has been pulled together across the split lines so that only propagators and external legs remain,

<sup>22</sup>If the diagram is thought of as a planar graph with external legs extending to infinity, the polygon partition is its graph dual.

resulting in several 2-gons that have to be drawn with curved lines. A geometric interpretation of the kinematic connection between the traces is hardly possible. With three or more traces in a single vertex, they must be allowed to commute, which is a rather un-geometric concept. Therefore, we keep the compact representation as a partitioned  $n$ -gon, from which the symmetries are still visible at least as well as in the diagram view.

Singlet propagators are more straightforwardly introduced by distinguishing certain lines that separate two pieces of at least  $\mathcal{O}(p^4)$ . Using a dashed line, we therefore have

$$\begin{array}{c} \diagup \\ \diagdown \end{array} \begin{array}{c} \diagdown \\ \diagup \end{array} \text{---} \text{---} \begin{array}{c} \diagdown \\ \diagup \end{array} \begin{array}{c} \diagup \\ \diagdown \end{array} \sim \text{hexagon with dashed line} \quad (5.5)$$

As is stated below (3.30), a singlet line removes any rotational symmetry held by the traces it connects.

## 5.2 Generating partitioned polygons

Partitions are generated by taking a blank  $n$ -gon and enumerating all distinct ways of dividing it with a line, giving all 2-piece partitions. Then, 3-piece partitions are generated by partitioning 2-piece partitions a second time, and so on until the list of partitions is exhaustive. Higher-order diagrams are generating by, for each new line, also enumerating all ways of redistributing the order of the partitioned piece. As an example, the three ways of adding a line to the following partition,

$$\text{shaded hexagon} \rightarrow \text{shaded hexagon with line} \text{, } \text{shaded hexagon with line} \text{, } \text{shaded hexagon with line} \text{, } \text{shaded hexagon with line} \text{, } \text{shaded hexagon with line} \text{, } \text{shaded hexagon with line} \text{, } \text{shaded hexagon with line} \text{, } \text{shaded hexagon with line} \text{, } \text{shaded hexagon with line} \text{, } \quad (5.6)$$

gives nine new partitions. The seventh is a duplicate of the fourth, and should be removed to avoid double-counting.

Flavour splits are generated by adding extra partitions inside the polygons, and care must be taken to only allow splits that are supported by the Lagrangian. Lastly, singlet propagators are easily generated by enumerating all ways to substitute one or more internal lines with special singlet lines, with the requirement that the line separates polygons that are at least  $\mathcal{O}(p^4)$ .

This procedure is guaranteed to generate all flavour-ordered diagrams, but will generate many duplicates. In order to avoid double-counting, the program must be able to tell when two partitions are equivalent. This can be achieved by reducing all partitions to a representation that is unique for each class of equivalent partitions, as is the focus of the next section.

## 5.3 A symmetry-respecting representation of partitions

As we will demonstrate below, all information contained in a partition, including kinematic connections between traces, can be encoded in its perimeter. The perimeter is circular,

which geometrically represents the cyclicity of flavour traces. For flavour-split diagrams, each trace gets its own circular parameter by pulling it apart in the manner of (5.4).

From these observations, we can develop a symmetry-respecting representation of partitions. To each corner of the perimeter, we assign some symbol that describes the information encoded in it. The entire perimeter of an  $n$ -gon partition can then be reduced to a string of  $n$  symbols. Cyclically shifting the string corresponds to rotating the partition, so all strings representing equivalent diagrams are cyclic shifts of each other. By defining a suitable ordering on the alphabet of such symbols, we can determine the *least cyclic shift* (LCS) of the string, i.e. the cyclic shift that makes the string “least” in the sense of lexicographic ordering. Then, all equivalent diagrams are reduced to the same string, making comparisons trivial. The computation of LCSs is a well-known problem with several efficient solutions such as Booth’s algorithm [33].

In order for such a representation to work, the assignment of symbols can not depend on the absolute position of any corner. For instance, if we label a corner “1” and state that it is connected to corner 4 with a line, the representation becomes worthless — an equivalent partition may label the corresponding corner “2” and say that it is connected to corner 5. If we instead drop the corner numbers and only state the relative distance — “this corner is connected to the corner 3 steps down the perimeter clockwise”, or “3” for short — we can represent all  $\mathcal{O}(p^2)$  partitions. For instance,

$$\begin{array}{c} 5 \\ \cdot \\ \cdot \\ \cdot \\ \cdot \\ \cdot \\ \cdot \\ 3 \end{array} \begin{array}{c} \cdot \\ \cdot \\ \cdot \\ \cdot \\ \cdot \\ \cdot \\ \cdot \\ \cdot \end{array} \begin{array}{c} \cdot \\ \cdot \\ \cdot \\ \cdot \\ \cdot \\ \cdot \\ \cdot \\ \cdot \end{array} \begin{array}{c} \cdot \\ \cdot \\ \cdot \\ \cdot \\ \cdot \\ \cdot \\ \cdot \\ \cdot \end{array} \rightarrow (\cdot \cdot 5 \cdot 3 \cdot \cdot 3, 5), \quad \begin{array}{c} \cdot \\ \cdot \\ \cdot \\ \cdot \\ \cdot \\ \cdot \\ \cdot \\ \cdot \end{array} \begin{array}{c} \cdot \\ \cdot \\ \cdot \\ \cdot \\ \cdot \\ \cdot \\ \cdot \\ \cdot \end{array} \begin{array}{c} \cdot \\ \cdot \\ \cdot \\ \cdot \\ \cdot \\ \cdot \\ \cdot \\ \cdot \end{array} \begin{array}{c} \cdot \\ \cdot \\ \cdot \\ \cdot \\ \cdot \\ \cdot \\ \cdot \\ \cdot \end{array} \rightarrow (\cdot \cdot 5 3 \cdot \cdot 5 3), \quad (5.7)$$

where the alphabet of symbols consists of (possibly empty) ordered sequences of line lengths, read counterclockwise. The obvious ordering for such an alphabet is lexicographic ordering of the sequences. The LCSs of the representations are shown. The second string is periodic, which stands in direct correspondence with the partition being symmetric. Note that each line is described twice, but that this redundancy is necessary — removing it would break the symmetry of many partitions.

For higher-order diagrams, additional information about order and flavour splits is needed. These are properties of vertices, and therefore of pieces of the partitions, but pieces can unambiguously be mapped onto lines: each line has exactly one piece to its left, in the direction it is drawn. This way, all pieces are described by at least one line, with the exception of 1-piece partitions. This case is easily covered by also counting the lines that make up the perimeter.

Flavour splits are, as mentioned above, best represented by separating the partition into traces and representing each one individually. For each vertex, we may then list the representations of all other traces connected to it. We may resolve the ambiguity created by the fact that traces commute by always sorting lists of representations lexicographically. However, we can not just cross-reference the representations to represent connections, since this would lead to reference loops that can be shown to make finding LCSs impossible for

sufficiently complex partitions. Instead, each vertex must maintain a “slave” copy of all traces connected to it. When a “slave” would list the connection back to its “master”, it instead inserts a dummy symbol with a fixed place in the lexicographic ordering, thereby removing all reference loops. The downside of this is that each trace is represented several times, once as a master and several times as the slave of other traces. However, this redundancy appears necessary.

The last thing to add is singlet propagators, which act as lines on the perimeter of a trace. The quality of being a singlet, as well as a reference to the trace it connects to, can simply be added to the list of properties of that line. With these rules in place, an illustrating example is given in figure 1.

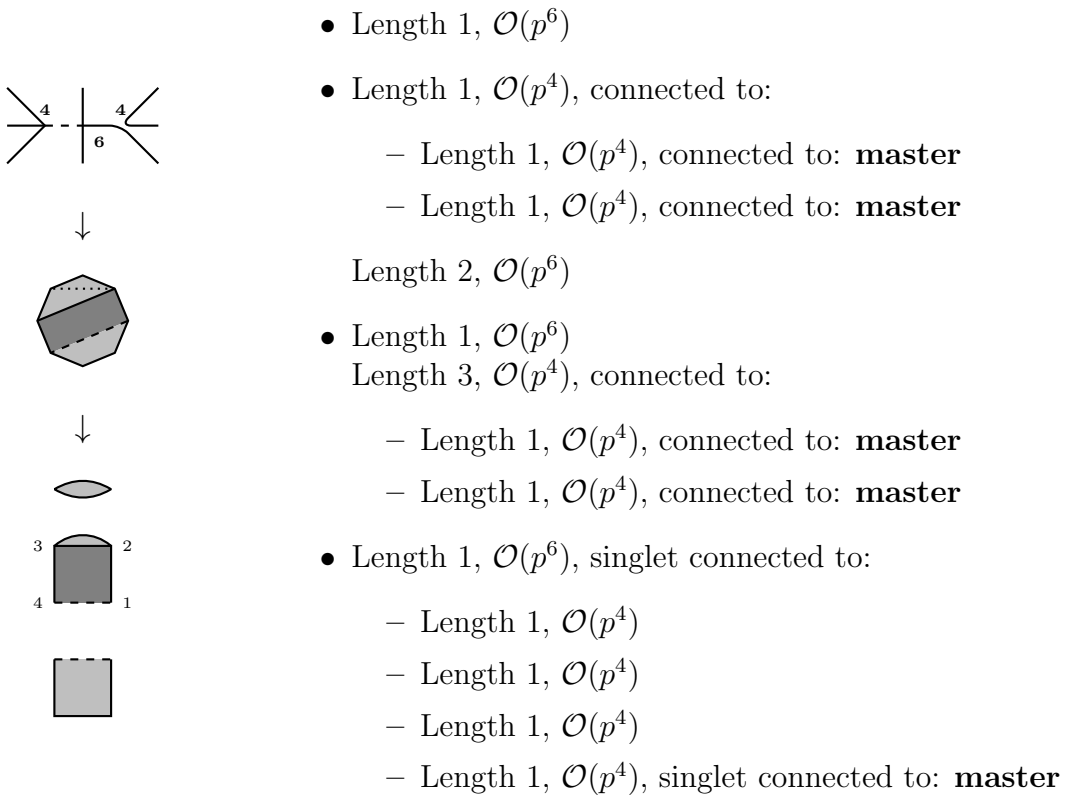


Figure 1: An  $\mathcal{O}(p^{10})$  diagram showcasing most features of flavour-ordered diagrams. The diagram is translated to a polygon partition, which is pulled apart into traces in the manner of (5.4). On the right, the LCS of the representation of the 4-trace is shown, with each bullet point being one symbol in the string. The trace is traversed in the order indicated by the numbers in the pulled-apart version of the partition. To find the LCS, the alphabet of symbols has been ordered by recursively applying lexicographic order to their subcomponents. Note how both the other traces appear as slaves least once.

With this representation defined, the method of generating flavour-ordered diagrams is completed. However, the most error-prone part of manually listing flavour-ordered diagrams is often the correct compensation for symmetries when applying  $\mathbb{Z}_R$ . At high orders,



many intricacies and caveats appear. An efficient solution to this issue is presented in the next section.

## 5.4 Determining diagram symmetries

As stated below (5.7), rotational symmetries of a diagram translates into periodicity in its representation. This holds also for the more detailed representation developed in the previous section — if it did not, the representation would not be valid. Therefore, the answer to the question “how many cyclic permutations should this trace be summed over?” is “the period of its representation”. This covers all the cycling rules described in section 3; specifically, any trace that is contained in a single vertex does not require cycling, since its string representation is always a repetition of a single symbol. The only exception is that the presence of a singlet breaks all cyclic symmetries of a trace, a rule which is easy to apply to the representation.

At a first look, symmetry under swapping equal-size traces appears equally straightforward: two traces are equivalent under swaps if and only if their representations are equal. Therefore, we should perform all swaps of traces that are equally large but not equivalent. Let us investigate this using the diagrams

$$\text{Diagram 1} \sim \text{12-gon} \quad \text{Diagram 2} \sim \text{12-gon} \quad \text{Diagram 3} \sim \text{12-gon} . \quad (5.8)$$

In the first diagram, the rule works correctly: the 2-traces are identical, and are not swapped. In the second diagram, the 2-traces “see” different mirror images of the non-symmetric 4-trace, and are therefore considered inequivalent, prompting a correct swap. In the third diagram, the 4-trace is symmetric, so the 2-traces end up identical. This gives symmetry under swapping the 2-traces, and a separate symmetry under cycling of the symmetric 4-trace, but this is wrong — we only have symmetry under both operations combined. If we were to blindly trust the symmetry of the representation, we would have

$$\text{Diagram 1} \equiv \text{Diagram 2} \equiv \text{Diagram 3} \equiv \text{Diagram 4} , \quad (5.9)$$

while only the first and the last labeling are actually equivalent. More such problems emerge in

$$\text{Diagram 1} \sim \text{12-gon} \quad \text{Diagram 2} \sim \text{12-gon} , \quad (5.10)$$

where we have distorted the 12-gon partition to make it more readable. The first diagram has four 2-traces, which we have labeled for the purposes of this example. The representation suggests symmetries under exchange of trace I and IV, and under exchange of

II and III, while the diagram is in fact only symmetric under both exchanges performed together. In the second diagram, the 4-trace has period 1 and all 2-traces are identical, but the diagram is only symmetric under cycling of the 4-trace combined with a similar cyclic permutation of the 2-traces.

These problems have a common cause: since traces are unlabeled, equivalent traces are seen as freely interchangeable, so we fail to recognise that we often need both a cycling and a swap to arrive at an equivalent labeling. The solution is the following rule: Whenever a symmetry relies on the equivalence of two or more traces, that equivalence shall not be used for any other symmetry. By further adding that cyclic symmetries are determined before swapping symmetries, all the above problems, and most likely all other problems of the same kind, are solved. The cyclicity of the 4-traces in (5.8-5.10) rely on the equivalence of the 2-traces, so the excessive swapping symmetry is removed. In the first diagram of (5.10), the equivalence of each pair of traces depends on the equivalence of the other pair, so swapping symmetry is only invoked once.

With these methods and rules laid down, we at last have a fully functional way to generate all flavour-ordered diagrams that contribute to a given process. In conjunction with this thesis, an implementation called `fodge` (flavour-ordered diagram generator), which interfaces with the FORM library used to perform the calculations, was written in C and used for the calculation of some of the larger amplitudes. More details can be found in appendix E.

## 6 Examples of amplitudes

Using the methods developed in the previous sections, we have computed several stripped NLSM amplitudes, some of which have not previously been determined. This section lists and explains some of those that are simple enough to write down in a sensible way.

### 6.1 4-point amplitudes

These amplitudes are by far the simplest, since their tree-level diagrams contain no propagators and only carry two flavour structures ( $\{4\}$  and  $\{2, 2\}$ ), or only one in the  $\mathcal{O}(p^2)$  case. At  $\mathcal{O}(p^6)$  and above, they only receive contributions from the Lagrangian terms with no more than four  $u_\mu$ 's, which is a tiny subset of the total Lagrangian.

#### 6.1.1 The $\mathcal{O}(p^2)$ amplitude

This is the simplest amplitude in all of the NLSM. It is given by a single diagram and a simple stripped amplitude,

$$\begin{array}{c} \diagup \\ \times \\ \diagdown \end{array} \quad -iF^2 \mathcal{M}_{2,\{4\}} = \frac{t}{2}, \quad (6.1)$$

where  $t$  is the Mandelstam invariant  $(p_1 + p_3)^2$ . We have pulled factors of  $i$  and  $F$  over to the left-hand side for clarity. The form of the right-hand side could in fact be guessed

based on symmetry, since  $t$  is invariant under  $\mathbb{Z}_4$ , whereas  $s$  and  $u$  transform into each other under it. The only other invariant kinematic structure would be  $s + u$ , which is simply  $-t$  due to conservation of momentum.

If we plug (6.1) into (3.15) and apply some  $SU(2)$  group algebra, we recover the familiar  $N_f = 2$  amplitude

$$\mathcal{M}_{2,4}^{abcd}(s, t, u) = \frac{-4i}{F^2} [s\delta^{ab}\delta^{cd} + t\delta^{ac}\delta^{bd} + u\delta^{ad}\delta^{bc}] \quad (6.2)$$

with the Mandelstam invariants defined as in section 4.2.

### 6.1.2 The $\mathcal{O}(p^4)$ amplitude

This amplitude consists of the two diagrams

$$\begin{array}{c} \diagup \quad \diagdown \\ \diagdown \quad \diagup \end{array} \quad - iF^4 \mathcal{M}_{4,\{4\}} = 2L_3(u^2 + s^2) + 4L_0t^2, \quad (6.3)$$

$$\begin{array}{c} \diagdown \quad \diagup \\ \diagup \quad \diagdown \end{array} \quad - iF^4 \mathcal{M}_{4,\{2,2\}} = 8L_1s^2 + 4L_2(t^2 + u^2), \quad (6.4)$$

which includes the simplest example of a flavour split. There are now two independent  $\mathbb{Z}_4$ -invariant kinematic structures,  $t^2$  and  $s^2 + u^2$ , and likewise two independent  $\mathbb{Z}_{\{2,2\}}$ -invariant ones,  $s^2$  and  $t^2 + u^2$ . All four are reflected in one term each, and neatly correspond to the LECs.

In analogy with (6.2), the complete  $SU(2)$   $\mathcal{O}(p^4)$  amplitude is

$$\begin{aligned} \mathcal{M}_{4,4}^{abcd}(s, t, u) = \frac{8i}{F^4} \left\{ \right. & [4L_0(u^2 + us) + 2L_1s^2 + L_2(t^2 + u^2) + 2L_3s^2] \delta^{ab}\delta^{cd} \\ & + [4L_0(s^2 + st) + 2L_1t^2 + L_2(u^2 + s^2) + 2L_3t^2] \delta^{ac}\delta^{bd} \\ & \left. + [4L_0(t^2 + tu) + 2L_1u^2 + L_2(s^2 + t^2) + 2L_3u^2] \delta^{ad}\delta^{bc} \right\}. \end{aligned} \quad (6.5)$$

The  $L_1, L_2$  sector is valid for any  $N_f$  (using  $\tau = 2$ ) due to the simplicity of 2-traces.

### 6.1.3 The $\mathcal{O}(p^6)$ amplitude

Like its lower-order analogue, this amplitude has only two diagrams,

$$\begin{array}{c} \diagup \quad \diagdown \\ \diagdown \quad \diagup \end{array} \quad - iF^4 \mathcal{M}_{6,\{4\}} = -L_{6,3}t(s^2 + u^2) - 2L_{6,4}t^3, \quad (6.6)$$

$$\begin{array}{c} \diagdown \quad \diagup \\ \diagup \quad \diagdown \end{array} \quad - iF^4 \mathcal{M}_{6,\{2,2\}} = -2L_{6,1}(t^3 + u^3) + \frac{2}{3}L_{6,2}(s^3 + t^3 + u^3). \quad (6.7)$$

Like at  $\mathcal{O}(p^4)$ , there are two independent  $\mathbb{Z}_4$ -invariant kinematic structures,  $t^3$  and  $t(s^2 + u^2)$ , and two independent  $\mathbb{Z}_{\{2,2\}}$ -invariant ones,  $s^3$  and  $s(t^2 + u^2)$ . These four correspond to the four LECs —  $s^3 + t^3 + u^3$  is a linear combination of  $s^3$  and  $s(t^2 + u^2)$ . We will not state the full amplitude, but its form is analogous to (6.2) and (6.5).

### 6.1.4 The $\mathcal{O}(p^8)$ amplitude

This is the only  $\mathcal{O}(p^8)$  amplitude that is even remotely simple to calculate, although the time consumption of the direct computation is comparable to that of much more complex amplitudes, such as the  $\mathcal{O}(p^4)$  8-point. Like all its analogues above  $\mathcal{O}(p^2)$ , it has only two diagrams,

$$\begin{array}{c} \text{X} \\ \text{X} \end{array} \quad -iF^4 \mathcal{M}_{8,\{4\}} = L_{8,4} s^2 u^2 + \frac{1}{2} L_{8,5} t^2 (s^2 + u^2) + L_{8,6} t^4, \quad (6.8)$$

$$\begin{array}{c} \text{X} \\ \text{X} \end{array} \quad -iF^4 \mathcal{M}_{8,\{2,2\}} = L_{8,1} s^2 (t^2 + u^2) + L_{8,2} (t^4 + u^4) + 2L_{8,3} t^2 u^2, \quad (6.9)$$

There are now three independent  $\mathbb{Z}_4$ -invariant kinematic structures,  $t^4$ ,  $t^2(s^2 + u^2)$  and  $s^2 u^2$ , and corespondingly three for  $\mathbb{Z}_{\{2,2\}}$ . This is reflected in the six LECs.

This sequence of diagrams can be continued to even higher orders, and determining the terms in the  $\mathcal{O}(p^{10})$  and  $\mathcal{O}(p^{12})$  Lagrangians that only contain four  $u_\mu$ 's should not be excessively difficult.<sup>23</sup> However, this is getting ahead of the more interesting problems of going to higher order or increasing the number of legs. Without dwelling longer on this, we will therefore move on with the latter.

## 6.2 The $\mathcal{O}(p^2)$ 6- and 8-point amplitudes

The leading order in the power counting offers a relatively simple playground for flavour-ordering, free from splittings and singlets. It is relatively well explored, and the amplitudes presented here were also calculated in [6]. Therefore, this section is mainly for comparison with the more complicated amplitudes below.

The 6-point amplitude is given by the diagrams

$$\begin{array}{c} \text{X} \\ \text{X} \end{array} \quad \begin{array}{c} \text{X} \\ \text{X} \end{array} \quad (6.10)$$

and has the amplitude

$$\begin{aligned} -4iF^4 \mathcal{M}_{2,6} = & s_{12} + s_{23} + s_{34} + s_{45} + s_{56} + s_{61} \\ & - \frac{(s_{12} + s_{23})(s_{45} + s_{56})}{s_{123}} - \frac{(s_{23} + s_{34})(s_{56} + s_{61})}{s_{234}} - \frac{(s_{34} + s_{45})(s_{61} + s_{12})}{s_{345}}, \end{aligned} \quad (6.11)$$

which suggests the reduced form (see section 4.3)<sup>24</sup>

$$-4iF^4 \mathcal{M}_{2,6} = \left\{ s_{12} - \frac{1}{2} \frac{(s_{12} + s_{23})(s_{45} + s_{56})}{s_{123}} \right\} + [\mathbb{Z}_6], \quad (6.12)$$

<sup>23</sup> $\mathcal{M}_{10,\{4\}}$  will be a linear combination of  $s^5$ ,  $s^3 tu$  and  $st^2 u^2$ , and  $\mathcal{M}_{10,\{2,2\}}$  will be a linear combination of  $t^5$ ,  $t^3 us$  and  $tu^2 s^2$ , since these are the only independent  $\mathcal{O}(p^{10})$  kinematic structures that are invariant under  $\mathbb{Z}_{\{4\}}$  and  $\mathbb{Z}_{\{2,2\}}$ , respectively. The coefficients will be linear combinations of the LECs of the terms in  $\mathcal{L}_{10}$  that only contain four  $u_\mu$ 's. These terms, along with the rest of  $\mathcal{L}_{10}$ , are currently unknown.

<sup>24</sup>The above amplitude has 6 + 12 terms in the form (4.12), organised into two separate orbits under  $\mathbb{Z}_6$ .

where the expression in braces is  $\mathfrak{m}_{2,\{6\}}$ , and  $[\mathbb{Z}_6]$  indicates summation over all cyclic permutations. Note the factor of  $1/2$ , which contains the statement that the second term has twofold symmetry under rotation, a trait that is shared by the second diagram. In the minimal parametrisation, the two terms (plus their cyclings) are in fact exactly the respective values of the two diagrams. In other parametrisations, additional terms show up and cancel to give this parametrisation-independent expression.

The 8-point amplitude is given by the diagrams

$$\begin{array}{cccc}
 \begin{array}{c} \diagup \\ \diagdown \\ \diagup \\ \diagdown \\ \diagup \\ \diagdown \\ \diagup \\ \diagdown \end{array} &
 \begin{array}{c} \diagup \\ \diagdown \\ \diagup \\ \diagdown \end{array} &
 \begin{array}{c} \diagup \\ \diagdown \\ \diagup \\ \diagdown \end{array} &
 \begin{array}{c} \diagup \\ \diagdown \\ \diagup \\ \diagdown \end{array} & , & (6.13)
 \end{array}$$

and its stripped amplitude is, in a similarly reduced form,

$$\begin{aligned}
 -8iF^6 \mathcal{M}_{2,8} = & \left\{ \frac{4s_{12} + s_{1234}}{2} - \frac{(s_{12} + s_{23})(s_{45} + s_{56} + s_{67} + s_{78} + s_{4567} + s_{5678})}{s_{123}} \right. \\
 & + \frac{1}{2} \frac{(s_{12} + s_{23})(s_{1234} + s_{4567})(s_{56} + s_{67})}{s_{123}s_{567}} \\
 & \left. + \frac{(s_{12} + s_{23})(s_{1234} + s_{45})(s_{67} + s_{78})}{s_{123}s_{678}} \right\} + [\mathbb{Z}_8] \quad (6.14)
 \end{aligned}$$

where there is again a rather direct correspondence between terms and diagrams, which is most manifest in the minimal parametrisation. This is the only 8-point amplitude that is simple enough to be presented in this fashion with any degree of readability.

### 6.3 The $\mathcal{O}(p^4)$ 6-point amplitude

This is a novel result of this work, and hinges decisively on the use of split-trace flavour ordering. It was also recently arrived at in a different form by [9]. The amplitude is given by the four diagrams

$$\begin{array}{cccc}
 \begin{array}{c} \diagup \\ \diagdown \\ \diagup \\ \diagdown \end{array} &
 \begin{array}{c} \diagup \\ \diagdown \\ \diagup \\ \diagdown \end{array} &
 \begin{array}{c} \diagup \\ \diagdown \\ \diagup \\ \diagdown \end{array} &
 \begin{array}{c} \diagup \\ \diagdown \\ \diagup \\ \diagdown \end{array} & . & (6.15)
 \end{array}$$

Note that unlike its  $\mathcal{O}(p^2)$  counterpart, the third diagram is not symmetric due to the asymmetric placement of vertices. The single-trace stripped amplitude is

$$\begin{aligned}
 -iF^6 \mathcal{M}_{4,6} = & L_3 \left\{ s_{12}(s_{12} + s_{34} + s_{45}) - \frac{(s_{12} + s_{23})(s_{45}^2 + s_{56}^2)}{s_{123}} \right\} + [\mathbb{Z}_6] \\
 & + 2L_0 \left\{ s_{12}(s_{12} + s_{34} + 2s_{45}) + s_{123}(s_{612} - s_{61}) - \frac{(s_{12} + s_{23})(s_{45} + s_{56})^2}{s_{123}} \right\} + [\mathbb{Z}_6] \quad (6.16)
 \end{aligned}$$

In order to find the reduced form of the flavour-split basis, it is extremely helpful to have a closed Mandelstam basis. In terms of the basis  $\hat{\mathcal{B}}_{\{2,4\}}$  of (D.1), it is

$$\begin{aligned}
-iF^6 \mathcal{M}_{4,\{2,4\}} = & \frac{L_1}{2} \left\{ t_1 [t_1 + 2t_2 + t_3 - 3(t_5 + t_6)] + \frac{(t_2 + t_3 + t_4)^2 [t_3 - 2(t_5 + t_6)]}{2t_1} \right\} + [\mathbb{Z}_{\{2,4\}}] \\
& + \frac{L_2}{8} \left\{ t_1 \left[ t_1 + 2t_2 + \frac{t_3}{2} - 3(t_5 + t_6) \right] + 4t_7^2 - 2t_9^2 \right. \\
& \left. + \frac{[(t_2 + t_3 + t_4)^2 + 4(t_7 + t_8 + t_9)^2] [t_3 - 2(t_5 + t_6)]}{2t_1} \right\} + [\mathbb{Z}_{\{2,4\}}]. \quad (6.17)
\end{aligned}$$

Note that the summation over cyclic permutations is replaced by summation over  $\mathbb{Z}_{\{2,4\}}$ .

## 6.4 Further amplitudes

We have computed the  $\mathcal{O}(p^6)$  6-point amplitude, and using the closed mandelstam bases presented in appendix D, it is possible to present its reduced form in two or three pages. However, the discovery of these bases came so late in the process of this work that we have not had the time to organise the amplitude in a satisfactory manner. Rather than presenting the raw result produced by FORM without the manual adjustments that place the amplitude in its most readable form, we have chosen to leave it out.

We have also computed several amplitudes whose expressions are too large to overview. They have been verified by checking their Adler zeroes, and in some cases by running brute-force Feynman diagram calculations. Further beyond that, we have generated the flavour-ordered diagrams of many more amplitudes using `fodge`. Evaluation of those amplitudes require more optimised handling in FORM, more computing power, or simply more time. Here, we only summarise the number and general properties of the diagrams to give an idea of how the complexity scales. The summary is given in table 3.

In the table, we note that the number of diagrams grow more rapidly with  $n$  (the number of particles) than with  $N$  (the power-counting order). Especially when  $N > n$ , the number of new diagrams is very small. This is also reflected in the computational effort needed: the  $\mathcal{O}(p^2)$  10-point,  $\mathcal{O}(p^6)$  8-point and  $\mathcal{O}(p^8)$  6-point amplitudes took approximately 10 minutes each to calculate with FORM, while the  $\mathcal{O}(p^4)$  10-point amplitude took almost an hour and the  $\mathcal{O}(p^2)$  12-point amplitude took over 2 days. At high  $N$ , the calculation of vertex factors takes significant time, while at high  $n$ , the conversion to Mandelstam variables is very time-consuming due to the large dimension of kinematic space.

As the table shows, we have calculated all amplitudes with less than 100 diagrams, excluding  $N \geq 10$ , where the Lagrangian is not yet known. If we decide to push the frontier of large  $n$  further in the future, we can expect the required computational effort to be severe.

| $\mathcal{O}(p^N)$ | $n$ | Number of diagrams |   |         |        |         |        | Computed?         |                               |
|--------------------|-----|--------------------|---|---------|--------|---------|--------|-------------------|-------------------------------|
|                    |     | $SU(N_f)$          | $U(N_f)$  | $SU(3)$ | $U(3)$ | $SU(2)$ | $U(2)$ |                   |                               |
| $\mathcal{O}(p^2)$ | 4   | 1                  |   |         |        |         |        | Yes (6.1)         |                               |
|                    | 6   | 2                  | <i>These columns equal <math>SU(N_f)</math></i> |         |        |         |        | Yes (6.12)        |                               |
|                    | 8   | 4                  |   |         |        |         |        | Yes (6.14)        |                               |
|                    | 10  | 16                 |   |         |        |         |        | Yes (see [6])     |                               |
|                    | 12  | 73                 |   |         |        |         |        | Yes*              |                               |
|                    | 14  | 414                |   |         |        |         |        | No                |                               |
| $\mathcal{O}(p^4)$ | 4   | 2                  |   |         |        | 1       | 1      | Yes (6.4)         |                               |
|                    | 6   | 4                  | <i>These columns equal <math>SU(N_f)</math></i> |         |        |         | 2      | 2                 | Yes <sup>†*</sup> (6.16-6.17) |
|                    | 8   | 18                 |   |         |        | 8       | 8      | Yes <sup>†*</sup> |                               |
|                    | 10  | 90                 |   |         |        | 43      | 43     | Yes*              |                               |
|                    | 12  | 577                |   |         |        | 283     | 283    | No                |                               |
| $\mathcal{O}(p^6)$ | 4   | 2                  | 2   | 2       | 2      | 1       | 1      | Yes (6.7)         |                               |
|                    | 6   | 10                 | 9   | 9       | 8      | 4       | 3      | Yes <sup>†*</sup> |                               |
|                    | 8   | 50                 | 45  | 48      | 43     | 18      | 14     | Yes*              |                               |
|                    | 10  | 358                | 316   | 348     | 316    | 128     | 97     | No                |                               |
| $\mathcal{O}(p^8)$ | 4   | 2                  | 2   | 2       | 2      | 1       | 1      | Yes* (6.9)        |                               |
|                    | 6   | 11                 | 10  | 10      | 9      | 4       | 3      | Yes*              |                               |
|                    | 8   | 104                | 84  | 97      | 77     | 34      | 21     | No                |                               |

Table 3: Summary of the number of  $\mathcal{O}(p^N)$   $n$ -point diagrams. The  $SU(N_f)$  column shows the general count, and the  $U(N_f)$  column shows the count without singlet diagrams. The  $SU(3)$  and  $SU(2)$  columns show the number of distinct diagrams left when some Lagrangian terms have been eliminated in the manner of section 2. Note that the distinction for  $N_f = 2$  and  $N_f = 3$  emerges first at  $\mathcal{O}(p^4)$  and  $\mathcal{O}(p^6)$ , respectively, and that the distinction between  $SU$  and  $U$  emerges first at  $\mathcal{O}(p^6)$ . The rightmost column states whether an amplitude has been computed by us, and provides references to the explicit amplitudes when possible. Amplitudes marked with an asterisk have to our knowledge not been calculated before; the  $\mathcal{O}(p^4)$  6-point amplitude was only recently reproduced by [9]. Amplitudes marked with a dagger have been verified with a brute-force Feynman diagram calculation; the remainder rely only on Adler zeroes for verification.

## 7 First steps towards generalisation

As the final part of the thesis, we will briefly cover some areas outside of its main scope. This includes the basic principles of how our flavour-ordering methods could be extended to the full  $\chi$ PT and to loop diagrams, with the hope that it might serve as the basis of future work.

### 7.1 A brief look at $\chi$ PT

The NLSM is a very general theory, but as mentioned before, it does not describe the full suite of meson properties when applied to low-energy QCD. Chiral perturbation theory ( $\chi$ PT) adds extensions to cover such shortcomings. This thesis makes very limited use of full  $\chi$ PT (the main exception is section 7.2), but it is illuminating to see the broader context in which our version of the NLSM lives.

$\chi$ PT can be derived from an extended QCD Lagrangian,

$$\mathcal{L}_{\text{QCD, ext.}} = \mathcal{L}_{\text{QCD}} + \bar{q}\gamma^\mu(v_\mu + \gamma_5 a_\mu)q - \bar{q}(s - i\gamma_5 p)q, \quad (7.1)$$

where  $\mathcal{L}_{\text{QCD}}$  is as in (2.17), and  $v_\mu$ ,  $a_\mu$ ,  $s$  and  $p$  are  $N_f \times N_f$  matrices that parametrise the additional couplings. In spacetime, they transform as a vector, axial vector, scalar, and pseudoscalar, respectively.

It is convenient to define the linear combinations  $r_\mu = v_\mu + a_\mu$ , which couples to right-handed quarks, and  $\ell_\mu = v_\mu - a_\mu$ , which couples to left-handed ones. The Lagrangian is invariant under chiral symmetry if the fields are given the transformation properties

$$\ell_\mu \xrightarrow{g} g_L \ell_\mu g_L^\dagger + i g_L \partial_\mu g_L^\dagger, \quad r_\mu \xrightarrow{g} g_R r_\mu g_R^\dagger + i g_R \partial_\mu g_R^\dagger, \quad s + ip \xrightarrow{g} g_R (s + ip) g_L^\dagger, \quad (7.2)$$

with  $g = (g_L, g_R) \in G$  as usual. Any symmetry-consistent coupling can be introduced through these fields; for instance, much of the Standard Model is contained in

$$r_\mu = -e\mathbf{Q}A_\mu, \quad \ell_\mu = -e\mathbf{Q}A_\mu - e(W_\mu^+ \mathbf{T} + \mathbf{T}^\dagger W_\mu^-), \quad s = \mathbf{M}, \quad p = 0, \quad (7.3)$$

where  $\mathbf{M} = \text{diag}(m_u, m_d, m_s, \dots)$  is the quark mass matrix,  $\mathbf{Q} = \text{diag}(\frac{2}{3}, -\frac{1}{3}, -\frac{1}{3}, \dots)$  is the quark charge matrix,  $e$  is the elementary charge,  $A_\mu$  and  $W_\mu^\pm$  are electroweak gauge fields, and  $\mathbf{T}$  is a quark mixing matrix. What remains is  $Z$  couplings in  $\ell_\mu$  and Higgs couplings in  $s$ , but more exotic couplings can be introduced if desired.<sup>25</sup>

Lagrangian building blocks similar to  $U, U^\dagger$  can be constructed as

$$\chi = 2B_0(s + ip), \quad F_L^{\mu\nu} = \partial^\mu \ell^\nu - \partial^\nu \ell^\mu - i[\ell^\mu, \ell^\nu], \quad F_R^{\mu\nu} = \partial^\mu r^\nu - \partial^\nu r^\mu - i[r^\mu, r^\nu], \quad (7.4)$$

where  $B_0$  is a new LEC.<sup>26</sup> These building blocks are  $\mathcal{O}(p^2)$  and transform as

$$\chi \xrightarrow{g} g_R \chi g_L^\dagger, \quad F_L^{\mu\nu} \xrightarrow{g} g_L F_L^{\mu\nu} g_L^\dagger, \quad F_R^{\mu\nu} \xrightarrow{g} g_R F_R^{\mu\nu} g_R^\dagger. \quad (7.5)$$

<sup>25</sup>One could also introduce the 2-tensor term  $\frac{1}{2}[\gamma_\mu, \gamma_\nu]t^{\mu\nu}$  to (7.1) to complete the family of Dirac bilinears and introduce couplings of 2-tensor nature through  $t^{\mu\nu}$ . This option is not considered in [13] and [16, 14], but is explored in [34].

<sup>26</sup> $F_{L,R}^{\mu\nu}$  are analogous to the field-strength tensor of a gauge theory, and are indeed equal to the electromagnetic field-strength tensor if only the electromagnetic couplings are added.



Note that  $F_{L,R}^{\mu\nu}$  are hermitian, but that  $\chi$ , in general, is not.

Following [14, 16], less cumbersome building blocks in the same family as  $u_\mu, \nabla_\mu$  can be defined as

$$\chi_\pm = u^\dagger \chi u^\dagger \pm u \chi^\dagger u, \quad f_\pm^{\mu\nu} = u F_L^{\mu\nu} u^\dagger \pm u^\dagger F_R^{\mu\nu} u. \quad (7.6)$$

When the gauge fields  $v_\mu, a_\mu$  are introduced, local invariance requires modification of  $u_\mu$ : in (2.23), we must change  $\partial_\mu u \rightarrow (\partial_\mu - ir_\mu)u$  and  $\partial_\mu u^\dagger \rightarrow (p_\mu - il_\mu)u^\dagger$ . The same changes apply to (2.24), and the right-hand side of (2.25) becomes  $-f_{-\mu\nu}$ .

These building blocks ( $u_\mu, \chi_\pm, f_\pm^{\mu\nu}$ ) along with the covariant derivative of (2.24) form the foundation of the full  $\mathcal{O}(p^8)$  Lagrangian of [14] and the unpublished  $\mathcal{O}(p^6)$  Lagrangian associated with it. At  $\mathcal{O}(p^2)$ ,  $\chi$ PT introduces only one additional term compared to the NLSM Lagrangian, since  $\chi_-$  has odd parity and  $f_\pm^{\mu\nu} = 0$ :

$$\mathcal{L}_2^{\chi\text{PT}} = \frac{F^4}{4} \langle u_\mu u^\mu + \chi_+ \rangle. \quad (7.7)$$

The additional LEC that would emerge is absorbed into  $B_0$ . At  $\mathcal{O}(p^4)$ , the full  $\chi$ PT Lagrangian [4, 5] takes the form

$$\begin{aligned} \mathcal{L}_4 = & L_0 \langle u_\mu u_\nu u^\mu u^\nu \rangle + L_1 \langle u_\mu u^\mu \rangle \langle u_\nu u^\nu \rangle + L_2 \langle u_\mu u_\nu \rangle \langle u^\mu u^\nu \rangle + L_3 \langle u_\mu u^\mu u_\nu u^\nu \rangle \\ & + L_4 \langle u_\mu u^\mu \rangle \langle \chi_+ \rangle + L_5 \langle u_\mu u^\mu \chi_+ \rangle \\ & + L_6 \langle \chi_+ \rangle^2 + L_7 \langle \chi_- \rangle^2 + \frac{L_8 + H_2}{2} \langle \chi_+^2 \rangle + \frac{L_8 - H_2}{2} \langle \chi_-^2 \rangle, \\ & - iL_9 \langle f_+^{\mu\nu} u_\mu u_\nu \rangle + \frac{2H_1 + L_{10}}{4} \langle f_+^{\mu\nu} f_{+\mu\nu} \rangle + \frac{2H_1 - L_{10}}{4} \langle f_-^{\mu\nu} f_{-\mu\nu} \rangle, \end{aligned} \quad (7.8)$$

where some LECs appear in linear combinations to conform with the original formulation in [4, 5], which uses  $\chi$  and  $F_{L,R}^{\mu\nu}$ . The  $H_i$  correspond to terms where all instances of  $\phi^a$  can be eliminated, leaving only the additional fields.

## 7.2 Flavour-ordering and mass

In order to more realistically model the light but non-massless mesons of low-energy QCD, we may borrow a minimal part of  $\chi$ PT where

$$\chi = 2B_0 \mathbf{M}, \quad \ell_\mu = r_\mu = 0, \quad (7.9)$$

where  $\mathbf{M} = \text{diag}(m_u, m_d, \dots)$  is the  $N_f$ -quark mass matrix. This inclusion adds the  $\chi_+$  term to the  $\mathcal{O}(p^2)$  Lagrangian in (7.7), and includes  $L_4, \dots, L_8$  and  $H_2$  in the  $\mathcal{O}(p^4)$  Lagrangian in (7.8).

### 7.2.1 Scalar meson masses

The  $\chi$ PT addition to  $\mathcal{L}_2$  generates masses through the expansion

$$\frac{F^2}{4} \langle \chi_+ \rangle = \frac{B_0 F^2}{2} \langle \mathbf{M}(U + U^\dagger) \rangle = B_0 F^2 \langle \mathbf{M} \rangle - B_0 \langle \mathbf{M} \Phi^2 \rangle + \mathcal{O}(\Phi^4). \quad (7.10)$$

The first term on the right is merely an additive constant, but the second expands to the canonical mass terms of the fields. However, it turns out that all  $\phi^a$  are not mass eigenstates; instead, the  $SU(2)$  Lagrangian grants well-defined masses to the linear combinations

$$\pi^\pm = \frac{\phi^1 \pm i\phi^2}{\sqrt{2}}, \quad \pi^0 = \phi^3, \quad (7.11)$$

where we have identified the states as the three lightest mesons. These are also charge eigenstates, and including electromagnetic interactions in  $\chi$ PT confirms that  $\pi^\pm$  are indeed the charged pions. All three fields gain the mass  $M_\pi^2 = B_0 \langle M_0 \rangle = B_0(m_u + m_d)$ .

For  $N_f = 3$ , the mass eigenstates and masses are

$$\begin{aligned} \pi^\pm &= \frac{\phi^1 \pm i\phi^2}{\sqrt{2}}, & M_{\pi^\pm}^2 &= B_0(m_u + m_d), \\ K^\pm &= \frac{\phi^4 \pm i\phi^5}{\sqrt{2}}, & M_{K^\pm}^2 &= B_0(m_u + m_s), \\ K^0, \bar{K}^0 &= \frac{\phi^6 \pm i\phi^7}{\sqrt{2}}, & M_{K^0}^2 &= B_0(m_d + m_s) \end{aligned} \quad (7.12)$$

for six of the fields. For the remaining two,  $\phi^3$  and  $\phi^8$ , there is a nontrivial mixing angle  $\delta$ , so we define the mass eigenstates

$$\pi^0 = \phi^3 \cos \delta + \phi^8 \sin \delta, \quad \eta = -\phi^3 \sin \delta + \phi^8 \cos \delta. \quad (7.13)$$

Carrying out the algebra for diagonalising the mass matrix, we arrive at

$$\tan(2\delta) = \frac{-\sqrt{3}(m_u - m_d)}{2m_s - (m_u + m_d)}, \quad (7.14)$$

which is a very small value when the conventional quark mass ratios  $m_s \approx 20m_d \approx 40m_u$  are used.<sup>27</sup> To leading order in  $\delta$ , we have

$$M_{\pi^0}^2 = B_0(m_u + m_d) - \varepsilon + \mathcal{O}(\varepsilon^2), \quad M_\eta^2 = B_0 \frac{m_u + m_d + 4m_s}{3} + \varepsilon + \mathcal{O}(\varepsilon^2), \quad (7.15)$$

using the small parameter

$$\varepsilon = \frac{B_0}{2} \frac{(m_u - m_d)^2}{2m_s - (m_u + m_d)} \approx 10^{-3} M_{\pi^\pm}^2. \quad (7.16)$$

These masses offer a reasonably accurate first approximation of the measured meson masses, although  $\varepsilon$  is significantly smaller than the physical difference between  $M_{\pi^0}^2$  and  $M_{\pi^\pm}^2$ . More  $\chi$ PT corrections can be introduced for greater accuracy; see e.g. [8].

---

<sup>27</sup>If the quark masses are instead taken to be equal, the mass eigenstates become degenerate and  $\delta$  is no longer well-defined.

This process can of course be carried on to larger  $N_f$ , but the difficulty increases while the physical relevance decreases, since the lightest vector mesons are lighter than the lightest scalar mesons containing charm quarks. The mass calculation can also be extended to  $U(3)$  to include the singlet particle  $\eta' \approx \phi^0$ , which mixes with  $\pi^0$  and  $\eta$ . This is algebraically messy, though, and offers a very poor approximation of the  $\eta'$  mass.

The  $\chi_{\pm}$ -containing terms in  $\mathcal{L}_4$  generate mass-dependent interaction vertices, some of which are 2-point, which makes them similar to the canonical mass term. The resummation of these gives corrections to the leading-order masses, and their presence gives rise to several new mass-dependent interaction vertices that must be taken into account. However, this is outside the scope of this thesis.

### 7.2.2 Massive propagators, equal-mass case

If all particles are granted equal masses, with  $m$  being that mass, the NLSM propagator generalises straightforwardly as

$$\frac{i\delta^{ab}}{q^2} \rightarrow \frac{i\delta^{ab}}{q^2 - m^2}. \quad (7.17)$$

This is easy to implement and does not interfere with flavour-ordering, but its effect on the soft limit is dramatic. Sending  $p_i \rightarrow 0$  is not compatible with  $p_i^2 = m^2$ , so our previous definition of Adler zeroes is invalidated. The simplest  $\chi$ PT amplitude,

$$-iF^2 \mathcal{M}_{2,4} = \frac{t}{2} - m^2, \quad (7.18)$$

does vanish at  $t = 2m^2$ , but this is not a permutation-invariant statement, and the dressed amplitude has different soft limits. With the  $N_f = 2$  mesons,

$$\begin{aligned} \mathcal{M}(\pi^0 \pi^{\pm} \rightarrow \pi^0 \pi^{\pm}) &\propto t - M_{\pi}^2, & \mathcal{M}(\pi^+ \pi^- \rightarrow \pi^+ \pi^-) &\propto t - 2M_{\pi}^2, \\ \mathcal{M}(\pi^{\pm} \pi^{\pm} \rightarrow \pi^{\pm} \pi^{\pm}) &\propto s - 2M_{\pi}^2, & \mathcal{M}(\pi^0 \pi^0 \rightarrow \pi^0 \pi^0) &\propto M_{\pi}^2. \end{aligned} \quad (7.19)$$

All other combinations yield zero — charge conservation is a global symmetry.

The lack of easily accessible Adler zeroes removes the main error checking procedure from our methods, and hides the fact that higher-ordered vertices are constructible from lower-order ones. It might be possible to circumvent this with generalised definitions of the soft limit, but due to these issues, no actual amplitude calculations involving massive particles have been carried out in this work.

### 7.2.3 Massive propagators, general case

Regardless of the problems introduced by masses, let us press on to the more general case. When the particle masses are unequal, the simple extension (7.17) is not possible. Instead, we will have

$$\frac{i\delta^{ab}}{q^2} \rightarrow i\Delta^{ab}(q), \quad (7.20)$$

where  $\Delta$  is some flavour-space matrix, which may be very messy in the general case. If all particles are mass eigenstates, it will have diagonal entries  $\Delta^{aa}(q) = 1/(q^2 - M_a^2)$ , with all other elements zero. Even in this simpler case, it is still not possible to apply (3.11) to achieve flavour ordering.

In order to diagonalise  $\Delta$ , we must change basis from  $\phi^a$  to a basis of mass eigenstates  $\pi^a$ , accompanied by a corresponding change to a different basis of generators  $t^a \rightarrow \tau^a$ , so that  $\Phi = \phi^a t^a = \pi^a \tau^a$ . If the fields are also to be charge eigenstates, such as the meson fields in (7.12), we must abandon the requirement that the generators be hermitian, but we can require that  $\tau^{a\dagger} = \tau^b$  for some  $b$  given  $a$ , since  $\pi^{a\dagger} = \pi^b$ . This allows us to generalise trace-orthogonality and commutation relations as

$$\langle \tau^a \tau^{b\dagger} \rangle = \tau \delta^{ab}, \quad [\tau^a, \tau^b] = i\kappa \varphi^{abc} \tau^{c\dagger} \quad \Rightarrow \quad \varphi^{abc} = \frac{-i}{\tau\kappa} \langle [\tau^a, \tau^b] \tau^c \rangle, \quad (7.21)$$

where  $\varphi^{abc}$  are the structure constants of the new basis. They are totally antisymmetric but not necessarily real; for instance,  $N_f = 2$  has  $\varphi^{123} = -i$ . With these definitions, we recover the familiar identities (3.11) and (3.12):

$$\frac{1}{\tau} \langle X \tau^a \rangle \langle \tau^{a\dagger} Y \rangle = \langle XY \rangle - \frac{1}{N_f} \langle X \rangle \langle Y \rangle, \quad \frac{1}{\tau} \langle X \tau^a Y \tau^{a\dagger} \rangle = \langle X \rangle \langle Y \rangle - \frac{1}{N_f} \langle XY \rangle. \quad (7.22)$$

With  $\Delta^{ab}(q)$  not proportional to  $\delta^{ab}$ , this is still not enough to do flavour ordering, but the generators offer a way to salvage it. In the *adjoint representation* (see appendix A, the generators

$$(\alpha_a)^{bc} = -i\varphi^{abc} \quad (7.23)$$

are  $(N_f^2 - 1) \times (N_f^2 - 1)$  matrices rather than  $N_f \times N_f$ , but can still be shown to have the same properties as  $\tau^a$ . For our purposes, the important thing is that one can form a basis for diagonal  $(N_f^2 - 1) \times (N_f^2 - 1)$  using squares of adjoint generators. That is, we can express

$$\Delta^{ab}(q) = \sum_{k=1}^{N_f^2-1} (\alpha_k^2)^{ab} x_k(q) \quad (7.24)$$

for some coefficients  $x_k(q)$ . For instance, with  $N_f = 2$  we have

$$\alpha_1^2 = \text{diag}(0, -1, -1), \quad \alpha_2^2 = \text{diag}(-1, 0, -1), \quad \alpha_3^2 = \text{diag}(-1, -1, 0), \quad (7.25)$$

which can be used to represent  $\Delta$  like

$$\Delta(q) = \alpha_3^2 \left[ \frac{1/2}{q^2 - M_{\pi^0}^2} - \frac{1}{q^2 - M_{\pi^\pm}^2} \right] + (\alpha_1^2 + \alpha_2^2) \left[ \frac{-1/2}{q^2 - M_{\pi^\pm}^2} \right], \quad (7.26)$$

where the bracketed expressions are the  $x_k(q)$ . A similar construction is possible for  $N_f = 3$ , where there are 5 different masses and 5 linearly independent  $8 \times 8$  diagonal matrices constructible from the generators. Most likely, the construction is possible for any  $N_f$ , but we have not checked larger values.

With an expression like (7.24) available, we can generalise the flavour contraction over a propagator like

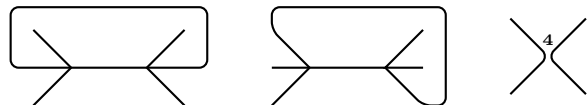
$$\begin{aligned}
\langle X \tau^a \rangle \Delta^{ab}(q) \langle \tau^{b\dagger} Y \rangle &= \sum_k x_k(q) \langle X \tau^a \rangle (\alpha_k^2)^{ab} \langle \tau^{b\dagger} Y \rangle \\
&= \sum_k^{N_f-1} x_k(q) \langle X \tau^a \rangle \varphi^{akc} \varphi^{ckb} \langle \tau^{b\dagger} Y \rangle \\
&= - \sum_k \frac{x_k(q)}{\tau^2 \kappa^2} \langle X \tau^a \rangle \langle \tau^{a\dagger} [\tau^{k\dagger}, \tau^{c\dagger}] \rangle \langle [\tau^c, \tau^k] \tau^b \rangle \langle \tau^{b\dagger} Y \rangle \\
&= - \sum_k \frac{x_k(q) \tau}{\kappa^2} \langle [X, \tau^{k\dagger}] [\tau^k, Y] \rangle,
\end{aligned} \tag{7.27}$$

making repeated use of various identities. When all masses (i.e. all  $x_k$ ) are equal, this reduces to (3.11).

The above expression represents a weakened form of flavour ordering. The ordering of  $X$  and  $Y$  is conserved, and  $x_k(q)$  are readily absorbed into the kinematic factors, but various extra generators are inserted into the traces. It is not entirely clear how their presence interacts with the orthogonality of flavour structures, but it seems likely that this allows a more complicated, but still valid, form of flavour-ordering to be carried out even with particles of unequal masses.

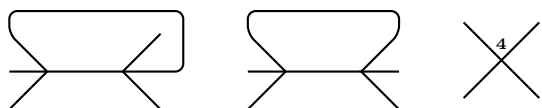
### 7.3 Flavour-ordering and loops

So far, all discussion has been about tree diagrams, but the flavour-ordering techniques developed here can be extended to loop diagrams. When connecting two legs of a diagram through a loop, the relevant flavour structure contraction is carried out through (3.12) if both flavour indices reside in the same trace. The first (multiplet) term splits the flavour structure into  $\langle X \rangle \langle Y \rangle$ , where  $X$  and  $Y$  can be interpreted as the “inside” and “outside” of the loop.<sup>28</sup> Therefore, the three diagrams



$$\tag{7.28}$$

are all  $\mathcal{O}(p^4)$  and have the same flavour structure, but have different symmetry properties. We have drawn the loops in odd shapes to emphasise the interpretation as further connections applied to an underlying tree diagram. Since  $\langle t^a \rangle = 0$ , the first diagram among



$$\tag{7.29}$$

<sup>28</sup>It is of course arbitrary which side is considered the inside, but the naming is nonetheless intuitive.

is zero, while the other two have the same order and flavour structure. The middle diagram gains a factor of  $\langle 1 \rangle = N_f$  from the empty inside.

When a loop connects two flavour indices residing in different traces, (3.11) is used, and the multiplet term joins the flavour structures. This applies equally well when adding a second loop between the inside and outside of another loop to form a non-planar diagram. Therefore,

(7.30)

are all  $\mathcal{O}(p^6)$  and have the same flavour structure.

In both cases, the singlet term can be interpreted as the subtraction of a diagram with a singlet particle in the loop. As can be seen from (3.11) and (3.12), singlet loops leave the existing flavour structures unchanged: insides and outsides are not separated, and separate flavour structures are not joined. Therefore, in the singlet loop diagrams

(7.31)

the first pair of diagrams shares order and flavour structure, as does the second pair. The last diagram is zero, since its flavour structure is split  $\{1, 3\}$ .

No actual loop calculations are carried out in this work, but the above flavour-ordering rules should hopefully simplify future developments.

## 8 Summary, conclusions and outlook

In this work, we have successfully developed a fully general framework for performing tree-level calculations in the NLSM with any number of legs and any number of derivatives in the Lagrangian. The methods significantly lessen the efforts needed to compute the amplitudes, and shortens the expressions needed to write them. We have shown how the procedure of obtaining an amplitude can be efficiently automated rather than depending on laborious hand-construction of diagrams. Lastly, we have as a side-effect simplified the act of squaring the amplitude into a cross-section (see the end of section 3.7).

Flavour-ordering has its limitations, though. It is constrained to the massless NLSM at tree-level, although extension to massive  $\chi$ PT and loop diagrams might be possible, as shown in section 7. The main limitation is that it is constrained to theories based on the group algebra of  $SU(N_f)$  and  $U(N_f)$ , since it relies on the existence of (3.11-3.12). In a different group, flavour-ordering is not guaranteed.<sup>29</sup> This limitation is not seen in soft

<sup>29</sup> $SO(N_f)$  has the (3.11)-analogue  $\langle Xt^a \rangle \langle t^a Y \rangle = \frac{1}{2}(\langle XY \rangle - \langle XY^T \rangle)$ , where the transpose reverses the order of the indices. This is less useful than true flavour-ordering, but might still offer some advantage compared to brute-force Feynman diagrams.

recursion (section 4.5), where a much larger range of theories (see examples given in [32]), many of which do not have the notion of stripped amplitudes, can be constructed.

Thus, we have a trio of methods with different advantages and drawbacks. Flavour-ordering is powerful, but specialised to  $SU(N_f)$ - or  $U(N_f)$ -based theories, and suffers from a rapidly growing number of diagrams. Soft recursion is more widely applicable, but algebraically involved and not as readily automated. The developments of [9] offers some improvements, but soft recursion is either way unable to calculate  $\mathcal{O}(p^N)$   $n$ -point amplitudes in a theory with soft degree  $\sigma$  if  $n \geq \sigma N$ . This mostly excludes  $\mathcal{O}(p^6)$  calculations in the NLSM, since the very complicated 6-point amplitude is required as a seed. Lastly, brute-force Feynman diagrams are universal and cover the cases where the other methods fail, but require orders of magnitude more tedious algebra than flavour-ordering.<sup>30</sup>

Most of the work in this thesis has been geared towards calculating amplitudes with more legs at higher orders, but as seen in section 6.4, we are approaching the limit of our current computational ability. The usefulness of such extreme amplitudes is limited, since even 6-point scattering can be expected to be rare in reality. Also, the large number of unknown LECs limits the predictive power of the high-order interactions. Another issue is that all tree-level diagrams beyond  $\mathcal{O}(p^2)$  share power-counting order with several loop diagrams, so there is no use in pursuing higher orders at tree-level until the corresponding loop level has been reached. On the other hand, our methods and results can hopefully serve as a useful backbone for such efforts, as outlined in section 7.

There are also other interesting directions to develop. We define flavour structures in a basis of traces, but such a basis is non-orthogonal (although section 3.7 shows that the  $SU(N_f)$  version comes close to orthogonality, especially for large  $N_f$ ) and overcomplete. In perturbative QCD, more well-behaved bases such as the DDM basis [35, 36] and multiplet bases [37, 38] have been used to define colour structures and perform e.g. BCFW recursion [39]. In light of the many analogies we have seen between our methods and perturbative QCD, similar constructions could be possible also for the NLSM, and may offer computational advantages.

## Acknowledgements

First and foremost, I would like to deeply thank my supervisors for letting me enjoy immense freedom in exploring the subject, for providing profound support and guidance when needed, and for the hard work in ensuring that the project was kept finite in the end. I also thank Nils Hermansson-Truedsson, Christian Reuschle and Malin Sjödal for interesting discussions about various side topics. I thank Torbjörn Lundberg for a very fruitful exchange of thoughts and ideas, and for proof-reading the thesis, for which I also thank Emil Boman. Lastly, I would like to thank all the PhD students, postdocs and staff for making the department into a very enjoyable second home during the thesis work, and my friends and flatmates for making my first home quite nice as well.

---

<sup>30</sup>As can be seen from (3.15), the reduction in effort due to flavour-ordering is  $\mathcal{O}(|\mathcal{S}_n|/|\mathbb{Z}_R|)$ , which ranges from  $(n-1)!$  for  $R = \{n\}$  to  $n!/[(n/2)! 2^{n/2}]$  for  $R = \{2, 2, \dots, 2\}$ . A similar ratio applies to each vertex factor.

## A The Lie algebra of $SU(N_f)$ and $U(N_f)$

This is a more thorough description and derivation of the group algebra used above.

### A.1 General definitions

In their usual representation,  $U(N_f)$  is the group of  $N_f \times N_f$  unitary matrices, and  $SU(N_f)$  is the subgroup of unitary matrices with determinant 1. Since a general complex matrix of that size has  $2N_f^2$  degrees of freedom, a unitary matrix has half that, so the dimension (number of generators) of the  $U(N_f)$  algebra is  $N_f^2$ . The extra constraint on  $SU(N_f)$  reduces this by 1.

In order to generate an infinitesimal element  $U$  with these properties through

$$U(\alpha) = \exp(i\alpha^a t^a), \quad (\text{A.1})$$

unitarity dictates that  $(t^a)^\dagger = t^a$ , and since  $\det U = \exp(i\alpha^a \langle t^a \rangle)$ ,  $SU(N_f)$  places the further constraint that  $\langle t^a \rangle = 0$ . It is convenient to let the generators of  $U(N_f)$  be the same as those of  $SU(N_f)$ , plus an extra non-traceless generator  $t^0$  that effectively generates  $\det U$ .

A sensible basis of generators should have an orthonormality relation. The most sensible option is to base it on the trace,

$$\langle t^a t^b \rangle = \tau \delta^{ab}, \quad (\text{A.2})$$

where  $\tau$  is some normalisation, for which multiple conventions exist. This relation is satisfied also for  $U(N_f)$  if  $t^0 = \mathbb{1} \sqrt{\tau/N_f}$ .

The  $SU(N_f)$  generators form a basis for the space of traceless hermitian matrices, and traces can be included by adding  $t^0$ . Therefore, for any  $N_f \times N_f$  matrix  $A$ ,

$$A = A^0 \mathbb{1} + A^a t^a, \quad A^a = \frac{1}{\tau} \langle A t^a \rangle, \quad A^0 = \frac{1}{N_f} \langle A \rangle, \quad (\text{A.3})$$

where  $\mathbb{1}$  is the  $N_f \times N_f$  unit matrix. In  $U(N_f)$ , we can simply let  $a$  run from 0 to  $N_f^2 - 1$  and drop the separate  $A^0$  term. When the coefficients  $A^0$  and  $A^a$  are real,  $A$  may be any hermitian matrix, so when they are purely imaginary, it may be any antihermitian matrix. Therefore, complex coefficients allow  $A$  to be any matrix.

Being a Lie algebra, the basis of generators is closed under application of the commutator, so we may define

$$[t^a, t^b] = i\kappa f^{abc} t^c, \quad (\text{A.4})$$

where  $f^{abc}$  are called the structure constants of the algebra, and  $\kappa$  is another normalisation. The values  $f^{abc}$  depend on the particular choice of basis. The structure constants are real, since the commutator is antihermitian, and they are antisymmetric in  $a$  and  $b$ , since the commutator is. They are in fact antisymmetric in all indices, since  $f^{abc} \propto \langle [t^a, t^b] t^c \rangle$  makes them cyclic in the indices. As a consequence, the  $U(N_f)$  structure constants are zero when any index is zero, since  $t^0$  commutes with all matrices.



Lastly, the generators also have well-defined anticommutation relations. They are fixed by  $\langle \{t^a, t^b\} \rangle = 2\langle t^a t^b \rangle$ , so the anticommutator must consist of something that satisfies (A.2), possibly plus something that is traceless and hermitian. In a similar fashion to the commutator, we therefore have

$$\{t^a, t^b\} = \frac{2\tau}{N_f} \delta^{ab} + \kappa d^{abc} t^c, \quad (\text{A.5})$$

where  $d^{abc}$  are the anticommutator analogues of the structure constants. Based on arguments similar to those for  $f^{abc}$ , they are real and totally symmetric. In  $SU(2)$ ,  $f^{abc} \propto \epsilon^{abc}$  and  $d^{abc} = 0$ , where  $\epsilon$  is the Levi-civita symbol with  $\epsilon^{123} = 1$ .

By combining the commutation and anticommutation relations, one gets the generator product rule

$$t^a t^b = \frac{[t^a, t^b] + \{t^a, t^b\}}{2} = \frac{\tau}{N_f} \delta^{ab} + \kappa (d^{abc} + i f^{abc}) t^c, \quad (\text{A.6})$$

which is useful for evaluating traces of more than two generators.

## A.2 Conventional values

For  $N_f = 2$ , the Pauli matrices make up the canonical choice of generators:  $t^a = \sigma^a$ . Here, the (anti)commutator relations reduce to  $f^{abc} = \epsilon^{abc}$  (the levi-civita symbol being the only totally antisymmetric  $3 \times 3 \times 3$  object) and  $d^{abc} = 0$ . For  $N_f = 3$  the most common choice in particle physics is the Gell-Mann matrices:  $t^a = \lambda^a$ . Both these bases usually have the normalisation  $\tau = \kappa = 2$ .

When discussing the generators for general  $N_f$ , different authors use different values for  $\tau$  and  $\kappa$ . Depending on the context, a particular choice of normalisation may reduce the amount of factors of 2 or  $\sqrt{2}$  that show up in expression. Besides  $(\tau, \kappa) = (2, 2)$  mentioned above, common choices include  $(\frac{1}{2}, 1)$  [40],  $(1, \sqrt{2})$  [6], and  $(1, 1)$  [7]. For compatibility with different sources, we choose to keep the normalisation general.

## A.3 Contractions in traces

The contraction identity (3.11), which is central to flavour-ordering, can be derived from a more general identity based on (A.3). Starting with an arbitrary complex matrix  $A$  and writing out the internal indices of the matrices, we have

$$A = \frac{1}{N_f} \langle A \rangle \mathbb{1} + \frac{1}{\tau} \langle A t^a \rangle t^a \quad \Rightarrow \quad A_{ij} - \left( \frac{1}{N_f} A_{kk} \delta_{ij} + \frac{1}{\tau} A_{\ell k} t_{k\ell}^a t_{ij}^a \right) = 0. \quad (\text{A.7})$$

With a few more  $\delta$ 's, we can rewrite this as

$$A_{\ell k} \left[ \delta_{i\ell} \delta_{jk} - \left( \frac{1}{N_f} \delta_{k\ell} \delta_{ij} + \frac{1}{\tau} t_{ij}^a t_{k\ell}^a \right) \right] = 0. \quad (\text{A.8})$$

Since  $A$  was arbitrary, the bracketed expression must be zero in general, so

$$\frac{1}{\tau} t_{ij}^a t_{kl}^a = \delta_{il} \delta_{jk} - \frac{1}{N_f} \delta_{ij} \delta_{kl}. \quad (\text{A.9})$$

This can now be used to contract two traces containing arbitrary matrices  $X$  and  $Y$ :

$$\frac{1}{\tau} \langle X t^a \rangle \langle t^a Y \rangle = \frac{1}{\tau} X_{ji} t_{ij}^a t_{kl}^a Y_{lk} = X_{jl} Y_{lj} - \frac{1}{N_f} X_{ii} Y_{kk} = \langle XY \rangle - \frac{1}{N_f} \langle X \rangle \langle Y \rangle, \quad (\text{A.10})$$

which proves (3.11). Similarly,

$$\frac{1}{\tau} \langle X t^a Y t^a \rangle = \frac{1}{\tau} X_{li} t_{ij}^a Y_{jk} t_{kl}^a = X_{ii} Y_{jj} - \frac{1}{N_f} X_{lj} Y_{jl} = \langle X \rangle \langle Y \rangle - \frac{1}{N_f} \langle XY \rangle \quad (\text{A.11})$$

proves (3.12).

In  $U(N_f)$ , the  $1/N_f$  term in (A.3) is not used, since  $t^0$  takes over its function. This carries through to (A.9), which loses its last term. Therefore, the  $1/N_f$  terms in (3.11) and (3.12) are not present in the  $U(N_f)$  case.

## A.4 The adjoint representation

For each set of Lie algebra generators  $t^a$ , one can also find a complementary set  $F^a$  known as the *adjoint representation*. A conventional definition is

$$(F^a)_{bc} = -i\kappa f^{abc}, \quad (\text{A.12})$$

where the last two flavour indices assume the role of the internal indices of  $(t^a)_{ij}$ . No distinction is made between upper and lower indices. The adjoint generators are  $(N_f^2 - 1) \times (N_f^2 - 1)$  matrices, and are traceless and hermitian due to the antisymmetry of  $f^{abc}$ .

The adjoint generators have mostly the same algebraic properties as  $t^a$ ; for instance,

$$\langle F^a F^b \rangle = -\kappa^2 f^{acd} f^{bdc} = \frac{1}{\tau^2} \langle t^a [t^c, t^d] \rangle \langle t^b [t^c, t^d] \rangle = 2\tau N_f \delta^{ab}, \quad (\text{A.13})$$

where the last equality is found by inserting (3.11) and (3.12) into the traces. Therefore, going to the adjoint representation changes the normalisation as  $\tau \rightarrow 2\tau N_f$ .

The commutation relations of the adjoint generators is a direct consequence of the Jacobi identity

$$f^{abe} f^{cde} + f^{bce} f^{ade} + f^{ace} f^{dbe} = 0, \quad (\text{A.14})$$

which holds for the structure constants of any Lie algebra, and can be verified by examining nested commutators. With some index shuffling, the Jacobi identity can be recast to

$$[F^a, F^b] = i\kappa f^{abc} F^c. \quad (\text{A.15})$$

The placement of  $\kappa$  in (A.12) preserves the normalisation of this relation.

The adjoint representation does not have anticommutator relations analogous to (A.5). Being closed under anticommutation is not a general feature of Lie algebras, and its occurrence in the  $SU(N_f)$  and  $U(N_f)$  algebras does not carry over to the adjoint representation. The existence of (A.5) hinges on  $t^a$  being a complete basis for traceless hermitian  $N_f \times N_f$  matrices, and since  $F^a$  are not a complete basis for traceless hermitian  $(N_f^2 - 1) \times (N_f^2 - 1)$  matrices, an analogue can not be expected.

## B The orthogonality of flavour structures

Here, we prove the orthogonality relation (3.31) used in section 3.7 to prove the uniqueness of stripped amplitudes. It relies on notation defined in that and previous sections.

Let  $\sigma, \rho \in \mathcal{S}_n$  be two permutations, and  $Q, R$  be two flavour splittings of total length  $n$ . We use these to build two flavour structures, and begin by focusing on the trace in  $\mathcal{F}_\sigma(Q)$  that contains  $a_{\sigma(n)}$  and the trace in  $\mathcal{F}_\rho(R)$  that contains  $a_{\rho(m)}$ , where we have picked  $m$  such that  $\rho(m) = \sigma(n)$ . If there are more traces present, we leave them as passive “spectators” for the time being. Then, we use (3.11) to contract  $a_{\sigma(n)}$  in

$$\mathcal{F}_\sigma(Q) \cdot [\mathcal{F}_\rho(R)]^* = \tau \left[ \langle X a_{\sigma(n-1)} a_{\rho(m-1)} Y \rangle - \frac{1}{N_f} \langle X a_{\sigma(n-1)} \rangle \langle a_{\rho(m-1)} Y \rangle \right] \cdot (\text{spectators}), \quad (\text{B.1})$$

where the product is defined as in (3.31).

From here on, we work only to leading order in  $N_f$ , so we can omit the second term above. (Note that we do not do this because  $N_f$  is necessarily large, but because we wish to use power counting of  $N_f$  to separate orthogonal flavour structures.) We then move on to contracting  $\sigma(n-1)$ , followed by  $\sigma(n-2)$ , and so on. Each time we contract  $\sigma(n-i)$ , the situation may be one of the following cases:

1.  $\rho(m-i) = \sigma(n-i)$ . We carry on through a special case of the contraction identity (3.12), and find

$$\langle X a_{\sigma(n-i)} a_{\rho(m-i)} Y \rangle = \tau \frac{N_f^2 - 1}{N_f} \langle XY \rangle. \quad (\text{B.2})$$

This may be repeated as long as there are indices left, and we gain a factor of  $N_f$  (plus  $\mathcal{O}(N_f^{-1})$ , which we ignore) each time.

2.  $\rho(m-i) \neq \sigma(n-i)$ , but  $\rho(m') = \sigma(n-i)$  is in the same trace as  $\sigma(n-i)$ . Here, (3.12) (after some reshuffling of  $X$  and  $Y$ ) gives

$$\langle X a_{\sigma(n-i)} Y a_{\rho(m-i)} \rangle = \tau \left[ \langle X \rangle \langle Y \rangle - \frac{1}{N_f} \langle XY \rangle \right]. \quad (\text{B.3})$$

the second term is suppressed by a factor of  $N_f^{-1}$ , and the first must eventually take a detour through (B.1) before continuing; in any case, this case falls behind case 1 by at least two factors of  $N_f$ .

3.  $\rho(m') = \sigma(n - i)$  is in a different trace than  $\sigma(n - i)$ . This forces us to bring in the spectator trace containing  $\rho(m')$  and go back to (B.1), so this case falls behind case 1 by at least one factor of  $N_f$ .
4. The trace is empty. We gain a factor of  $\langle \mathbb{1} \rangle = N_f$ , and if there are no spectator traces left, we are done. Otherwise, we bring in the next pair of spectators and continue from (B.1).

If  $Q = R = \{n\}$  and  $\sigma \equiv \rho \pmod{\mathbb{Z}_R}$ , we will only encounter case 1 until we finish with a case 4, and will gain a total factor of  $\tau^n N_f^n [1 + \mathcal{O}(N_f^{-2})]$ . If  $Q = R \neq \{n\}$  on the other hand, we will encounter case 4 at each split, but the leading power of  $N_f$  stays the same.

If  $\sigma \not\equiv \rho \pmod{\mathbb{Z}_R}$ , we must eventually encounter case 2, so this falls behind the  $\sigma \equiv \rho \pmod{\mathbb{Z}_R}$  case by at least two powers of  $N_f$ . If  $Q \neq R$ , we will encounter case 3 (without a corresponding case 4) whenever there is a mismatch in the flavour splits, so we will fall behind the  $Q = R$  case by at least one power of  $N_f$ . This is the reason for the values of  $\gamma$  stated below (3.31).

Thus, we have proven

$$\mathcal{F}_\sigma(Q) \cdot [\mathcal{F}_\rho(R)]^* = \tau^n N_f^{n-2} (N_f^2 - 1) \begin{cases} 1 + \mathcal{O}(N_f^{-2}) & \text{if } Q = R \text{ and } \sigma \equiv \rho \pmod{\mathbb{Z}_R}, \\ \mathcal{O}(N_f^{-\gamma}) & \text{otherwise } (\gamma \geq 1) \end{cases} \quad (\text{B.4})$$

which is (3.31). The factor of  $(N_f^2 - 1)$  is common to all cases, since the final pair of indices is always contracted as  $\langle a_{\sigma(1)} a_{\sigma(1)} \rangle$ .

## C The double soft limit

This appendix provides a derivation of (4.19), which is used to calculate the double soft limit of stripped amplitudes. We start by quoting (4.17), which is proven in [6] and gives the double soft limit of the full amplitude:

$$\lim_{\varepsilon \rightarrow 0} \mathcal{M}_{N,n+2}^{aba_1 \dots a_n}(\varepsilon p, \varepsilon q, p_1, \dots, p_n) = -\frac{1}{\kappa^2 F^2} \sum_{i=1}^n f^{abc} f^{a_i dc} \frac{p_i \cdot (p - q)}{p_i \cdot (p + q)} \mathcal{M}_{N,n}^{a_1 \dots a_{(i-1)} da_{(i+1)} \dots a_n}(p_1, \dots, p_n). \quad (\text{C.1})$$

In order to find the corresponding expression for a stripped amplitude, we project it out by contracting both sides with  $[\mathcal{F}_{\text{id}}(R)]^*$  over all flavour indices (see (3.15) and section 3.7). On the left-hand side of (C.1), this will project out  $\lim_{\varepsilon \rightarrow 0} \mathcal{M}_{N,n+2,R}$ . For simplicity, we start with  $R = \{n + 2\}$  before moving on to the general multi-trace case. According to (3.15), the right-hand side of (C.1) has the form (schematically, with kinematic terms omitted)

$$\sum_{\sigma \in \mathcal{S}_n / \mathbb{Z}_n} f^{abc} f^{a_i dc} \langle a_{\sigma(1)} \dots a_{\sigma(i-1)} da_{\sigma(i+1)} \dots a_{\sigma(n)} \rangle \quad (\text{C.2})$$

plus flavour-split structures, but those can be ignored due to (3.31). We have omitted the algebra generators for readability;  $a_i$  means  $t^{a_i}$ . The structure constants can be contracted in using (3.11) and  $f^{abc} = \frac{-i}{\tau\kappa} \langle t^a [t^b, t^c] \rangle$ , leaving

$$-\frac{1}{\kappa^2} \langle a_{\sigma(1)} \cdots a_{\sigma(i-1)} [[a, b], a_{\sigma(i)}] a_{\sigma(i+1)} \cdots a_{\sigma(n)} \rangle. \quad (\text{C.3})$$

With appendix B in mind, we immediately see that this is orthogonal to  $\mathcal{F}_{\text{id}}(n+2)$  unless  $\sigma = \text{id}$ . The nested commutators expand to

$$[[a, b], a_i] = aba_i - baa_i - a_iab + a_i ba. \quad (\text{C.4})$$

Since  $a$  comes before  $b$  in  $\mathcal{F}_{\text{id}}(n+2)$ , the second and fourth terms vanish under the projection. Also,  $ab$  occurs at the beginning (or, equivalently, the end) of the flavour structure, so the first term only contributes when  $i = 1$ , and the third term only contributes when  $i = n$ . This collapses the sum in (C.1) to those two cases, leaving

$$\lim_{\varepsilon \rightarrow 0} \mathcal{M}_{N, n+2, \{n+2\}}(\varepsilon p, \varepsilon q, p_1, \dots, p_n) = \frac{1}{\kappa^4 F^2} \left\{ \frac{p_1 \cdot (p - q)}{p_1 \cdot (p + q)} - \frac{p_n \cdot (p - q)}{p_n \cdot (p + q)} \right\} \mathcal{M}_{N, n, \{n\}}(p_1, \dots, p_n). \quad (\text{C.5})$$

If we now move on to general  $R$ , we see that  $a$  and  $b$  must reside in the same trace, since the nested commutator on the right-hand side is inside a single trace. This is essentially the condition stated for the validity of (4.19), with  $(p_n, p, q, p_1)$  mapping to  $(p_{i-1}, p_i, p_j, p_{j+1})$ . The trace they reside in can be treated exactly like the single-trace flavour structure of (C.5), and all other traces in the flavour structure follow along as ‘‘spectators’’, as in a normal application of (3.31). The reduction  $\{n+2\} \rightarrow \{n\}$  in (C.5) then generalises to  $R \rightarrow R'$  as described below (4.19). This generalisation therefore results in (4.19), which is thereby proven.

## D Closed Mandelstam bases

Here, we show the derivation of closed Mandelstam bases for all 6-particle flavour structures as described in section 4.3. Note that neither basis is unique, and that better basis choices may exist.

### D.1 The basis for $R = \{2, 4\}$

This is the only basis other than  $\mathcal{B}_{\{6\}}$  that is needed at  $\mathcal{O}(p^4)$ . Since  $\mathbb{Z}_{\{2,4\}}$  is abelian, the last 5 elements of  $\mathcal{B}_{\{2,4\}}$  in (4.13) transform rather simply. It is therefore possible to form closed linear combination by inspection with a little help from trial and error. This gives

the closed basis  $\hat{\mathcal{B}}_{\{2,4\}} = \{t_1, \dots, t_9\}$  with elements

$$\begin{aligned}
t_1 &= s_{123}, & t_2 &= s_{124}, & t_3 &= s_{125}, & t_4 &= s_{126}, \\
t_5 &= s_{45} + \frac{s_{124} - s_{123}}{2}, & t_6 &= s_{56} + \frac{s_{125} - s_{124}}{2}, \\
t_7 &= s_{14} + s_{15} + \frac{s_{123} + s_{126}}{2}, & t_8 &= s_{15} + s_{16} + \frac{s_{123} + s_{124}}{2}, \\
t_9 &= s_{14} + s_{16} + \frac{s_{123} + s_{125}}{2}.
\end{aligned} \tag{D.1}$$

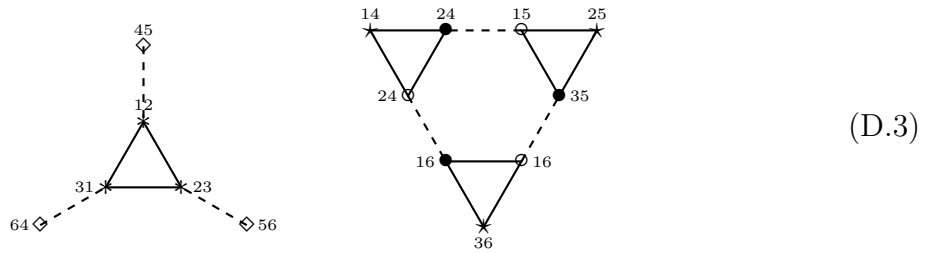
Under the action of  $\mathbb{Z}_{\{2,4\}}$ , they transform as

$$\begin{aligned}
21\ 3456 : & \quad \{t_1, \dots, t_6, t_7, t_8, t_9\} \rightarrow \{t_1, \dots, t_6, -t_7, -t_8, -t_9\}, \\
12\ 4563 : & \quad \{t_1, \dots, t_6, t_7, t_8, t_9\} \rightarrow \{t_2, t_3, t_4, t_1, t_6, t_5, +t_8, -t_7, -t_9\},
\end{aligned} \tag{D.2}$$

where the first permutation cycles the 2-trace, and the second cycles the 4-trace; together, they generate all of  $\mathbb{Z}_{\{2,4\}}$ . Note that  $\mathbb{Z}_{\{2,4\}}$  does not act as a true permutation on the basis, since some elements change sign. This appears to be unavoidable, but is not a problem — in fact, any complex phase can be applied without breaking the  $\mathbf{m}$ -finding procedure.

## D.2 The basis for $R = \{3, 3\}$

The group  $\mathbb{Z}_{\{3,3\}}$  is generated by the permutations  $g_1 = 231\ 456$  and  $g_2 = 456\ 123$ . They do not commute, so the group is non-abelian, which makes its effects less predictable. Among all kinematic invariants, only  $s_{123}$  maps to itself under both generators, and is also the only squared propagator momentum permitted by this flavour structure. The 15 invariants  $s_{ij}$  decompose into a sextuplet and a nonet under the group, and can be mapped out in a variant on a Cayley graph:



Each node in the graph represents  $s_{ij}$  and is marked with  $ij$ . The action of  $g_1$  is represented by following the solid-drawn triangles clockwise, and  $g_2$  is represented by following the dashed lines. The 9 distinct invariants  $s_{ijk}$  with  $ijk \neq 123$  also form a nonet with the same structure as the one above, replacing 14 by 126, etc.

We must now extract the 8 basis elements  $t_2, \dots, t_9$  (with  $t_1 = s_{123}$ ) such that they are closed under  $\mathbb{Z}_{\{3,3\}}$ . In the nonet, we have marked three sets of invariants with  $\star$ ,  $\bullet$  and  $\circ$ . They map to each other as  $(\star, \bullet, \circ) \rightarrow (\bullet, \circ, \star)$  under  $g_1$  and as  $(\star, \bullet, \circ) \rightarrow (\star, \circ, \bullet)$  under  $g_2$ , so suitable linear combinations of the elements in each set will be closed under  $\mathbb{Z}_{\{3,3\}}$ .

Similarly, we can find two sets,  $\diamond$  and  $*$ , from the sextet. The corresponding sets from the nonet of  $s_{ijk}$ 's are not linearly independent from  $s_{123}$  and the sets of  $s_{ij}$ 's, so they can be ignored.

Unfortunately, it appears impossible to form real linear combinations without sacrificing either linear independence or closedness. Guided by the fact that  $g_1$  has period 3, we instead insert the third root of unity,  $\omega = e^{2\pi i/3}$ , and find the closed and complete basis  $\hat{\mathcal{B}}_{\{3,3\}}$  with

$$\begin{aligned}
t_1 &= s_{123}, \\
t_2 &= s_{24} + \omega s_{35} + \omega^2 s_{16}, & t_3 &= s_{15} + \omega s_{26} + \omega^2 s_{34}, & t_4 &= s_{36} + \omega s_{14} + \omega^2 s_{25}, \\
t_5 &= \omega^2 s_{24} + \omega s_{35} + s_{16}, & t_6 &= \omega^2 s_{15} + \omega s_{26} + s_{34}, & t_7 &= \omega^2 s_{36} + \omega s_{14} + s_{25}, \\
t_8 &= s_{12} + \omega s_{23} + \omega^2 s_{31}, & t_9 &= s_{45} + \omega s_{56} + \omega^2 s_{64},
\end{aligned} \tag{D.4}$$

where  $t_2, \dots, t_7$  come from the nonet ( $t_2$  and  $t_5$  from  $\bullet$ , etc.) and  $t_8, t_9$  come from the sextet. They transform as

$$\begin{aligned}
g_1 : & \quad \{t_1, t_2, t_3, t_4, t_5, t_6, t_7, t_8, t_9\} \rightarrow \{t_1, \omega t_3, \omega t_4, \omega t_2, \omega^2 t_6, \omega^2 t_7, \omega^2 t_5, \omega t_8, \omega t_9\}, \\
g_2 : & \quad \{t_1, t_2, t_3, t_4, t_5, t_6, t_7, t_8, t_9\} \rightarrow \{t_1, t_3, t_2, t_4, t_6, t_5, t_7, t_9, t_8\}.
\end{aligned} \tag{D.5}$$

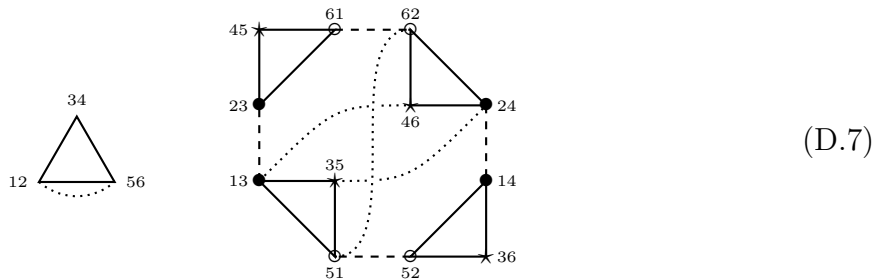
Since stripped amplitudes are real, the complex basis must be compensated for by complex coefficients. Still,  $\hat{\mathcal{B}}_{\{3,3\}}$  is just as valid as a real basis, and is useable for finding  $\mathbf{m}$ .

### D.3 The basis for $R = \{2, 2, 2\}$

The group  $\mathbb{Z}_{\{2,2,2\}}$  is also non-abelian, and can be tackled similarly to  $\mathbb{Z}_{\{3,3\}}$ . We choose the generators  $g_1 = 21\ 34\ 56$ ,  $g_2 = 34\ 56\ 12$  and  $g_3 = 65\ 43\ 21$  with the hopes that they be well-behaved, since  $\mathcal{B}_{\{6\}}$  is closed under the latter two. This flavour structure admits the six distinct propagators included in  $\mathcal{B}_{\{2,2,2\}}$  of (4.13). We arrange the corresponding invariants as



where  $g_1$  and  $g_2$  are represented as in (D.3), and the dotted lines represent the action of  $g_3$ . The four remaining  $s_{ijk}$ 's are not useful, but the  $s_{ij}$ 's decompose into a well-structured triplet and 12-plet:



Like in (D.3), we have marked three closed sets of  $s_{ij}$ 's. From these, it is possible to construct three linearly independent elements that close the basis without need for the triplet. Thus,  $\hat{\mathcal{B}}_{\{2,2,2\}}$  has elements

$$\begin{aligned} t_1 &= s_{123}, & t_2 &= s_{126}, & t_3 &= s_{156}, & t_4 &= s_{124}, & t_5 &= s_{125}, & t_6 &= s_{134}, \\ t_7 &= \frac{s_{61} - s_{62} + s_{52} - s_{51}}{2}, & t_8 &= \frac{s_{23} - s_{24} + s_{14} - s_{13}}{2}, & t_9 &= \frac{s_{45} - s_{46} + s_{36} - s_{35}}{2}, \end{aligned} \quad (\text{D.8})$$

where the factors of 1/2 remove some large powers of 2 that show up when writing amplitudes in this basis. Unlike in  $\hat{\mathcal{B}}_{\{3,3\}}$ , there was no need to resort to complex numbers. The basis transforms as

$$\begin{aligned} g_1 : & \quad \{t_1, t_2, t_3, t_4, t_5, t_6, t_7, t_8, t_9\} \rightarrow \{t_1, t_2, t_6, t_4, t_5, t_3, -t_7, -t_8, t_9\}, \\ g_2 : & \quad \{t_1, t_2, t_3, t_4, t_5, t_6, t_7, t_8, t_9\} \rightarrow \{t_2, t_3, t_1, t_5, t_6, t_4, t_8, t_9, t_7\}, \\ g_3 : & \quad \{t_1, t_2, t_3, t_4, t_5, t_6, t_7, t_8, t_9\} \rightarrow \{t_1, t_3, t_2, t_4, t_6, t_5, t_7, t_9, t_8\}. \end{aligned} \quad (\text{D.9})$$

No basis element is a fixed point, which makes the basis harder to work in.

## E Implementation details

This is a brief summary of the code used in this work. It can be obtained from [www.github.com/mssjo/flavour-order](https://www.github.com/mssjo/flavour-order) and [www.github.com/mssjo/fodge](https://www.github.com/mssjo/fodge), and more information is available in the documentation found in the source code itself. The FORM library requires FORM, which can be acquired from [nikhef.nl/~form](https://nikhef.nl/~form).

The code was written gradually during the process of this work, and therefore contains deprecated sections, different nomenclature than used in this thesis, and several bugs and incomplete features. Fixes and improvements may be uploaded in the future.

### E.1 The FORM library

This library contains FORM procedures for calculating flavour-ordered amplitudes. It is based on brute-force Feynman diagram calculation procedures written by Johan Bijnens. The library contains several files with names `foMnpN.frm` that are used to compute the  $n$ -point  $\mathcal{O}(p^N)$  amplitude using flavour-ordering.

All definitions needed to use the library are included in `defs.hf`, and the flavour-ordering routines are initiated by `init-fo.hf`. The procedure `sfrule` creates a stripped Feynman rule (i.e. stripped vertex factor) at a given order and flavour splitting using the `vertex` procedure, which contains all NLSM Lagrangian terms up to  $\mathcal{O}(p^8)$ . Diagrams are then drawn using the `diagram` function followed by a call to the `diagram` procedure; how to do this is documented in that procedure. Finally, the `mandel` procedure rewrites the amplitude in terms of Mandelstam invariants, and `prettymandel` may be called to write the result in a more human-readable fashion.



The amplitude may be checked for Adler zeroes by calling the `adler` procedure. For complicated amplitudes, the symbolic algebra capabilities of FORM may not be enough to reveal a zero, and `mandelrand` can be called to give all Mandelstam invariants pseudo-random numerical values. Instead of checking Adler zeroes, reduced stripped amplitudes can be found by using the `group` and `uncycle` procedures together with a change of Mandelstam basis like those contained in `mandelbasis`.

The library contains several other more-or-less useful procedures, most of which are sufficiently documented in their source code to use without an introduction here.

## E.2 The diagram generator fodge

The program `fodge` (flavour-ordered diagram generator) generates flavour-ordered diagrams using the methods described in section 5. It runs on the command line and has a `man` page containing information on how to use it. It can generate a `.tex` file for drawing the diagrams (in polygon form) using `TikZ`, or generate a set of `.hf` files for use with the FORM library. It can also print a summary of the generated diagrams, which was used to generate table 3. The program is fully general, and can generate diagrams at any order as long as the `TikZ` drawing functions are modified to draw higher-order vertices.

## References

- [1] M. Gell-Mann and M. Levy, *The axial vector current in beta decay*, *Nuovo Cim.* **16** (1960) 705.
- [2] A. S. Gliozzi and A. Parola, *Nonlinear sigma models and quantum spin systems*, *Phys. Rev. B* **64** (2001) 184439.
- [3] S. Weinberg, *Phenomenological Lagrangians*, *Physica* **A96** (1979) 327.
- [4] J. Gasser and H. Leutwyler, *Chiral Perturbation Theory to One Loop*, *Annals Phys.* **158** (1984) 142.
- [5] J. Gasser and H. Leutwyler, *Chiral Perturbation Theory: Expansions in the Mass of the Strange Quark*, *Nucl. Phys.* **B250** (1985) 465.
- [6] K. Kampf, J. Novotný and J. Trnka, *Tree-level Amplitudes in the Nonlinear Sigma Model*, *JHEP* **05** (2013) 032 [1304.3048].
- [7] J. Bijnens and J. Lu, *Meson-meson Scattering in QCD-like Theories*, *JHEP* **03** (2011) 028 [1102.0172].
- [8] J. Bijnens and N. Hermansson Truedsson, *The Pion Mass and Decay Constant at Three Loops in Two-Flavour Chiral Perturbation Theory*, *JHEP* **11** (2017) 181 [1710.01901].

- [9] I. Low and Z. Yin, *Soft Bootstrap and Effective Field Theories*, 1904.12859.
- [10] F. A. Berends and W. Giele, *The Six Gluon Process as an Example of Weyl-Van Der Waerden Spinor Calculus*, *Nucl. Phys.* **B294** (1987) 700.
- [11] C. Reuschle and S. Weinzierl, *Decomposition of one-loop QCD amplitudes into primitive amplitudes based on shuffle relations*, *Phys. Rev.* **D88** (2013) 105020 [1310.0413].
- [12] T. Schuster, *Color ordering in QCD*, *Phys. Rev.* **D89** (2014) 105022 [1311.6296].
- [13] A. Pich, *Effective Field Theory with Nambu-Goldstone Modes*, in *Les Houches summer school: EFT in Particle Physics and Cosmology Les Houches, Chamonix Valley, France, July 3-28, 2017*, 2018, 1804.05664.
- [14] J. Bijnens, N. Hermansson-Truedsson and S. Wang, *The order  $p^8$  mesonic chiral Lagrangian*, *JHEP* **01** (2019) 102 [1810.06834].
- [15] G. Ecker, J. Gasser, A. Pich and E. de Rafael, *The Role of Resonances in Chiral Perturbation Theory*, *Nucl. Phys.* **B321** (1989) 311.
- [16] J. Bijnens, G. Colangelo and G. Ecker, *The Mesonic chiral Lagrangian of order  $p^6$* , *JHEP* **02** (1999) 020 [hep-ph/9902437].
- [17] J. Sawada, *A fast algorithm for generating nonisomorphic chord diagrams*, *SIAM Journal on Discrete Mathematics* **15** (2002) 546.
- [18] J. Wess and B. Zumino, *Consequences of anomalous Ward identities*, *Phys. Lett.* **37B** (1971) 95.
- [19] E. Witten, *Global Aspects of Current Algebra*, *Nucl. Phys.* **B223** (1983) 422.
- [20] C. Cheung, K. Kampf, J. Novotný, C.-H. Shen and J. Trnka, *A Periodic Table of Effective Field Theories*, *JHEP* **02** (2017) 020 [1611.03137].
- [21] M. L. Mangano and S. J. Parke, *Multiparton amplitudes in gauge theories*, *Phys. Rept.* **200** (1991) 301 [hep-th/0509223].
- [22] S. L. Adler, *Consistency conditions on the strong interactions implied by a partially conserved axial vector current*, *Phys. Rev.* **137** (1965) B1022.
- [23] S. Weinberg, *The quantum theory of fields*, vol. 2. Cambridge university press, 1996.
- [24] C. Cheung, K. Kampf, J. Novotný and J. Trnka, *Effective Field Theories from Soft Limits of Scattering Amplitudes*, *Phys. Rev. Lett.* **114** (2015) 221602 [1412.4095].
- [25] N. Arkani-Hamed, F. Cachazo and J. Kaplan, *What is the Simplest Quantum Field Theory?*, *JHEP* **09** (2010) 016 [0808.1446].

- [26] S. Weinberg, *The quantum theory of fields*, vol. 1. Cambridge university press, 1995.
- [27] J. A. Cronin, *Phenomenological model of strong and weak interactions in chiral  $U(3) \times U(3)$* , *Phys. Rev.* **161** (1967) 1483.
- [28] J. Bijnens, K. Kampf and S. Lanz, *Leading logarithms in  $N$ -flavour mesonic Chiral Perturbation Theory*, *Nucl. Phys.* **B873** (2013) 137 [1303.3125].
- [29] J. R. Ellis and B. Renner, *On the relationship between chiral and dual models*, *Nucl. Phys.* **B21** (1970) 205.
- [30] R. Britto, F. Cachazo and B. Feng, *New recursion relations for tree amplitudes of gluons*, *Nucl. Phys.* **B715** (2005) 499 [hep-th/0412308].
- [31] R. Britto, F. Cachazo, B. Feng and E. Witten, *Direct proof of tree-level recursion relation in Yang-Mills theory*, *Phys. Rev. Lett.* **94** (2005) 181602 [hep-th/0501052].
- [32] C. Cheung, K. Kampf, J. Novotný, C.-H. Shen and J. Trnka, *On-Shell Recursion Relations for Effective Field Theories*, *Phys. Rev. Lett.* **116** (2016) 041601 [1509.03309].
- [33] K. S. Booth, *Lexicographically least circular substrings*, *Information Processing Letters* **10** (1980) 240.
- [34] O. Cata and V. Mateu, *Chiral perturbation theory with tensor sources*, *JHEP* **09** (2007) 078 [0705.2948].
- [35] V. Del Duca, A. Frizzo and F. Maltoni, *Factorization of tree QCD amplitudes in the high-energy limit and in the collinear limit*, *Nucl. Phys.* **B568** (2000) 211 [hep-ph/9909464].
- [36] V. Del Duca, L. J. Dixon and F. Maltoni, *New color decompositions for gauge amplitudes at tree and loop level*, *Nucl. Phys.* **B571** (2000) 51 [hep-ph/9910563].
- [37] M. Sjö Dahl and J. Thorén, *Decomposing color structure into multiplet bases*, *JHEP* **09** (2015) 055 [1507.03814].
- [38] M. Sjö Dahl and J. Thorén, *QCD multiplet bases with arbitrary parton ordering*, *JHEP* **11** (2018) 198 [1809.05002].
- [39] Y.-J. Du, M. Sjö Dahl and J. Thorén, *Recursion in multiplet bases for tree-level MHV gluon amplitudes*, *JHEP* **05** (2015) 119 [1503.00530].
- [40] M. E. Peskin and D. V. Schroeder, *Quantum field theory. The Advanced Book Program*. Perseus Books Reading, Massachusetts, 1995.